



TECHNISCHE  
UNIVERSITÄT  
WIEN

## Diploma thesis

# High-efficient photo base generators for visible light initiation of oxa-ene Michael addition reactions

carried out at the

Research Group Polymer Chemistry and Technology  
Institute of Applied Synthetic Chemistry  
Technische Universität Wien

under supervision of

Senior Scientist Dipl.-Ing. Dr.techn. Patrick **Knaack**  
Univ. Prof. Dipl.-Ing. Dr. techn. Robert **Liska**

by

**Edma Gjata, BSc**

11843593

---

Edma Gjata, BSc

## Acknowledgements

Firstly, I would like to thank Prof. Robert Liska for the exiting topic and the opportunity to conduct my master thesis in his research group. Thank you for your valuable scientific input whenever I needed it.

I wish to extend my thanks and gratitude to my direct supervisor, Patrick. Thank you for your support, encouragement, and contribution to this thesis. I have yet a lot to learn from the openness and creativity you approach science with.

I thank all the current and former members of the FBMC working group for creating a welcoming environment I am genuinely happy to be a part of. I also thank you, Dagmar, Jürgen, and Walter, for the organizational support.

I am thankful to you, Ralle, for inspiring the start of this polymer chemistry quest through my first FBMC internship.

Further, since my thesis started existing because of yours, I thank you, Klaus, for your help along the way.

Thank you to the NMR operators, Dani, Toni, Kaja, Carola, and Klaus, for dealing with the extensive amount of NMR tubes on my account.

My dear H25 lab cannot go unmentioned. Thank you Flocke, my bench buddy, for the great support and unlimited (excel) tips and tricks. Thank you, Michi and Björn, for our talks, coffee breaks, and sometimes *even* the music in the lab. I have now realized the real luxury is sharing a lab with you three.

Next, I wish to thank all the dear friends I have met during my studies who have enriched these years in so many ways for me.

My special thank belongs to my parents and my brother for making all this possible by their unconditional love and everlasting support. Thank you for giving me courage to follow my dreams.

And lastly, Sebastian, I want to thank you for standing by my side. You always help me remember what *really* is important even in times of doubt. I wish to share every accomplishment with you.

## Abstract

Photopolymerization is one of the most promising techniques to obtain polymeric materials in a rapid and highly-efficient manner. This is reflected on the development of advanced manufacturing processes relying on photopolymerization, e.g. coating and 3D printing techniques.

At the core of every photoreaction stands the photoinitiating system. With the rise of new photoinitiators that shift the attention towards photogeneration of an acid or a base, photobase generators (PBGs) have gathered momentum in the last decade. They are superior to their radical generating counterparts, as they do not suffer from oxygen inhibition and are usually linked to less structural defects of the final material triggered by volume shrinkage upon polymerization. Moreover, unlike acid initiating species, they do not corrode metallic substrates, rendering their application in automotive and electronic industries possible.

However, most literature-known PBGs suffer from a rather weak basicity of the active species (e.g. primary or secondary amines), short wavelength absorption confined within harmful UV light, low quantum yields, as well as poor thermal and chemical stabilities.

The work carried out with this thesis opts to overcome these challenges through synthesis and investigation of new PBGs. Paired with their ability to liberate extremely strong phosphazene superbases with a high efficiency, their photosensitive moieties allow absorption of the incident light at high wavelengths, extending to the visible light region. Characterization of their thermal behavior and photoreactivity was carried out via thermogravimetric analysis and UV/Vis spectroscopy. Additionally, the synthesis of a new phosphazene base is explored with the intention of tuning basicity levels and enabling availability beyond commercial compounds.

The applicability of the prepared PBGs was tested on an oxa-ene Michael addition model system in a photo-DSC setup. Firstly, a monofunctional study was investigated including thorough screening of reaction conditions. This approach was further extended to a difunctional system with successful attempts towards expanding the library of photopolymerization reactions that involve a Michael addition mechanism.

## Kurzfassung

Photopolymerisation zählt zu den vielversprechendsten Methoden, um Polymere schnell und energieeffizient herzustellen. Insbesondere Beschichtungs- und 3D Druck Industrie profitieren durch die Entwicklung photopolymerisationsbasierter Fertigungstechnologien.

Im Mittelpunkt aller Photoreaktionen stehen photoinitiierende Systeme, nämlich Photoradikalgeneratoren (PRG), Photosäuregeneratoren (PAG) und Photobasengeneratoren (PBG). Die industriell relevantesten Initiatoren sind PRGs, obwohl deren Anwendung einige Limitierungen mit sich bringt, wie z.B. Sauerstoff Inhibition und polymerisationsinduzierter Volumenschrumpf, die zu defekten Materialien führen können. Dem gegenüber repräsentieren PBGs eine relativ neue Klasse an Initiatoren, welche von diesen Nachteilen nicht betroffen sind. Sie wirken darüber hinaus im Gegensatz zu PAGs nicht korrosiv gegenüber Metallen und sind deswegen geeigneter für Anwendungen in Automobil- und Elektronikindustrie.

Jedoch setzen herkömmliche PBGs schwach basische aktive Spezies frei (z.B. primäre oder sekundäre Amine), die für die meisten Anwendungen unzureichend sind. Sie absorbieren oft kurzwelliges Licht im schädlichen UV-Bereich mit geringen Quantenausbeuten und weisen eine geringe thermische und chemische Stabilität auf.

In der vorliegenden Arbeit wurden neue PBG Systeme synthetisiert und untersucht, die sehr starke Phosphazen-*N*-Superbasen höchsteffizient freisetzen können. Deren photosensitive Strukturen erlauben Lichtabsorption bei höheren Wellenlängen, welche den sichtbaren Bereich erreichen. Für die thermische und photochemische Charakterisierung wurden thermogravimetrische Analyse und UV/Vis Spektroskopie eingesetzt. In weiterer Folge wurde die Synthese einer modifizierten Phosphazen-Superbase als potentiell neue, zugänglichere aktive Spezies konzipiert. Die Anwendbarkeit der synthetisierten PBGs wurde anhand einer Oxa-En-Michael Addition mittels Photo-DSC untersucht. Eine grundlegende monofunktionelle Studie wurde erfolgreich durchgeführt, indem die Einflüsse von Temperatur, Lichtintensität und PBG Konzentration bestimmt wurden. Besonderer Fokus lag überdies auf die Erweiterung der Methodologie auf ein analoges difunktionelles System, wobei der Oxa-Michael Mechanismus eine vielversprechende Strategie zur Weiterentwicklung neuer Photopolymerklassen darstellt.

# Table of contents

Introduction	1	
Coatings	1	
Photopolymerization	4	
Photo base generators (PBG)	9	
Phosphazene superbases	11	
The oxa-Michael addition reaction	14	
<b>Objective</b>	<b>17</b>	
<b>State of the Art</b>	<b>18</b>	
<b>Results and discussion</b>	<b>R&amp;D</b>	<b>Exp.</b>
1. Synthesis	22	62
1.1 Phosphazene superbase	24	62
1.1.1 First P-fragment	24	62
1.1.1.1 The <i>n</i> -pentane route	24	62
1.1.1.2 The tetrachloroethane route	25	63
1.1.2 Second P-fragment	26	64
1.1.2.1 The NaOH approach	27	65
1.1.2.2 The KO-t-Bu/MeOH approach	28	65
1.1.3 Coupling of the two P-fragments	29	66
1.1.3.1 Reaction in THF at 30 °C	32	67
1.1.3.2 Reaction in toluene at 120 °C	33	67
1.2 Chromophore	34	67
1.3 PBGs	36	69
1.3.1 Thioxanthone-based <b>TP</b>	36	69
1.3.2 Isoxepac-based <b>IP</b>	37	69
2. Characterization	38	70
2.1 Thermogravimetric analysis (TGA)	38	70
2.2 Storage stability	40	70

2.3 UV/Vis spectroscopy	45	71
3. Monofunctional system	48	72
3.1 Preliminary studies	49	72
3.2 Optimization	51	73
3.2.1 Temperature screening	51	73
3.2.2 Irradiation intensity screening	53	73
3.2.3 PBG concentration screening	54	74
3.3 Formulation storage stability	55	74
4. Difunctional system	57	75
4.1 Towards oxa-Michael addition polymerization	57	75
<b>Conclusions</b>		<b>78</b>
<b>Materials and methods</b>		<b>81</b>
<b>Bibliography</b>		<b>83</b>
<b>Appendix</b>		<b>S1</b>

# Introduction

## Coatings

Far before the beginning of the Industrial Age, humankind deemed the protection of their belongings through coating important. First, they shielded their roofs by combining beeswax and clay for waterproofing and extending longevity,<sup>1</sup> then they added color to their homes through lacquers and varnishes for aesthetic appeal.<sup>2</sup> For hundreds of years that followed, ancient coating materials underwent development, improvement, and extension, shaping the advanced protective and decorative coatings industry as we know it. To date, their broad application field ranges from polymer coatings for infrastructure, automobiles, electronics, biomedicine, extending to even keratin coating treatments of human hair.<sup>3</sup>

Common manufacturing routes for polymer coatings have been traditionally limited to the use of organic solvents as a dispersion medium, which are associated with major drawbacks. Upon drying, volatile organic compounds (VOCs) are emitted from the organic solvents, causing adverse health and environmental issues. Reflecting the urgency of regulations for the worldwide minimization of VOCs, the coatings industry has nowadays shifted its attention towards the development of environmentally friendlier alternatives to organic solvents such as high solid, water-based or solventless coatings (e.g. powder, radiation curable etc.).<sup>4</sup> Their advantages and drawbacks are briefly outlined in Figure 1 and discussed below.

High solid coatings have found broad application in especially automotive, aerospace, and marine industries.<sup>5</sup> They resemble the conventional solvent-based coatings but contain up to 80 % solids. As a result thereof, a higher viscosity is expected, rendering the application of the coating rather difficult. To overcome this issue, high solid coatings utilize low molecular weight oligomers,<sup>6</sup> which require high functionalization for molecular weight increase and crosslinking during the curing process. With a higher functional group content, however, a decreased stability and consequently a relatively short pot life is expected.<sup>5</sup>

Another viable strategy towards VOC emission reduction are water-based coatings. Their advantage lies in the use of water as a solvent to disperse resins, e.g. water-reducible polyacrylates

or polyesters,<sup>7</sup> therefore offering an environmentally safer option for reduction of toxic waste disposal. Despite providing a very good surface finish and protection, they still suffer from high costs, prolonged drying times, and susceptibility to foaming when surfactants for improved wetting are added.<sup>7, 8</sup>

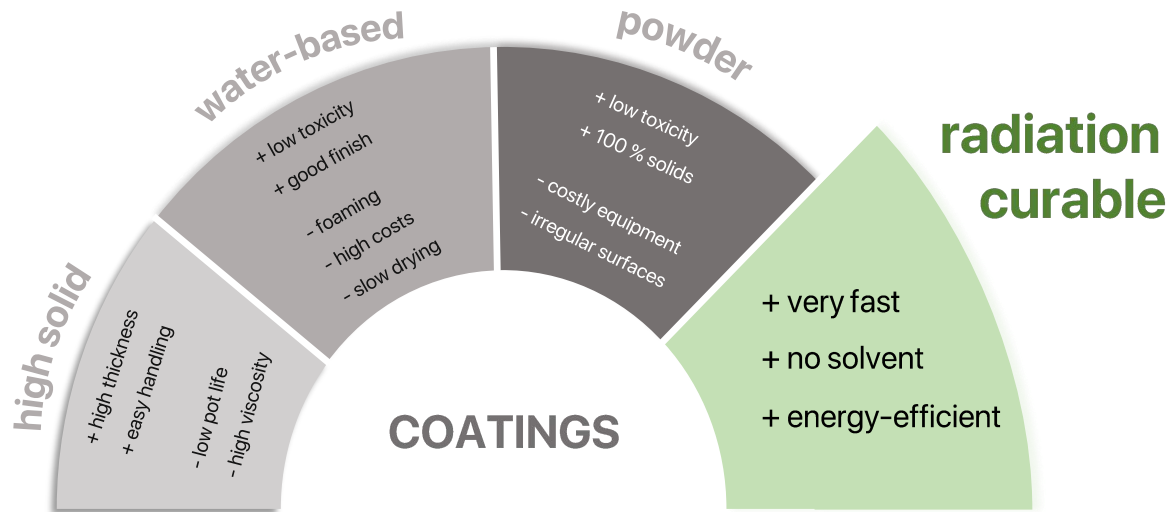


Figure 1: Comparison of modern polymer coating systems

Powder coatings represent a further alternative to conventional solvent coatings, since all their constituents are assembled in a dry, completely solventless form before being subjected to heat for thermal curing. However, their use is limited by the formation of irregular surface structures, e.g. pinholes or “orange-peel” textures.<sup>4, 5</sup>

Instead, radiation curable coatings outperform all the other coating techniques. They undergo an alternative mechanism to conventional thermal curing, which uses the energy of photons (photocuring) or electrons (electron beam curing) to convert a reactive liquid system to a solid crosslinked network.<sup>4</sup> Remarkable features of these solventless systems are their high curing rate, low energy and material consumption, and their virtually zero emission of VOCs.<sup>4, 9</sup>

Due to their higher relevance in industrial applications, photocuring methods based on hardening via UV, visible or even IR light,<sup>10</sup> have been at the forefront of new coating technologies. Owing to its energy-efficiency, a more controlled initiation, waste reduction, and excellent mechanical



properties achieved, radiation-based curing has gained ever-growing importance in numerous industrial applications,<sup>11, 12</sup> including temperature sensitive substrates (e.g. wood, paper), clear coats (e.g. furniture, flooring), automotive coatings, as well as protective coatings on glass fiber wires and electronic parts.<sup>4</sup>

## Photopolymerization

The use of light as a trigger to set a chemical reaction in motion has emerged as a versatile tool in modern chemistry. Indeed, over the past few decades, incorporation of photochemistry into the realm of polymer and material science has been a topic of great interest, giving rise to the well-known photopolymerization technologies.<sup>13</sup>

Compared to traditional thermal polymerization, which demands elevated temperatures to form the initiating species, photopolymerization reactions are unique insofar as they rely solely on light as a mild trigger.<sup>13, 14</sup> The advantages that they offer are threefold: firstly, photopolymerizations are generally carried out in solvent-free conditions, thereby avoiding volatilization. Secondly, light initiation enables spatial and temporal control, suggesting the user can precisely control when and where polymerization will occur.<sup>13, 15</sup> Thirdly, a remarkably high polymerization speed can be achieved, making this a feature of notable interest for various industrial applications including coatings, tissue engineering, photolithography, 3D printing, etc.<sup>15</sup>

A photopolymerization reaction involves a photoinitiator (PI), a photosensitive formulation and a suitable light source (Figure 2) and a strong interplay should exist between them.

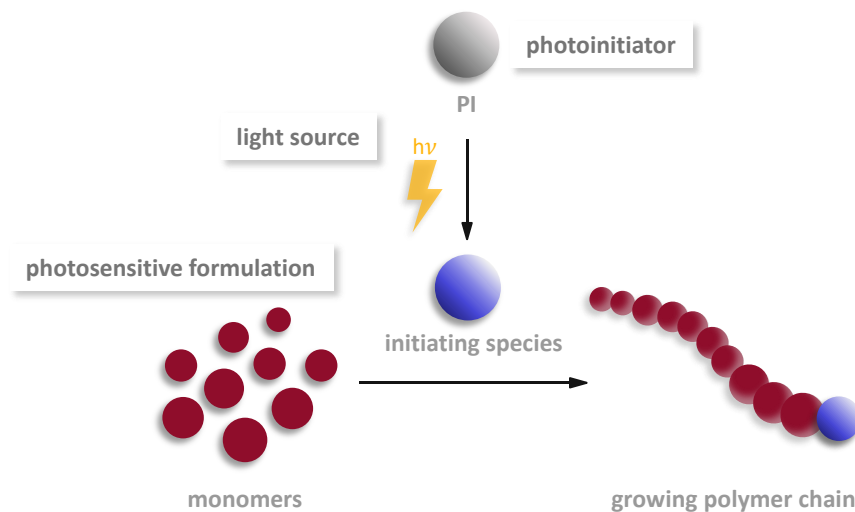


Figure 2: Simplified representation of a photopolymerization reaction

## Photoinitiator (PI)

Photoinitiators are radiation sensitive molecules that have the ability to absorb energy from the incident light and convert it into electronic excitation energy within the PI molecule. The light absorption itself is attributed to the presence of certain structural motives in the PI structure that dictate wavelength absorption, the so-known chromophores.<sup>16</sup>

Upon absorption of a photon, the chromophoric groups are responsible for the transition between a ground state (singlet state  $S_0$ ) and an excited state (singlet state  $S_1$ ) in the PI molecule.<sup>17</sup> From its excited singlet state  $S_1$ , the PI can undergo different energy dissipation pathways, which are depicted in the Jablonski diagram (Figure 3).

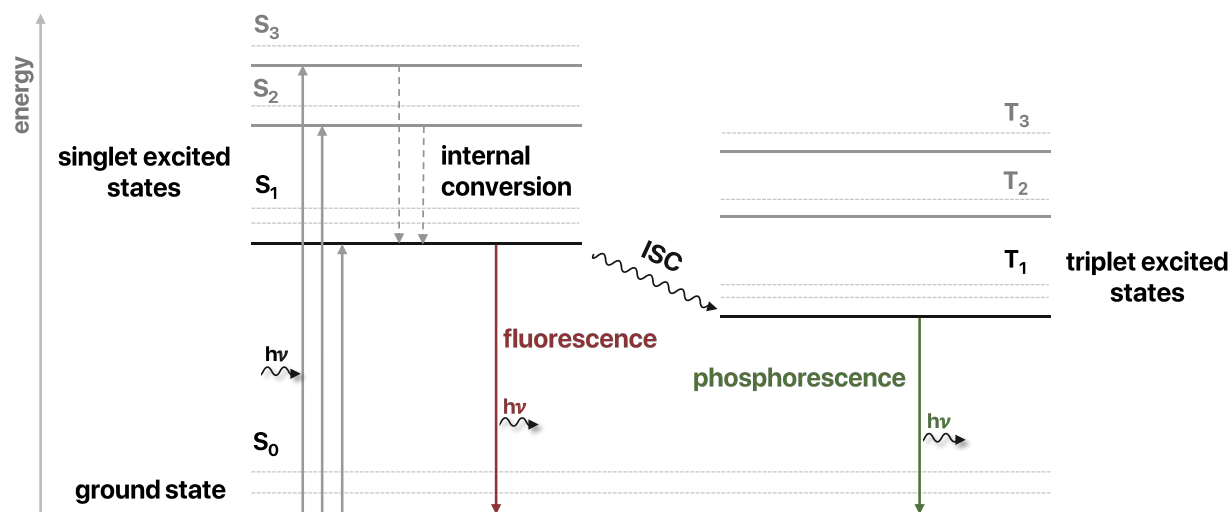


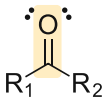
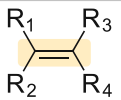
Figure 3: Jablonski diagram, adapted from <sup>17</sup>

Through an intersystem crossing (ISC) process, the energy is transferred to an excited triplet state  $T_1$ . Another possible event which competes with this transition is fluorescence, which is a radiative emission from  $S_1$  back to the ground state  $S_0$ .<sup>17</sup> In  $T_1$ , there are also several photophysical processes that can occur, i.e., phosphorescence, triplet-triplet annihilation ( $T_1 + T_1$  reaction) or quenching ( $T_1 + S_0$  reaction).<sup>17</sup>

Generation of the initiating species, however, proceeds through a photochemical process from a  $S_1$  or  $T_1$  state and is defined as such because the initial PI molecule undergoes a chemical change, leading to the formation of the intermediate initiating species for a photopolymerization reaction.

Population of  $S_1$  or  $T_1$  can happen directly via PI absorption or be facilitated indirectly via a so-called photosensitizer which transfers energy to the PI via a triplet-triplet transfer.<sup>17</sup> From a molecular orbital viewpoint, the excitation process induced by a photon absorption corresponds to the jump of an electron from an occupied MO to an empty MO in the PI molecule. The commonly used organic PIs possess nonbonding (n),  $\pi$  or  $\sigma$  (bonding) and their counterparts  $\pi^*$  or  $\sigma^*$  (antibonding) MOs.<sup>17</sup> The transition types encountered between these MOs can be classified into three categories, which are shortly introduced in Table 1.

Table 1: MO transition types in PI molecules in their usual UV/Vis wavelength range and their features, assembled from Fouassier<sup>17</sup>

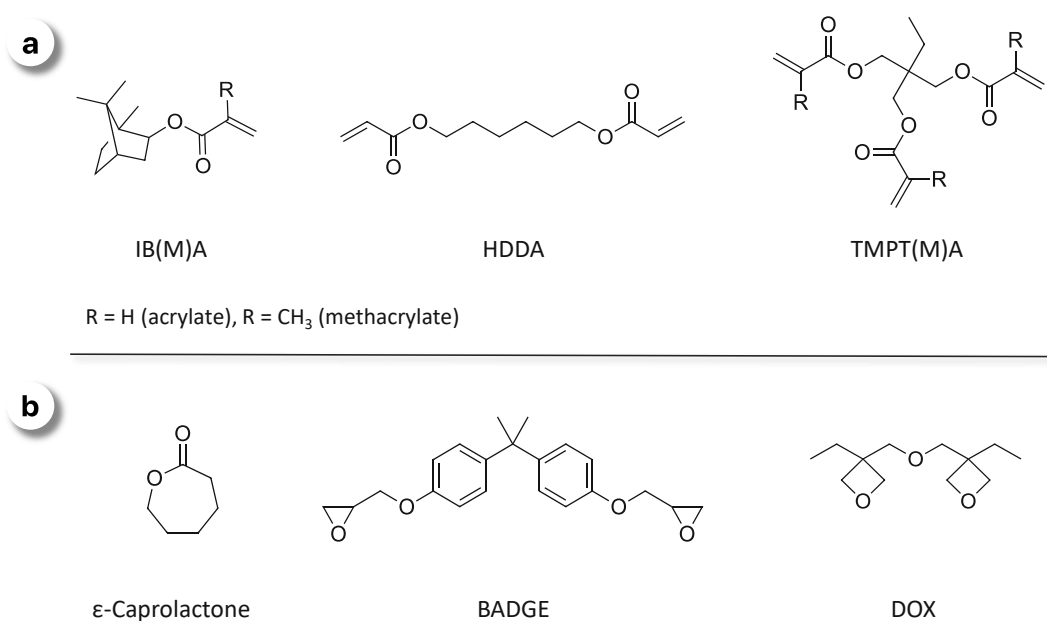
transition	example	type	absorption coefficient	absorption wavelength	excitation energy
$n\pi^*$		symmetry forbidden	low	long	localized
$\pi\pi^*$		symmetry allowed	high	often short	delocalized (e.g. $\pi$ conjugated)
charge transfer (CT)	polarized substituted molecules, etc.		high	redshifted	strongly delocalized

Depending on the PI structure, the formed species may be a radical, an ion (cation, anion), an acid, or a base, which can then respectively initiate free radical, cationic, and anionic photopolymerization or participate in an acid- or base-mediated photocrosslinking reactions.<sup>14, 17</sup>

## Photosensitive formulation

Although PIs have earned well-deserved attention in the field of photopolymerization, it is also important to acknowledge the role of the photosensitive formulation, i.e. monomers. As monomers dictate the chemical and (thermo)mechanical properties of the final material, a set of criteria has to be considered while selecting them, including their reactivity rate, storage stability, curing efficiency, toxicity level, odor, etc.<sup>17</sup>

The frontrunners in radical photopolymerization reactions, for example, are the versatile mono- or multifunctional (meth)acrylates, some of which are depicted in Scheme 1. For cationic photopolymerizations, an additional wide range of monomers is made available due to their susceptibility to be attacked by a cation as an initiating source. They include lactones, epoxides, or cyclic ethers such as oxetanes. From another point of view, epoxides also allow an anionic ring opening via an anion as the initiating species. However, the use of anionic photopolymerization in industry is limited and therefore a lot of monomers still remain inaccessible.<sup>17, 18</sup>



Scheme 1: Selection of common monomers suitable for **a) radical**, e.g. isobutyl(meth)acrylate (iB(M)A), 1,6-hexanediol diacrylate (HDDA), trimethylolpropane tri(meth)acrylate (TMPT(M)A) and **b) cationic photopolymerization**, e.g. ε-caprolactone, bisphenol-A-diglycidylether (BADGE), 3,3'-(oxybis(methylene))bis[(3-ethyl)oxetane] (DOX)

## Light source

The electromagnetic spectrum of light spans a wide frequency and wavelength range between gamma rays to radiofrequency rays (Figure 4). Because of the absorption patterns that most organic PIs employed in photopolymerizations demonstrate, the research interest lies in the UV and visible light regions of the spectrum. UV light ranges between 200-400 nm, with three distinguished groups, namely UV-A (320-400 nm), UV-B (290-320 nm), and UV-C (190-290 nm), whereas visible light covers wavelengths between 400 (violet light) and 700 nm (red light).<sup>17</sup>

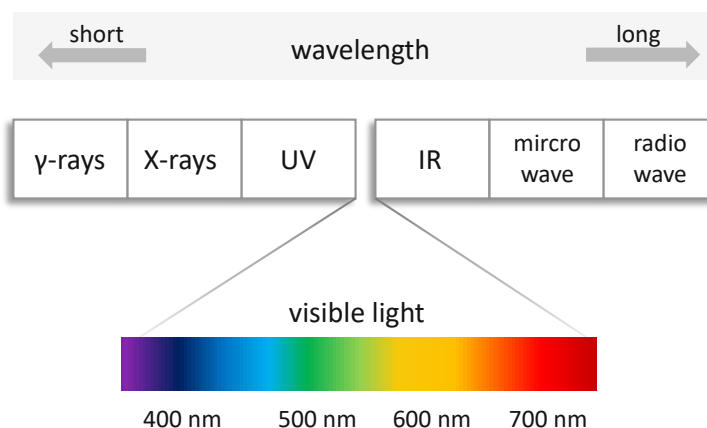


Figure 4: Electromagnetic spectrum of light

The absorbance of most PIs is confined within the UV region, which corresponds to lower wavelengths and high energy photon emissions. Despite its efficiency, high-energy UV light is responsible for a set of shortcomings, such as low penetration depth of light into the material and consequently low curing depths, ozone generation, as well as compromised radiation safety.<sup>13, 18</sup>

To mitigate the challenges UV radiation poses, a lot of scientific effort in the past few years has been gravitating towards longer wavelength absorbing PIs. A red-shifting of the absorption patterns – extending even to the visible light region – translates into higher curing depths. For this, new and existing PIs are developed and modified to finely tune their absorbance upon exposure to mild-energy visible light. Among useful strategies, electron donating substituents and halogens, or extended  $\pi$ -conjugation are introduced.<sup>19</sup>

## Photo base generators (PBG)

Photosensitive molecules with the ability to generate a base when irradiated are known as photo base generators (PBG) (Figure 5). The released base from a PBG can be utilized as an initiating species for anionic photopolymerizations, as a catalyst for imidization reactions,<sup>20</sup> sol-gel hydrolysis-condensation processes,<sup>21</sup> or as of more recently, in base-catalyzed thiol-epoxy, thiol-isocyanate and Michael additions.<sup>22, 23</sup>

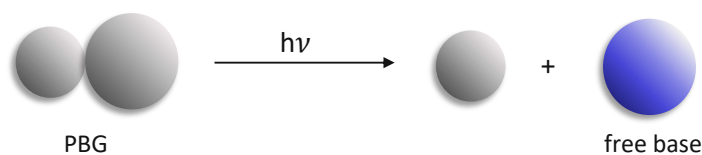
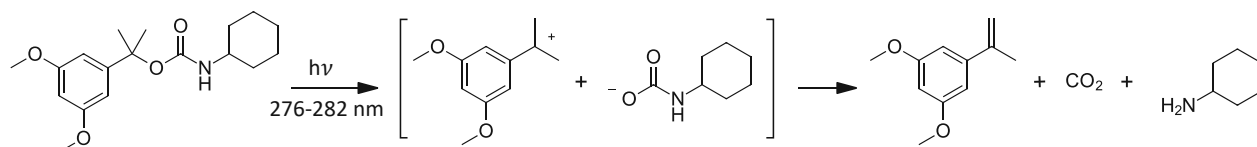


Figure 5: Photoinduced generation of a free base from a PBG

The concept of a PBG was formerly introduced in 1987, demonstrating the light induced release of a Lewis base from a cobalt(III) complex.<sup>24</sup> Shortly after, Cameron and Fréchet developed the first organic PBG generating a cyclohexylamine from a photoactive carbamate group via UV irradiation, thus setting an important example in this newly found field of PIs (Scheme 2).<sup>25</sup>



Scheme 2: Phototriggered liberation of a primary amine from a carbamate via UV light, reported by Cameron and Fréchet<sup>25</sup>

This successful example of photolabile carbamates serving as protecting groups for free amines, served as a starting point for the development of new related structures many decades ago.<sup>18</sup> The generated amines from such PBG systems originally found use in photoinduced curing of epoxy resins<sup>26</sup> and polyurethane isomers via terminal isocyanate groups for coating and photolithography applications.<sup>27</sup>

When compared to the widely used photo radical generators (PRG) for free radical polymerizations or to photo acid generators (PAG), which induce cationic polymerizations upon acid release, PBGs still remain a relatively uncharted field.<sup>18</sup>

They are, however, superior to their radical generating counterparts, as they mitigate oxygen inhibition, are linked to a significantly lower polymerization-induced volume shrinkage of the final material, and could be applied to a broader scope of monomers.<sup>18, 23</sup> Moreover, unlike PAGs, PBGs do not engage in corrosive reactions with metallic substrates and are therefore more suitable for applications in automotive and electronic industries.<sup>22</sup>

Given the low efficiency of primary and secondary amines that most reported PBGs liberate, however, their overall applicability in polymerization techniques necessitating stronger bases remained rather scarce for a long time. In most cases, post-exposure thermal treatment is additionally required for better conversion and complete polymerization.<sup>27, 28</sup> Apart from the insufficient basicity the released primary or secondary amines, PBGs tend to suffer from low thermal stability<sup>28</sup> and low quantum yields.<sup>29</sup> Moreover, base liberation is generally triggered by rather low wavelengths confined in the UV-C and UV-B region with short and harmful light below 320 nm.<sup>18, 23, 30</sup>

Considering their challenges as well as promising features, development of new PBGs so that they are able to absorb longer wavelength UV-A and visible light by generating stronger bases with high efficiencies has become a topic of great interest.<sup>22</sup> Indeed, several other PBG classes that incorporate stronger bases have emerged in the last few years, based on e.g. *O*-acyloximes, *O*-carbamoyloximes,  $\alpha$ -aminoketones and salts.<sup>22, 31</sup>



## Phosphazene superbases

Due to their remarkable utility as catalysts or auxiliary reagents in organic synthesis encompassing deprotonation processes, non-ionic organic superbases have gained widespread interest during the last decades.<sup>32, 33</sup> Examples of well-established organic bases with superbasicity potential and outstanding properties include phosphazenes,<sup>34</sup> phosphatranes,<sup>35</sup> guanidino-phosphazenes,<sup>36</sup> (bi)guanidines,<sup>37</sup> etc. Some representative structures of each family are depicted in Figure 6.

Interestingly, the basicity center of phosphatranes is located on the phosphorous atom (Figure 6, B), unlike the three other representatives which comprise a nitrogen basicity center instead.<sup>38</sup>

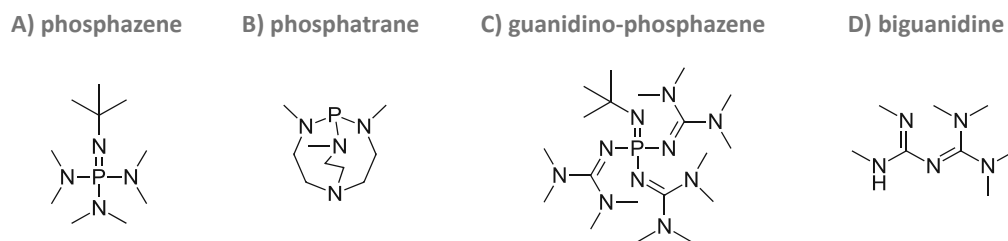
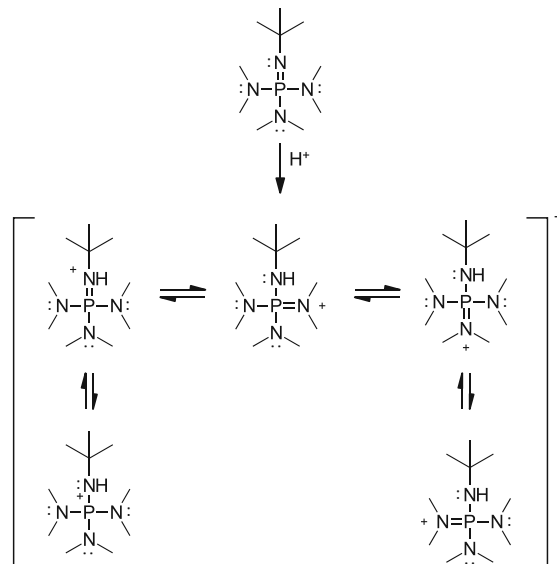


Figure 6: Examples of organic superbases: A) phosphazene, B) phosphatranes, C) guanidino-phosphazene, D) biguanidine

Among nitrogen-centered superbases, the so-known Schwesinger's phosphazenes (Figure 6, A) play an indispensable role, which is also reflected in their broad commercial availability.<sup>32, 33, 38</sup> Along with their outstanding stability towards oxygen and hydrolysis combined with thermal and chemical stability they are distinguished by extremely high  $^{\text{MeCN}}\text{p}K_{\text{BH}^+}$  values in solution ranging from 26.9 to 42.7.<sup>33, 34</sup>

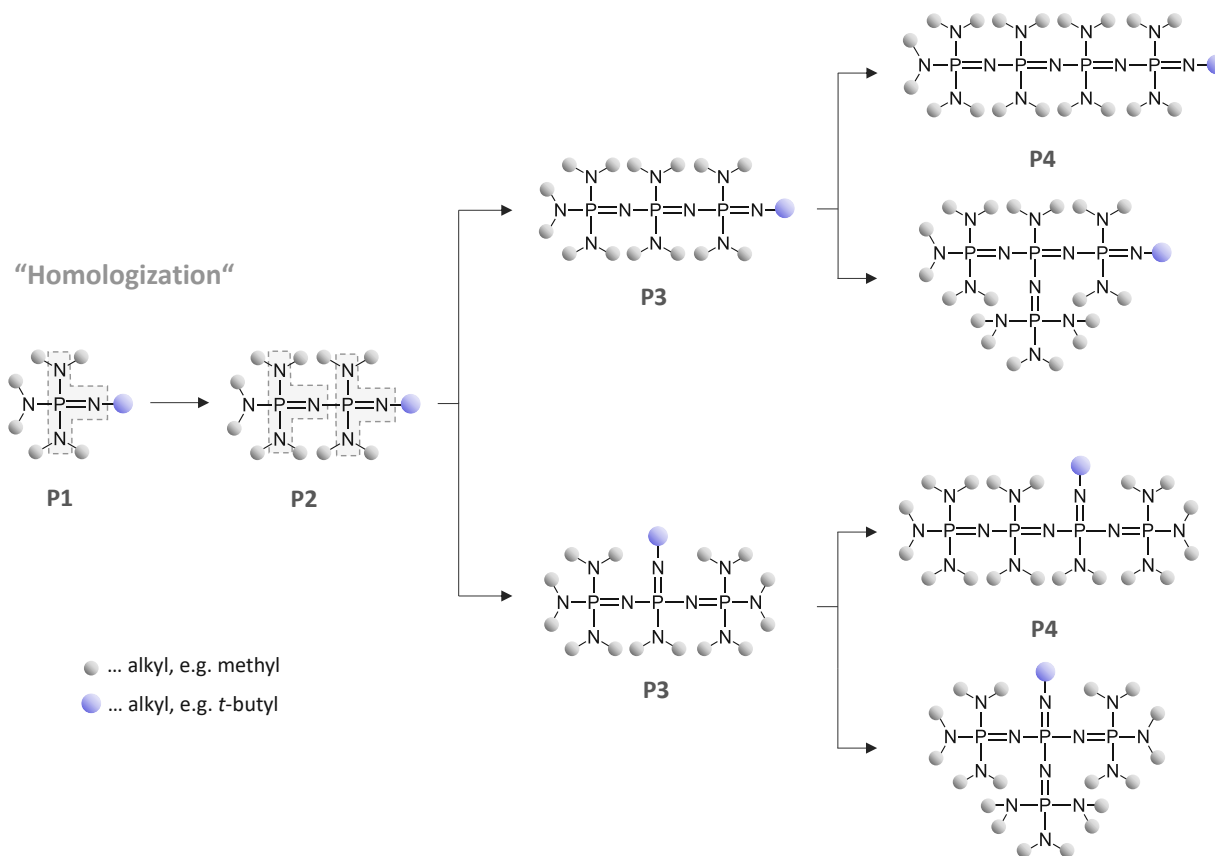
Their exceptionally high Brønsted basicity can be rationalized with simple considerations concerning their structural elements. As protonation takes place at the nitrogen center of the imino group ( $t\text{Bu-N=P}$ ),  $\pi$ -donating dimethylamino substituents bound to the phosphorous atom have the ability to enhance the donor capacity of the nitrogen lone pair, while also enabling a delocalization of the positive charge.<sup>33, 38</sup> The delocalized positive charge in form of resonance structures is exemplified below with a monophosphazene base (Scheme 3).



Scheme 3: Resonance structures of a protonated monophosphazene, based on literature <sup>33</sup>

Replacing these dialkylamino fragments with phosphazeryl groups comprising a  $-N=P(NR_2)_3$  unit increases the  $\pi$ -donating strength of the substituents and consequently the basicity of the phosphazene, as a more enhanced electron density resides at the basicity center.<sup>38</sup>

This illustrates a key principle described by Schwesinger for basicity enhancement of phosphazenes, which is referred to as the homologation strategy.<sup>34</sup> The approach can be simplified by considering a  $PN_3$  structural element as a “basicity battery cell”. Through successive expansion of a monophosphazene superbases via stepwise addition of these increments, e.g. in form of phosphazeryl substituents, an extraordinary increase of up to several orders of magnitudes in basicity of the resulting di-, tri-, tetraphosphazenes etc., can be achieved.<sup>34</sup> A simplified representation thereof is given in Scheme 4. Accordingly, the used nomenclature reflects the number of basicity battery cells, leading to  $P_1$ ,  $P_2$ ,  $P_3$ , etc. phosphazene superbases. Systems comprising more than two phosphorous units are characterized by the presence of isomeric structures.<sup>34</sup>



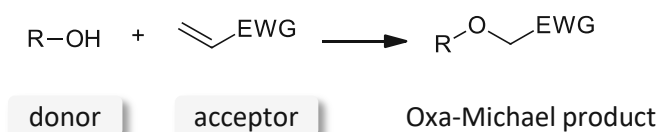
Scheme 4: Homologization principle for basicity enhancement of phosphazenes, assembled from Schwesinger et al.<sup>34</sup>

There is indeed a correlation between basicity and the number of basicity battery cells present. For a P1 superbases with dimethylated amine substituents and a *t*-butyl residue on the basicity center, a  $^{\text{MeCN}}\text{pK}_{\text{BH}^+}$  of 26.88 is observed. Further homologization to an analogous P2, P3, and P4 system profit by an increase by respectively 6, 12, and 16 orders of magnitude in basicity. This remarkable effect, however, becomes less prevalent in larger phosphazenes as P6 or P7, where only marginal changes in pK values are reported.<sup>34</sup>

## The oxa-Michael addition reaction

The reaction between an oxygen-containing nucleophile donor (e.g. an alcohol) with an electron deficient  $\alpha,\beta$ -unsaturated acceptor leading to the formation of an ether bond is known as the oxa-Michael addition (Scheme 5). The oxa-Michael reaction is considered as a hetero-type of the Michael addition, which is regarded as a pivotal C-C bond formation strategy in organic chemistry.<sup>39</sup>

As early as 1878, Loydl reported the synthesis of malic acid from fumaric acid by addition of an alkoxide to an  $\alpha,\beta$ -unsaturated carbonyl, thus setting the first example of an oxa-Michael reaction, even preceding the popular Michael reaction.<sup>40</sup>



Scheme 5: Generalized oxa-Michael addition reaction

Due to its remarkable versatility and functional group tolerance paired with high efficiency under mild operating conditions, the oxa-Michael reaction is a widely employed synthetic tool in organic chemistry.<sup>41</sup> However, although popular in small molecule, and natural product synthesis,<sup>42</sup> its potential still remains relatively unrecognized in polymer chemistry.<sup>41</sup>

Other subclasses of Michael reactions, e.g. aza-Michael using amines, thia-Michael using thiols, or carba-Michael employing C-H acidic compounds (e.g. malonates) as donors, have received a lot more attention in polymerization reaction strategies and are more frequently described in literature.<sup>41, 43-45</sup> This stems from their inherently higher nucleophilicity and consequently higher reactivity compared to alcohols as Michael donors.

Nevertheless, alcohols benefit from a set of advantages over amine- or thiol-based reagents. They exhibit significantly reduced health risks due to their lower toxicity and odor, rendering their application very attractive.<sup>41</sup> This is particularly relevant in polymer chemistry, as the utilization of multifunctional alcohol donors and acceptors gives access to a broad palette of oxa-Michael

polymers containing stable ether-bonds, e.g. poly(ether)s,<sup>46</sup> poly(ether-sulfone)s,<sup>47</sup> poly(ether-ester)s,<sup>48</sup> etc.

As mentioned, in order to generate a more nucleophilic and reactive alkoxide, alcohols necessitate a deprotonating base catalyst, which can in turn initiate the addition reaction.<sup>49</sup> For this, both Brønsted or Lewis bases can be used and their proposed initiation mechanisms. They differ in several aspects as outlined below (Figure 7).

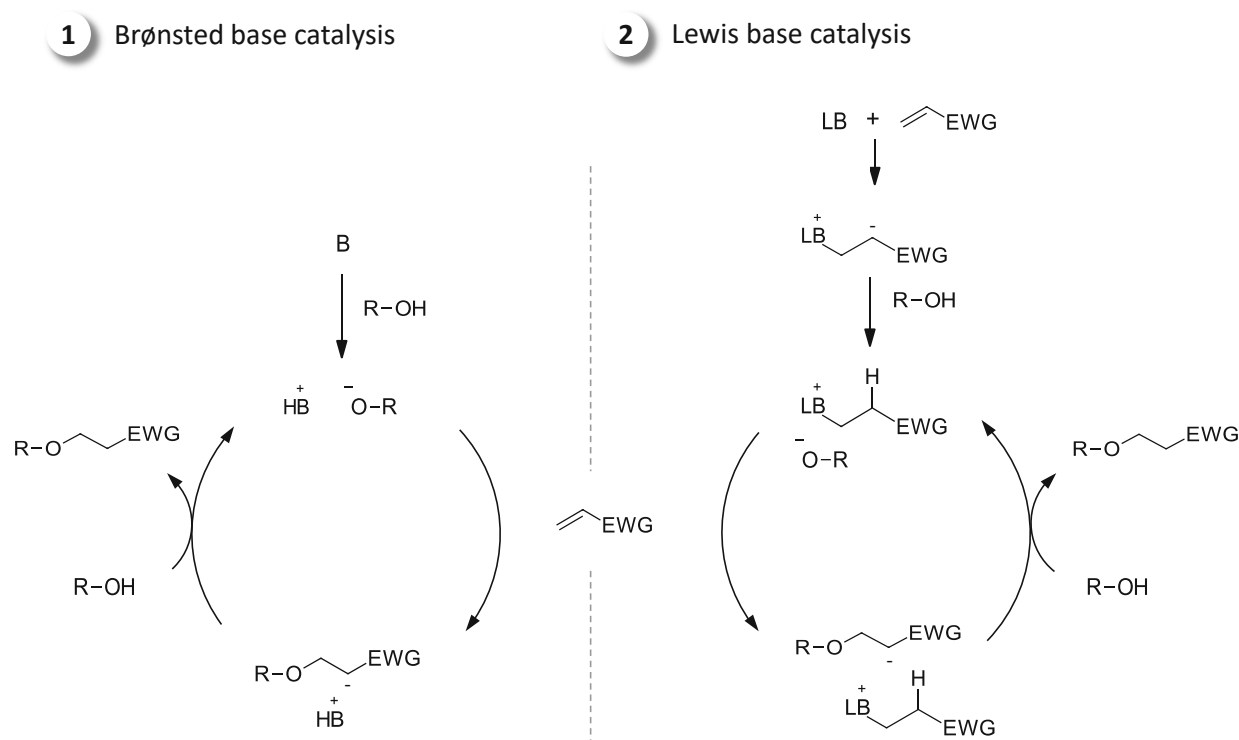


Figure 7: Literature proposed mechanistic pathways of an oxa-Michael addition reaction initiated with (1) Brønsted base and (2) Lewis base<sup>41</sup>

The Brønsted base catalyzed reaction pathway is driven by a direct deprotonation of the alcohol donor. The newly formed alkoxide nucleophile can then react with the electron-deficient Michael acceptor via conjugate addition to form a carbanion intermediate.<sup>41</sup> Subsequently, hydrogen abstraction from a further alcohol finally yields the oxa-Michael product.

In contrast, a Lewis base catalysis does not initiate by deprotonating the alcohol, as it relies on the addition of the electron rich neutral base to the Michael acceptor double bond, generating an energetically disfavored basic zwitterion.<sup>50</sup> In the next step, proton transfer from the alcohol to

the zwitterionic species occurs. The formed alkoxide in the ion pair can then undergo conjugate addition to a further Michael acceptor, which in turn generates a carbanion. Similarly to the Brønsted mediated pathway, the catalytic cycle is completed with the protonation by another alcohol, thus enabling the formation of an oxa-Michael ether.<sup>41, 51</sup>

Commonly used Brønsted and Lewis bases for oxa-Michael addition polymerization range from phosphines or inorganic bases to more recently utilized organocatalysts (e.g. *N*-heterocyclic carbenes, phosphazenes, amidines, etc.).<sup>41, 46, 48</sup> Relevant examples thereof are depicted in Figure 8.

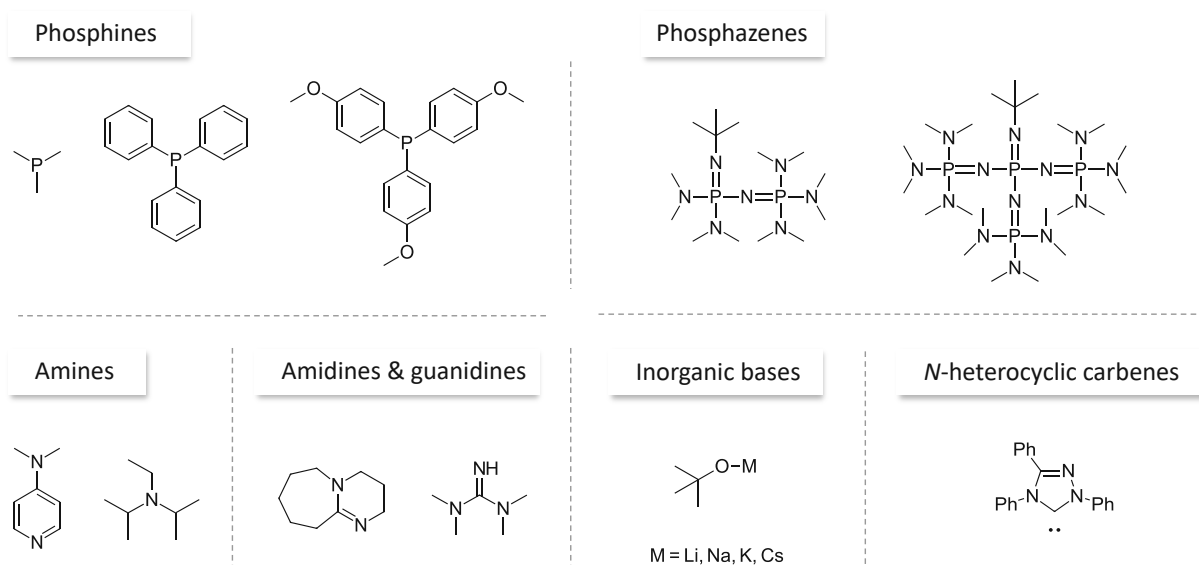


Figure 8: A selection of different bases utilized as catalysts for oxa-Michael additions, as reported in literature<sup>41</sup>

Among commonly used catalysts that qualify as Lewis bases, triarylphosphines (e.g. PPh<sub>3</sub>) and *N*-heterocyclic carbenes display a high nucleophilicity and reactivity. They are, however, associated with high moisture and air sensitivity and demand treatment under exclusion of oxygen.<sup>41, 52</sup> In contrast, many phosphazene superbases, such as P2-*t*-Bu, are free of stability issues, as they can be used under ambient atmosphere conditions while still allowing an exceptionally strong Brønsted basicity. Regardless of their elevated prices and sometimes hygroscopic nature (e.g. P4-*t*-Bu), phosphazenes stand out as highly efficient base catalysts for oxa-Michael polymerizations.<sup>41, 48</sup>

## Objective

The aim of this thesis is to expand the promising, yet challenging and relatively uncharted field of photo base generators (PBGs). Considering that they are mostly limited to the generation of active species with low basicities, their application spectrum remains quite narrow. Following recent developments that report the utilization of stronger bases, such as guanidines or amidines, this work should utilize the phosphazene superbases P2-*t*-Bu because of its notably higher basicity.

Therefore, the first goal of this work is the design of a new synthetic strategy towards a structurally modified P2-*t*-Bu superbases, which is otherwise only commercially accessible. Further, synthesis of new PBGs in form of stable salts combining the P2-*t*-Bu superbases together with a carboxylate functionalized chromophore should be performed. With the purpose of meeting the demand for higher wavelength absorbing moieties which can liberate the base with high efficiency, synthetic effort will be focused on the preparation of a thioxanthone acetic acid in a highly selective manner. A further commercially available structural analog chromophore will be additionally employed. In the next step, the two synthesized PBGs should be characterized regarding their thermal behavior via thermogravimetric analysis, light absorption properties via UV/Vis spectroscopy and stability upon long term storage.

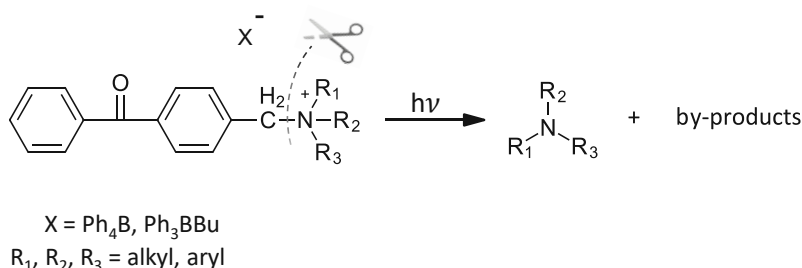
To demonstrate the applicability of the prepared PBGs a monofunctional model system based on an oxa-Michael addition reaction will be designed. On this basis, optimization of reaction conditions including temperature, light intensity, and PBG concentration will be carried out via photo-DSC studies and NMR spectroscopy. Along with the herein synthesized PBGs, a similar reference compound will be included for a better system comparability.

Finally, this protocol will be extended to a difunctional oxa-Michael system with the purpose of exploring possibilities for the preparation of linear poly(ether-amide)s via a PBG-mediated photopolymerization.

## State of the Art

Considerable progress in broadening the domain of photo base generators (PBGs) was seen in the early 2000s when quaternary ammonium salts were utilized for the generation of tertiary amines as free bases upon C-N bond cleavage.<sup>53-55</sup> In these systems, as exemplified in Scheme 6, the tertiary amine is attached via a methylene spacer to a photosensitive electron acceptor complexed as a quaternary ammonium salt with an electron donor anion, i.e. tetraorganylborate.

Despite their positive features, the efficiency of such PBGs is rather low, since the involved photoinduced electron transfer reaction is usually hindered by back electron transfer.<sup>53</sup> They are additionally constrained by poor solubility in organic solvents and oftentimes low thermal stability.<sup>18</sup> Moreover, variation of substituents on nitrogen is rather restricted, as photocleavage efficiency is also highly dependent on the exerted steric demand.<sup>18, 54</sup>

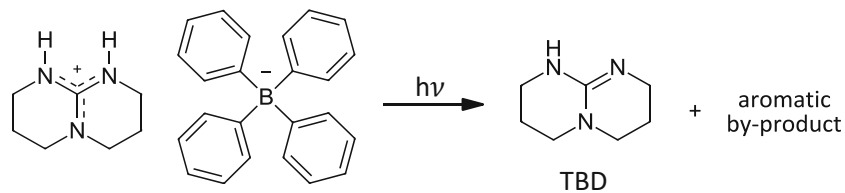


Scheme 6: Generation of a tertiary amine upon C-N bond scission from a quaternary ammonium salt PBG, based on Sarker et al.<sup>54</sup>

A significantly improved approach was proposed by Sun and co-workers,<sup>56</sup> where the strong guanidine base TBD was photocaged within a borate salt (TBD · HPh<sub>4</sub>) in its protonated form (Scheme 7). The “cage” implies that the base remains inactive insofar as there is no exposure to irradiation. In this example, photogeneration of the free base proceeded via a base deprotonation step triggered by 254 nm UV light.

This pioneering work enabled the first light-triggered ring opening polymerization of  $\epsilon$ -caprolactam and showed compatibility with a variety of bases, e.g. carbenes, tertiary amines or even phosphazenes.<sup>56</sup>

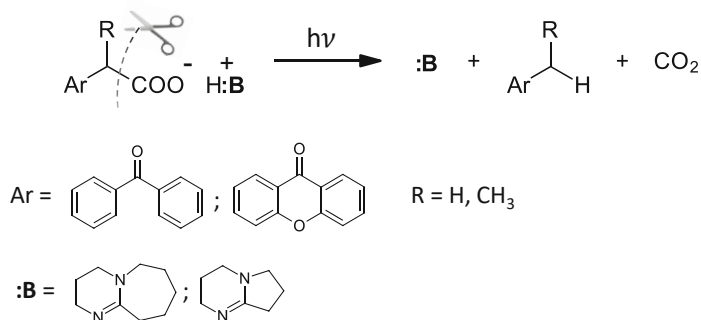




Scheme 7: Photoactivation of a tetraphenylborate based PBG by Sun et al. via deprotonation <sup>56</sup>

Still, the inherently low quantum yield ( $\phi_{254\text{ nm}} = 0.18$ ) and short wavelength absorption of the chromophore limit the use of these borate-based PBG salts.<sup>29</sup>

This issue was addressed later on by Arimitsu et al.<sup>29</sup> who paired the previously introduced concept of a photocaged protonated base with a carboxylate functionalized chromophore. They designed PBG salts consisting of ketoprofen or xanthone acetic acid as relatively high quantum yield chromophores in combination with strong bases, e.g. DBU, DBN, TBD, etc. which were applied for thiol-epoxy crosslinking under UV light (Scheme 8).<sup>29</sup>



Scheme 8: Photoinduced decarboxylation and base liberation of PBG salts based on chromophores functionalized with a carboxylic acid <sup>29</sup>

In this case, light absorption sets an irreversible photodecarboxylation reaction in motion. This enables the release of the caged base at a high efficiency, as the issue of back electron transfer is circumvented by the dissociative nature of the reaction. Additionally,  $\text{CO}_2$  is formed as a by-product.<sup>22</sup>

This concept has inspired research on numerous PBGs following a photodecarboxylation mechanism with many successful applications in various photopolymerization and base-mediated cross-linking reactions, e.g. thiol-yne-epoxy,<sup>57</sup> thiol-thiol coupling,<sup>58</sup> thiol-promoted epoxide

crosslinking,<sup>28</sup> or as of more recently even polyurethane photopolymerization from multifunctional alcohols and isocyanates.<sup>59</sup> Some of the PBGs utilized for these prominent examples reported in the past few years are summarized in Figure 9.

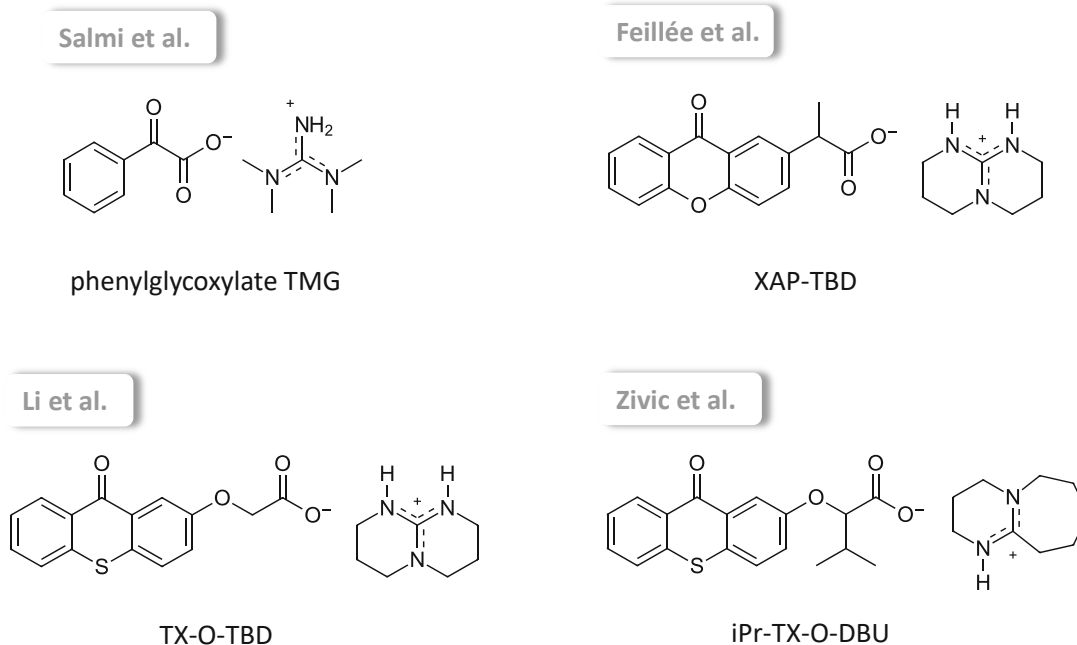


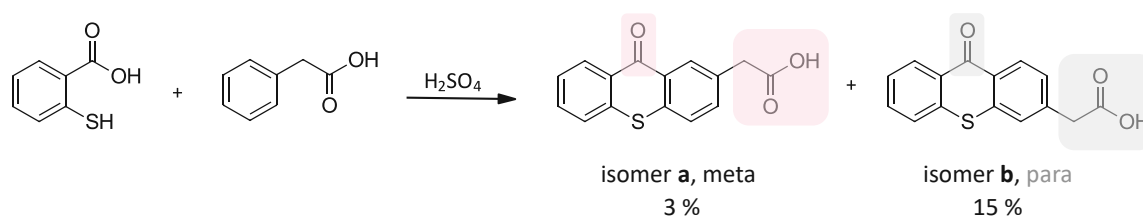
Figure 9: PBGs operating via photodecarboxylation; a) phenylglycolic acid salt of TMG,<sup>28</sup> b) xanthone propionic acid salt of TBD,<sup>58</sup> and thioxanthone derivatives with carboxylate functions with the ability to liberate c) TBD,<sup>57</sup> d) DBU<sup>59</sup>

PBGs containing thioxanthone-based acetic acid derivatives as chromophores withhold the potential of red-shifting the absorption patterns to the visible light portion of the spectrum.<sup>57</sup> Indeed, it has been argued that they enable a highly efficient photoinduced decarboxylation combined with high quantum yields.<sup>60</sup> The simplest structure among the many derivatives reported is an unmodified thioxanthone acetic acid.

To date, the synthesis of thioxanthone acetic acid is limited to only one procedure, which involves 2-phenylacetic acid and thiosalicylic acid whilst requiring strong acidic conditions, namely concentrated sulfuric acid.<sup>30, 60</sup> Generally, moderate to very good yields are reported, accompanied by the appearance of the product as a blue solid, which, within the context of its expected absorbance behavior, is rather atypical. Furthermore, the corresponding reaction mechanism is not yet fully elucidated.

Prior to this thesis, the same synthetic procedure had been performed in our laboratory,<sup>61</sup> leading to interesting findings, which are in disagreement with literature. The reaction led to the formation of two thioxanthone acetic acid isomers, namely a and b in a 1:5 ratio with a low yield of 18 % in total, obtained as a blue solid (Scheme 9).

On the one side, this result introduces an isomer separation problem. On the other side, the positioning of the acetic acid group relative to the chromophoric carbonyl has a notable effect on the photodecarboxylation process.<sup>62</sup> As described by Zimmerman through the so-called “meta effect”,<sup>62</sup> a much lower reactivity would be expected for the para-arrangement (isomer b). An alternative protocol is therefore needed to address this discrepancy.



Scheme 9: Revision of the literature-known procedure<sup>30</sup> for synthesis of thioxanthone acetic acid, performed in our laboratory<sup>61</sup>

# Results and discussion

## 1. Synthesis

### 1.1 Phosphazene superbases

The phosphazene base envisaged in this thesis should replace methyl residues of the commercially available Schwesinger homologue P2-*t*-Bu through a subtle structural modification by introducing ethyl groups, as shown in Figure 10. The slightly altered steric demand thereof could potentially imply changes in its synthesis and performance.

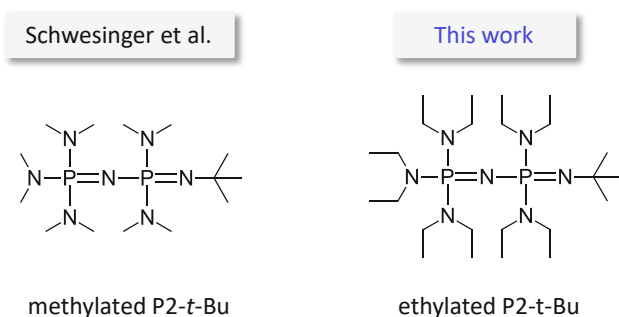


Figure 10: Structures of the literature known methylated P2-*t*-Bu and its ethylated homologue

This chapter describes the synthesis and isolation of the two required precursors, namely the phosphorimidic fragments **1** and **2** from  $\text{PCl}_5$ , as well as the coupling reaction thereof to form the desired ethylated P2-base **3** (Figure 11).

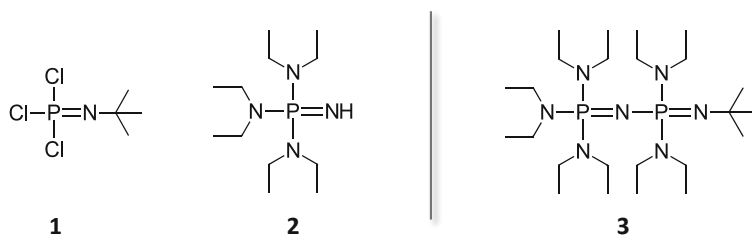
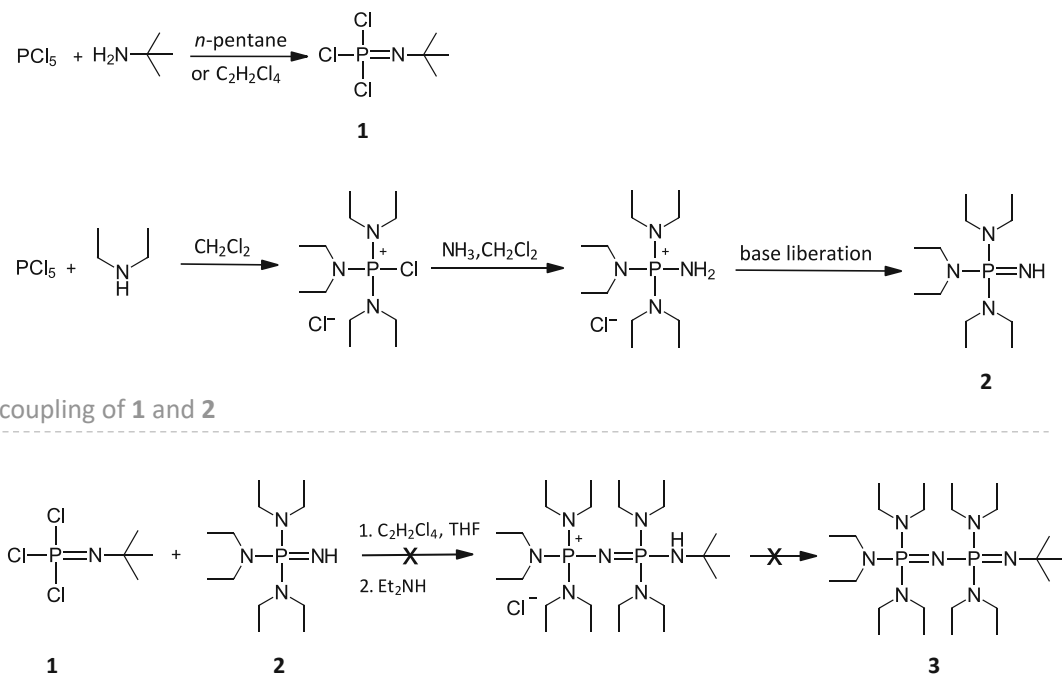


Figure 11: Structures of the targeted phosphorimidic compounds **1**, **2** and **3**

The summarized synthetic scheme is depicted in Scheme 10.



Scheme 10: General reaction scheme for the synthesis of the phosphazene superbase **3** from the building blocks **1** and **2**

### 1.1.1 First P-fragment

The first phosphorous fragment **1** (*N-tert*-butylphosphorimidic trichloride) depicted in Figure 12 is a precursor for the synthesis of the ethylated phosphazene P2-*t*-Bu base. For this, two literature known synthetic routes were exploited.<sup>63, 64</sup>

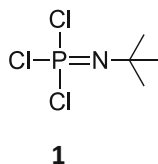
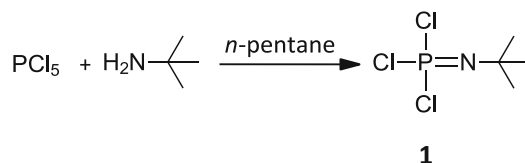


Figure 12: Structure of *N-tert*-butylphosphorimidic trichloride (**1**)

#### 1.1.1.1 The *n*-pentane route

The first route was based on a synthesis described by Weitkamp et al.<sup>63</sup> and is presented in Scheme 11.



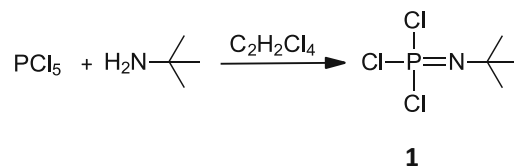
Scheme 11: Synthesis of the first P-fragment **1** via a *n*-pentane pathway<sup>63</sup>

Herein, the starting material phosphorous pentachloride was suspended in *n*-pentane before addition of a *t*-butylamine solution in the same solvent. The <sup>31</sup>P NMR spectrum of the filtered crude material was in compliance with the product peak reported in literature (-78.2 ppm). However, no product could be isolated via distillation, most probably due to the very air-sensitive nature of this reaction. As confirmed by further <sup>31</sup>P and <sup>1</sup>H NMR measurements, product was found in the liquid sump residue. Nonetheless, since the residue amount was minimal – with almost no quantitative significance – the synthesis was repeated aiming satisfactory exclusion of oxygen and moisture.

Performing the reaction for a total of three times achieved no better outcome. Sensitivity towards hydrolysis in conjunction with the considerably low boiling point of *n*-pentane (bp: 36 °C) seemed to be the limiting factors.

#### 1.1.1.2 The tetrachloroethane route

In the second pathway depicted in Scheme 12, two parameters were altered from the *n*-pentane route. Firstly, the higher-boiling solvent 1,1,2,2-tetrachloroethane was used in alignment with a similar literature procedure reported by Bell et al.<sup>64</sup>



Scheme 12: Synthesis of the first P-fragment **1** via a tetrachloroethane pathway<sup>64</sup>

Secondly, rather than adding the *t*-butylamine to the suspended phosphorous pentachloride, an inversed sequence was followed. Phosphorous pentachloride was added to a solution of *t*-butylamine in tetrachloroethane instead.

The overall handling and manipulation of the crude mixture was made easier most likely due to the low vapor pressure of the used solvent. Distillation afforded three fractions and in all three of them, the desired product **1** (bp: 161 °C) as well as the solvent (bp: 147 °C) were found. Further separation steps were not undertaken because of potential risk of product hydrolysis.

This obstacle notwithstanding, the tetrachloroethane route allowed product formation and an arguably easier purification procedure. Product isolation and yield estimation are nonetheless not possible, so that the product can only be manipulated in solution for the final synthesis step of the ethylated P2 base. The expected discrepancy in mole ratio should, however, not hinder P2 base formation.

### 1.1.2 Second P-fragment

The second targeted phosphorous building block was the ethylated P1 phosphazene base (*N,N,N',N',N'',N''*-hexaethylphosphorimidic triamide, **2**) shown in Figure 13.

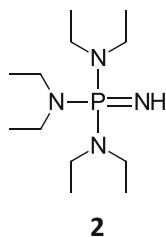


Figure 13: Structure of *N,N,N',N',N'',N''*-hexaethylphosphorimidic triamide (**2**)

The conventional synthetic route for its methylated counterpart, which has been extensively studied before by Schwesinger et al.,<sup>34</sup> demands the employment of highly volatile starting materials, namely dimethylamine and ammonia, which are gaseous at rt.

In our attempt to introduce somehow safer, easy-to-handle substances, the synthesis presented herein utilizes liquid diethylamine instead (Figure 14). This slightly altered course of alkylation could indicate changes in basicity.

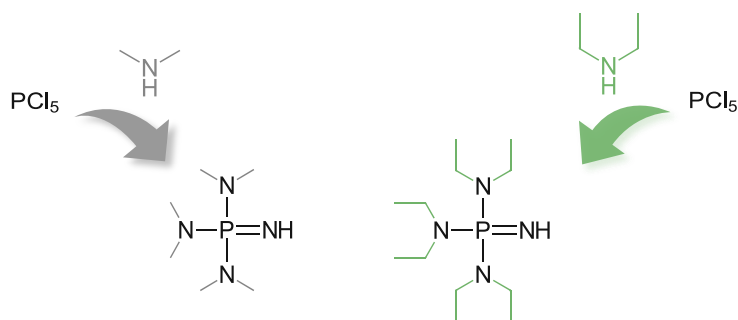
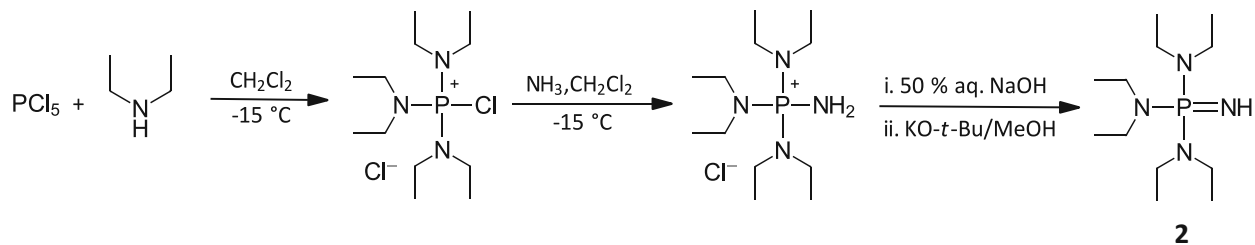


Figure 14: Different alkylation patterns for the phosphazene P1 base; left: methylation, right: ethylation

The target compound **2** was successfully synthesized in line with an already established protocol<sup>65</sup> in a two-step reaction employing ammonia gas, whereupon the intermediate chloride salt of the base was isolated as an orange solid (Scheme 13).





Scheme 13: Two-step synthesis of the second P-fragment **2** based on a literature reported procedure <sup>65</sup>

For the final base liberation, two possible approaches were taken into consideration. Both methods were performed on a small scale and are elaborated below. Ultimately, the NaOH approach was followed, affording the ethylated P1 base as an orange oil at 43 % yield.

#### 1.1.2.1 The NaOH approach

Treatment of the crude reaction mixture with a 50 wt % aqueous NaOH solution afforded the product in a fast and straightforward manner, without showing sensitivity to atmospheric air or moisture. This was confirmed via <sup>1</sup>H and <sup>31</sup>P NMR analysis in CDCl<sub>3</sub> in which recorded spectra were in compliance with literature,<sup>65</sup> showing no formation of hydrolysis by-products (Figure 15).

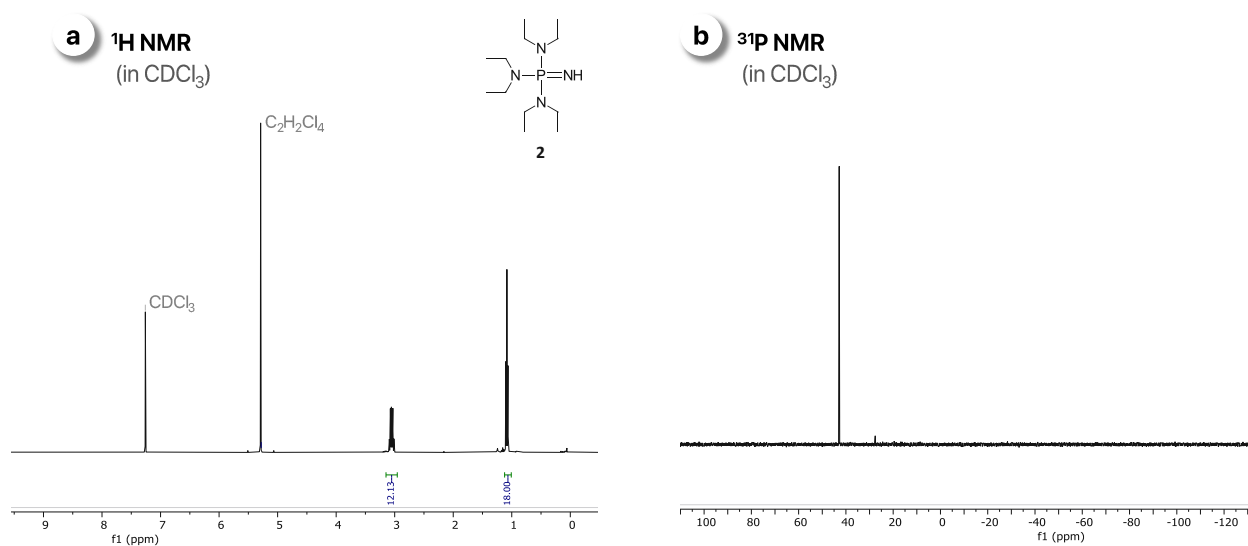


Figure 15: Ethylated P1 base liberation with NaOH; a) <sup>1</sup>H NMR, b) <sup>31</sup>P NMR

### 1.1.2.2 The KO-*t*-Bu/MeOH approach

Alternatively, KO-*t*-Bu in MeOH was used as a strong basic agent to liberate the ethylated P1 base (2) from its chloride salt.<sup>34</sup> In comparison to the aforementioned NaOH approach, this method required a 24-times longer reaction time and demanded an additional purification step via distillation. Due to the small scale in which the experiment was carried out, distillation of the intermediate product was not possible, so that a mixture of the product and HO-*t*-Bu were observed in the recorded NMR spectra (Figure 16).

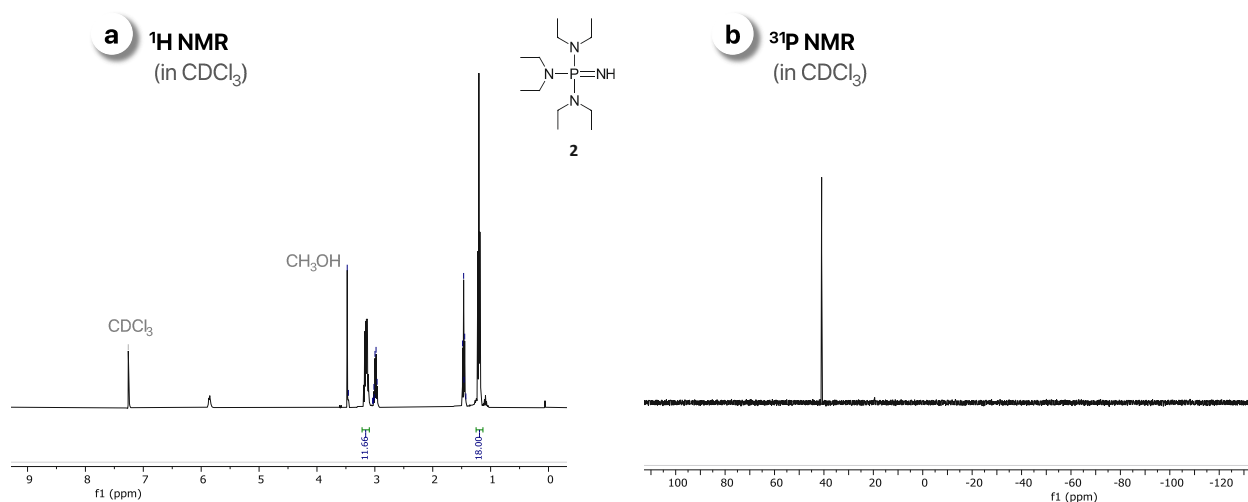
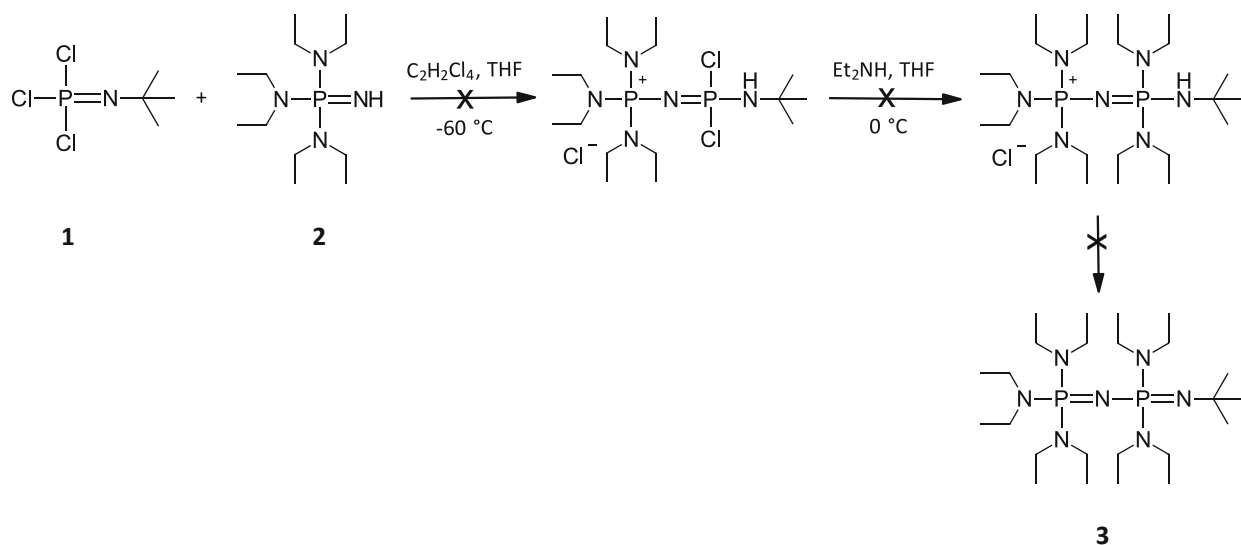


Figure 16: Ethylated P1 base liberation with KO-*t*-Bu/MeOH; a) <sup>1</sup>H NMR, b) <sup>31</sup>P NMR

Furthermore, the hygroscopic, air sensitive nature of KO-*t*-Bu and its incompatibility with many solvents make this method less attractive than treatment with NaOH. For these reasons, the NaOH route was selected as the preferred base liberation procedure for the crude reaction mixture.

### 1.1.3 Coupling of the two P-fragments

Since the designed ethylated P2-base ([[(tert-butylimino)bis(diethylamino)-λ5-phosphanyl]-*N,N,N',N'',N''*-hexaethylphosphorimidic triamide, **3**) and its synthesis have not been explored in the literature yet, the conventional procedure for the methylated Schwesinger P2-*t*-Bu was followed with some alterations (Scheme 14).<sup>34</sup>



Scheme 14: Coupling of the two P-fragments **1** and **2** for the synthesis of the ethylated P2-base **3**, adapted from Schwesinger et al.<sup>34</sup>

The synthesis involved the coupling of the two previously synthesized P-fragments **1** (in tetrachloroethane) and **2** and was performed in two steps at low temperatures (-60 °C to 0 °C).

The recorded <sup>31</sup>P NMR spectrum of the obtained crude product indicated a very pronounced peak at 40 ppm, which is allocated to the precursor ethylated P1 base (compound **2**, Figure 17). Three further peaks were evident in the range 0-20 ppm, which are tentatively allocated to either hydrolysis by-products or product formation at a very modest extent.

**<sup>31</sup>P NMR**  
(in CDCl<sub>3</sub>)

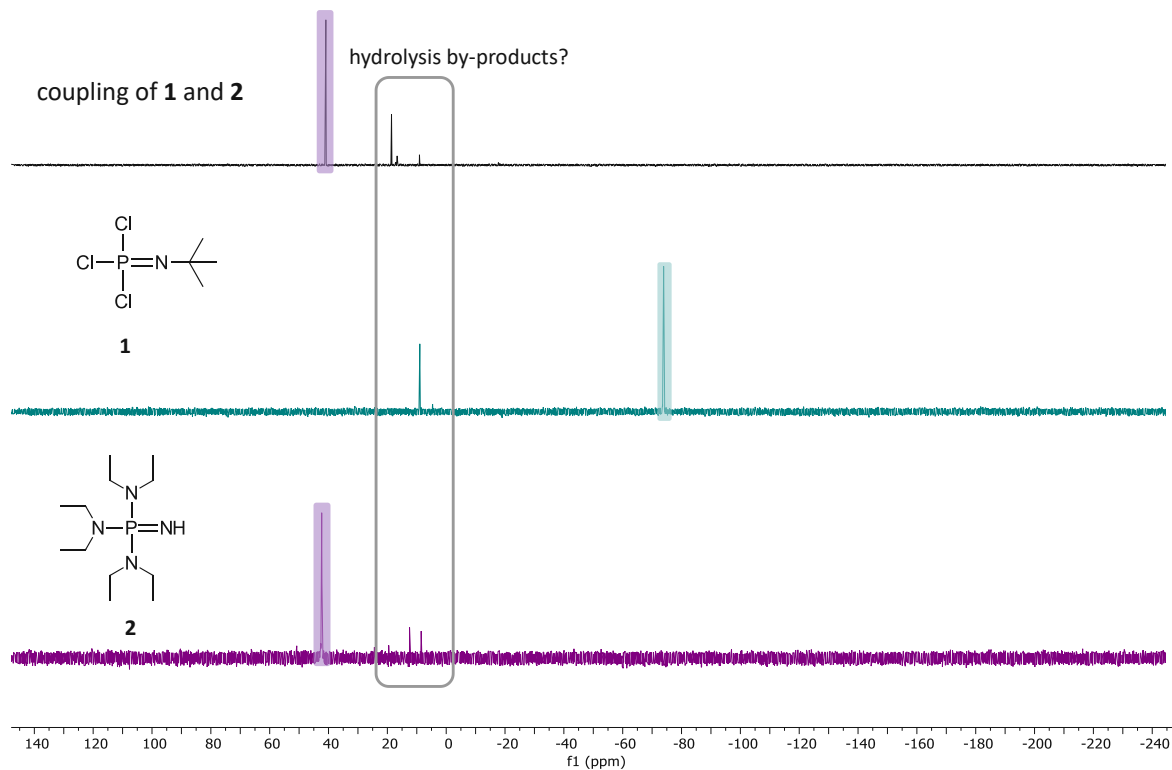


Figure 17: <sup>31</sup>P NMR spectra of the crude reaction mixture (top), P-fragment **1** (middle) and P-fragment **2** (bottom)

Unfortunately, neither could be ruled out via <sup>1</sup>H NMR analysis due to the expected proximity of the proton signals of the starting material **2** and the desired ethylated P2 base **3** (Figure 18). Further insights were gained via LC-MS analysis, revealing the presence of the precursor P-fragment **2**. Only traces of the P-fragment **1** were found. The molar mass of the desired ethylated P2 base was not found, indicating that no product formation had taken place.

**$^1\text{H}$  NMR**  
(in  $\text{CDCl}_3$ )

coupling of **1** and **2**

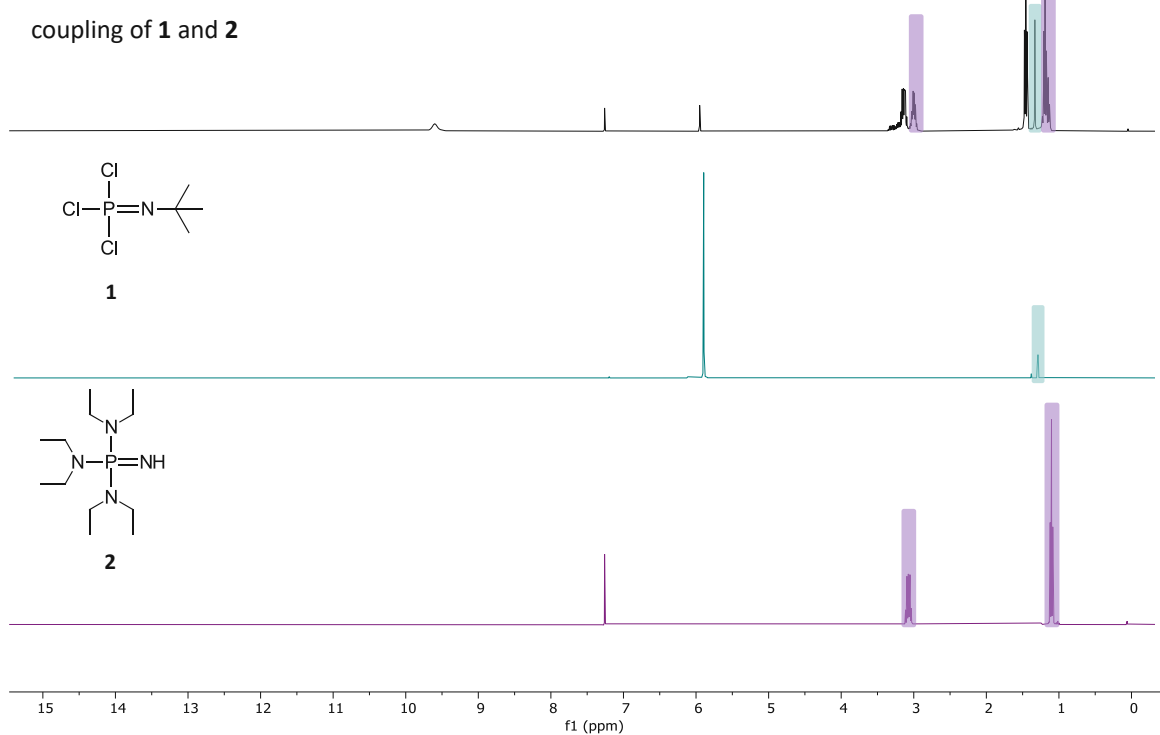


Figure 18:  $^1\text{H}$  NMR spectra of the crude reaction mixture (top), P-fragment **1** (middle) and P-fragment **2** (bottom)

This could be explained by numerous reasons. On the one hand, the steric bulk induced through the ethyl residues in contrast to methyl groups, although of minor difference, could hinder product formation, especially considering that low temperatures are applied during the reaction. Secondly, the reaction stoichiometry is unknown because of the trichloro-P-fragment **1** which, as discussed above, was used in tetrachloroethane with no yield information. An insufficient amount thereof could have rendered the conversion impossible. A further inconvenient influence is the highly sensitive nature towards moisture and air of fragment **1**, implying a possible hydrolysis, which leaves no place for product formation.

In a final attempt to react the precursor P-fragments in the crude mixture, assuming they are both present and intact in the crude mixture, two further experiments were carried out by elevating the reaction temperature and are outlined below.

#### 1.1.3.1 Reaction in THF at 30 °C

First, a small-scale reaction of the crude mixture was performed at 30 °C in THF aiming coupling of the two P-fragments **1** and **2** by temperature elevation. However, the recorded  $^1\text{H}$  and  $^{31}\text{P}$  NMR spectrum (Figure 19) were not indicative of product formation.

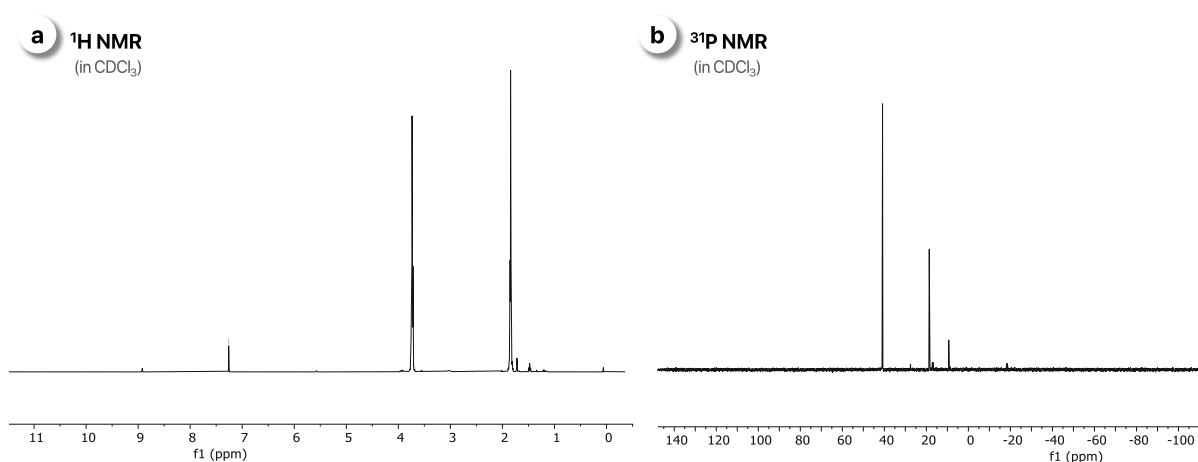


Figure 19: a)  $^1\text{H}$  and b)  $^{31}\text{P}$  NMR spectra measured after reaction of the crude mixture in THF at 30 °C

As far as the  $^{31}\text{P}$  NMR spectrum is concerned, the peak at 40 ppm, which is ascribed to the precursor P-fragment **2**, remains dominant. For the desired ethylated P2-*t*-Bu product, two peaks at equal intensities corresponding to two P-atoms within one molecule would be expected. This is unfortunately not the case. Signals detected in the region 0-20 ppm can be therefore assigned to hydrolysis by-products of both P-fragments **1** and **2**.

### 1.1.3.2 Reaction in toluene at 120 °C

Inspired by a literature procedure concerning the synthesis of cyclic phosphazenes from the same ethylated P1 base as a precursor and a chloro-cyclophosphazene,<sup>65</sup> a small-scale reaction of the crude mixture was performed in toluene instead of THF and refluxed at 120 °C overnight. Again, no conversion was observed in <sup>1</sup>H and <sup>31</sup>P NMR spectra, as depicted in Figure 20.

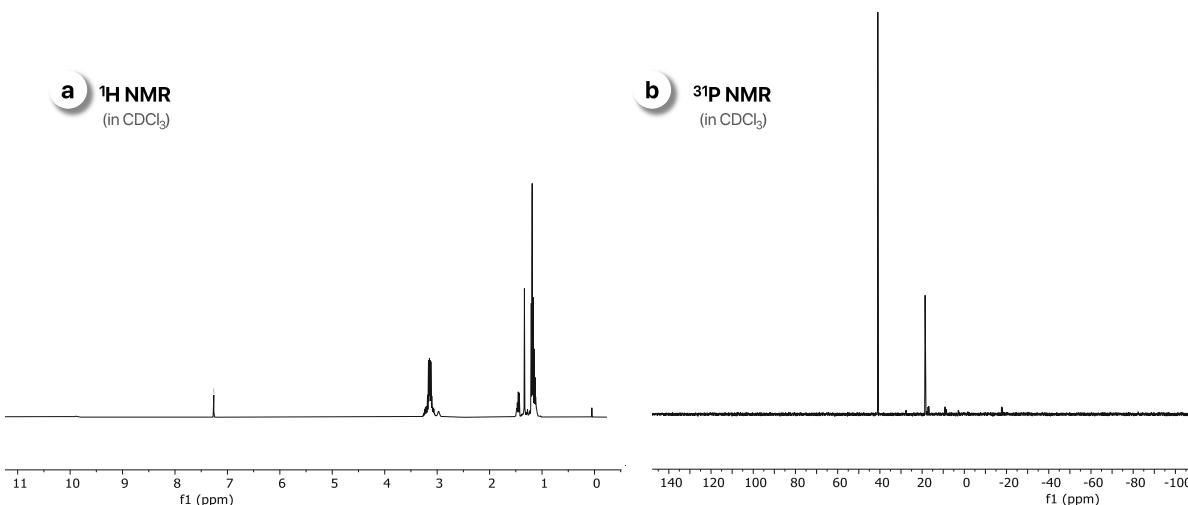


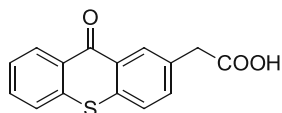
Figure 20: a) <sup>1</sup>H and b) <sup>31</sup>P NMR spectra measured after reaction of the crude mixture in toluene at 130 °C

Aligned with previous observations in the experiment performed in THF at 30 °C (Section 1.1.3.1), it is unfortunately obvious that a temperature elevation approach for improved kinetics cannot lead to the coupling of the two P-fragments **1** and **2**. The unstable nature of the reagents presents itself as the explanation, especially with regards to the highly moisture and air sensitive P-fragment **1**.

In case of a partial hydrolysis of the ethylated P1 base, its structure resembles the methylated analog hexamethylphosphoramidate, which is anticipated to be a human carcinogen. Due to the significant health risks posed by its handling, no further synthetic attempts towards the ethylated P2-*t*-Bu base were undertaken. The results presented herein, however, provide useful information that could facilitate future efforts in alternative phosphazene synthesis.

## 1.2 Chromophore

(10-Oxo-9-thia-3-anthryl)acetic acid, shortly referred to as thioxanthone acetic acid, represents a potentially powerful photoactive compound for the base liberation in PBG systems, owing to the proximity of its absorption bands near UV or even visible light wavelengths.



(10-Oxo-9-thia-3-anthryl)acetic acid

Figure 21: Structure of (10-Oxo-9-thia-3-anthryl)acetic acid

Reportedly, the homologue *O*-based structure xanthone acetic acid can be synthesized via a copper(I) catalyzed Ullmann coupling reaction under basic conditions, which leads to the formation of an aryl-oxygen bond.<sup>62</sup> Following this approach, an adapted synthetic pathway was pursued for the thioxanthone acetic acid targeted in this thesis.

The first step synthesis involved thiosalicylic acid and (4-iodophenyl)acetic acid, catalyzed by a Cu(I) catalyst complex formed between Cu(I)Cl salt and the chelating ligand tris[2-(2-methoxyethoxy)ethyl]amine (TDA-1). A possible mechanism for the catalysis is proposed in accordance to literature in Figure 22.<sup>66</sup>

Firstly, deprotonation of the thiosalicylic acid by the employed base  $\text{Cs}_2\text{CO}_3$  allows its coordination to the Cu(I) complex. Then, addition of the aryl halide starting material to the Cu(I) center forms an oxidized Cu(III) intermediate, which is followed by a reductive elimination of the product, namely 2-[4-(carboxymethyl)phenylthio]benzoic acid, and recovery of the catalyst complex Cu(I) TDA-1.



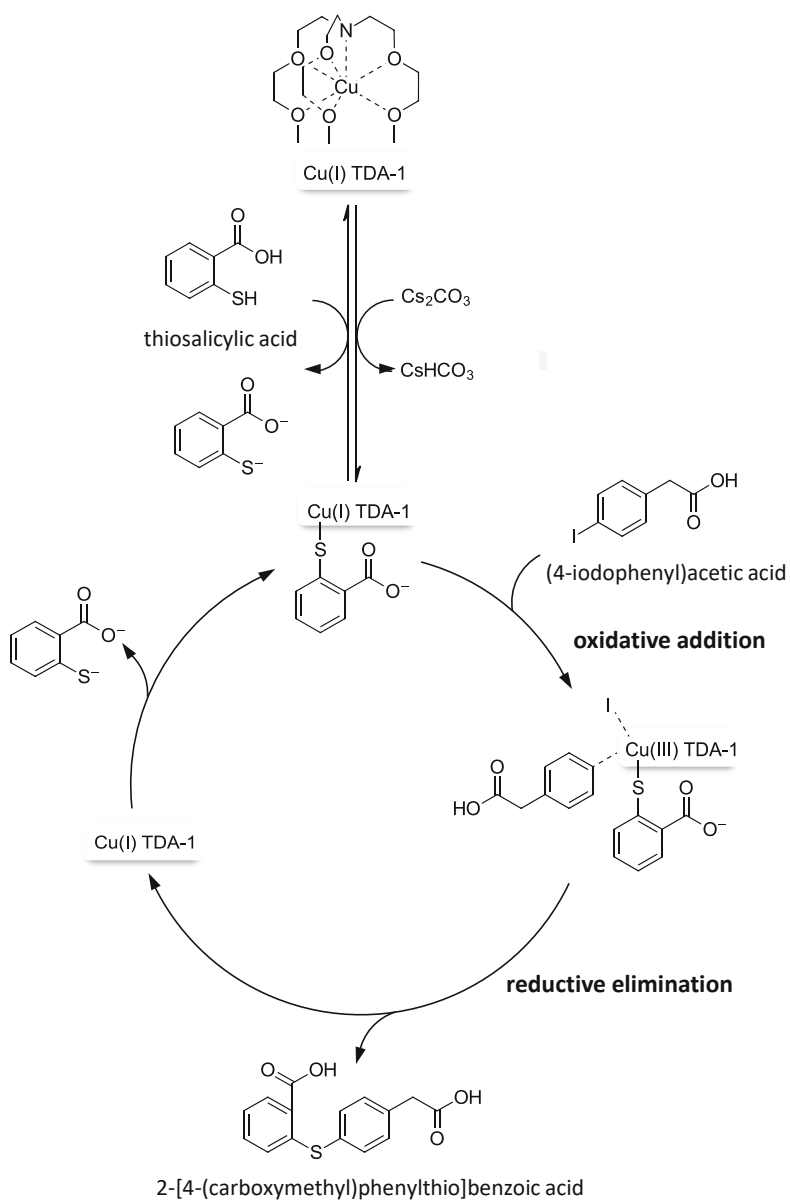


Figure 22: Proposed catalytic cycle for the thioxanthone acetic acid synthesis via an Ullmann coupling

In the second step, a condensation reaction of the isolated intermediate biaryl thioether product was performed in concentrated sulfuric acid at 100 °C. The ring-closure proceeds via an intramolecular Friedel-Crafts acylation, the mechanism of which is briefly outlined in Figure 23.

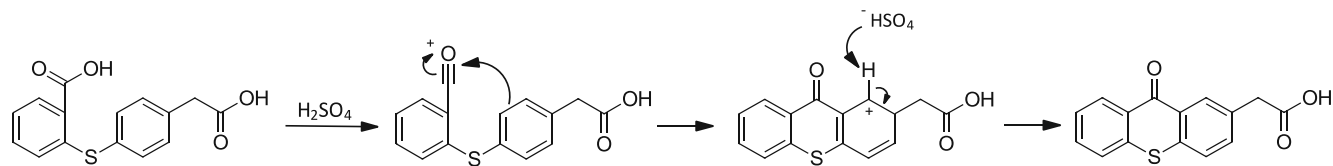


Figure 23: Intramolecular Friedel-Crafts acylation with concentrated  $\text{H}_2\text{SO}_4$

This route afforded the successful isolation of the target compound as an orange powder at a high yield (73 %). Its identity and isomeric purity were confirmed via  $^1\text{H}$  and  $^{13}\text{C}$  NMR analysis.

### 1.3 PBGs

To meet the demand for new decarboxylation-based PBGs which combine high photolysis efficiency at longer wavelengths paired with the ability to generate a superbase as the initiating species, two photoinitiators were designed.

#### 1.3.1 Thioxanthone-based TP

The first photobase generator, referred to as **TP** (Figure 24), combines the successfully synthesized thioxanthone acetic acid as the photoactive compound and the Schwesinger superbase P2-*t*-Bu. A straightforward synthetic procedure in accordance with preceding work done in our laboratory<sup>61</sup> was performed in THF employing an equimolar ratio of the thioxanthone acetic acid and the commercially obtainable phosphazene P2-*t*-Bu as a 0.25 M solution in THF.

Through participation of both compounds in a proton exchange reaction, the PBG salt was obtained as a sticky, viscous orange product. However, removal of THF proved to be a rather tedious task. Even after prolonged drying in vacuo, residual solvent was still traceable in  $^1\text{H}$  NMR spectra, pointing towards a potential solvent trapping within the PBG.

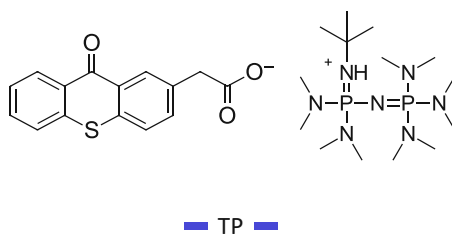


Figure 24: Structure of the **TP** photobase generator

### 1.3.2 Isoxepac-based IP

An additional PBG was prepared in a similar way, employing the same phosphazene base P2-*t*-Bu and the commercial compound 2-(11-oxo-6,11-dihydrodibenzo[*b,e*]oxepin-2-yl)acetic acid, commonly known as isoxepac (Figure 25). As a nonsteroidal anti-inflammatory drug, isoxepac is often associated with its numerous uses in medical treatments.<sup>67</sup> Interestingly, its additional role as an effective part of photoprotection compositions that reduce skin damage upon acute exposure to harmful UV light has also been reported.<sup>68</sup>

The only structural difference of isoxepac to thioxanthone acetic acid, where the biaryl motif is bridged by a sulfur atom, consists in the presence of an oxygen-methylene bridge instead. Considering its commercial availability and ease of handling, it is reasonable to incorporate isoxepac in a PBG system, referred to as **IP**, and accordingly investigate it together with the thioxanthone-based **TP**.

After preparation of the isoxepac-based **IP** salt and evaporation of the solvent, the title product was obtained as an off-white, viscous liquid. Similarly to **TP**, the phenomenon of residual solvent being trapped in the PBG was observed in this case as well.

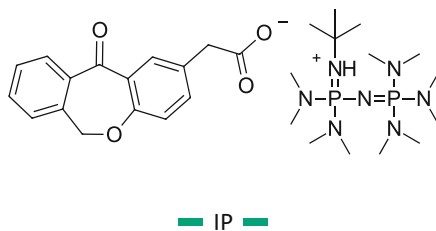


Figure 25: Structure of the **IP** photobase generator

## 2. Characterization

### 2.1 Thermogravimetric analysis (TGA)

To gain insight into the thermal stability of the thioxanthone-based **TP**, isoxepac-based **IP**, and the reference initiator, thermogravimetric analysis (TGA) was performed.

The TGA signal of the **TP** PBG indicates three profiles with a decline in mass (Figure 26). The first mass loss is most probably attributed to solvent evaporation, which is trapped in the photobase despite drying for several days in the high vacuum pump, which is in line with previous observations. This mass loss of 12 % starts at around 68 °C and stops at 130 °C, which is in good compliance with the boiling point of THF (66 °C) and of water.

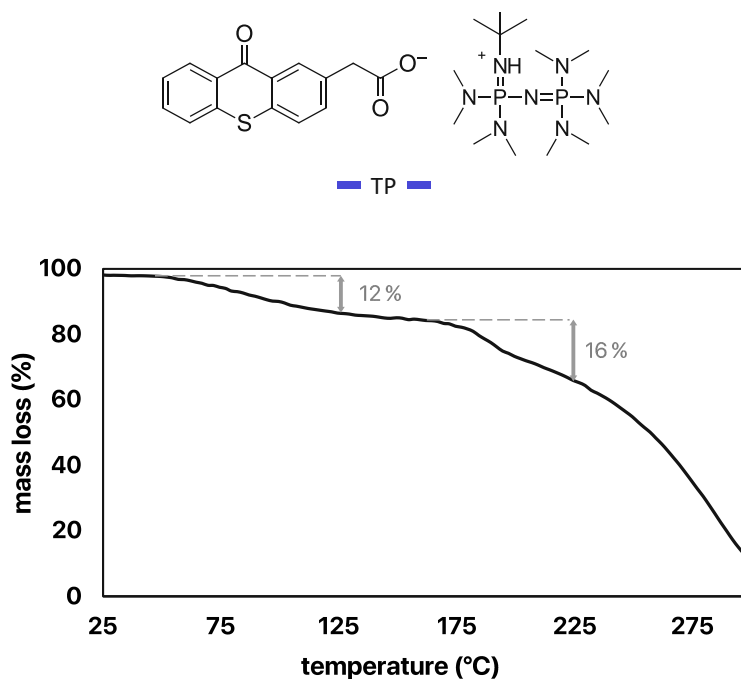


Figure 26: TGA measurement of **TP**

Thereafter, a second thermal decomposition causing a further weight loss of about 16 % takes place from 173 °C to 255 °C. From 255 °C onwards, more than 91 % of the PBG mass is lost.

The TGA curve for the isoxepac-based **IP** PBG exhibits two profiles with a decline in mass (Figure 27). The first mass loss is, similar to **TP**, most likely caused by evaporation of the solvent (THF) and eventually water regardless of prolonged drying.

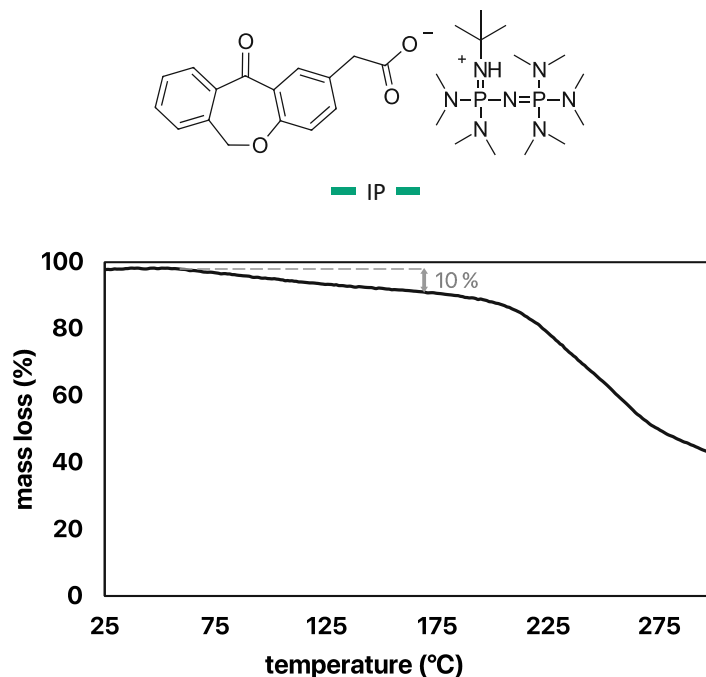


Figure 27: TGA measurement of **IP**

The second and most significant mass loss is ascribed to thermal decomposition starting at around 208 °C to 300 °C, which is the maximal temperature set for the measurement. More than half of the PBG perishes during this process.

The thermal behavior of **TP** and **IP** was compared to that of an analog PBG, which had been previously synthesized in our laboratory employing the P2-*t*-Bu superbase and ketoprofen as a chromophore, hereafter referred to as ketoprofen-based **KP**.<sup>61</sup> The corresponding curve of the retrieved thermal analysis data is depicted in Figure 28.

Similarly to **TP** and **IP**, the first mass loss amounting to 10 % is attributed to solvent residues (THF) evaporation. A good thermal stability of up to 203 °C is observed,<sup>61</sup> rendering all three PBGs comparable regarding their thermal behavior.

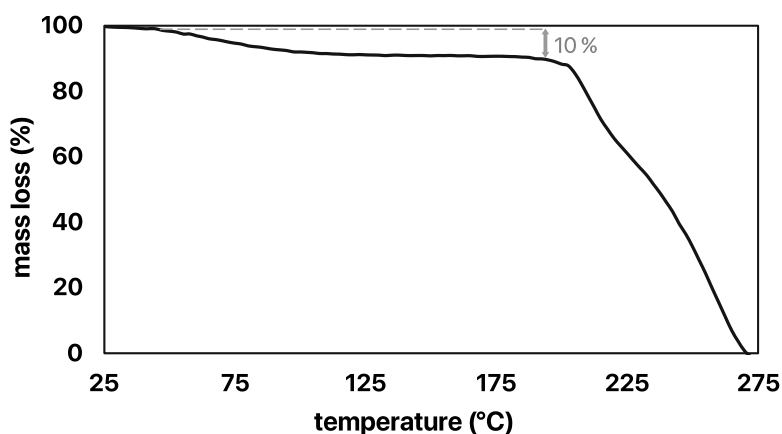
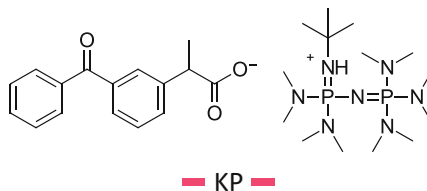


Figure 28: TGA measurement of the reference PBG KP, retrieved from previous work performed in our laboratory<sup>61</sup>

## 2.2 Storage stability

Since the prepared PBGs in this work are salts, the investigation of their storage stability is of high interest. For this, the thioxanthone-based **TP**, the isoxepac-based **IP**, and the reference initiator stored under Ar at 4 °C in the dark were subjected to <sup>1</sup>H NMR measurements, based on the presumption that a possible equilibrium shift of the salt would affect the proton signals in their respective spectra.

As far as **TP** is concerned, <sup>1</sup>H NMR analysis upon storage over 6 months revealed an altered ratio of the thioxanthone acetic acid signals to those of the P2-*t*-Bu base. Based on the comparison of the peak area integrations (Figure 29), a P2-*t*-Bu base excess of approximately 25 % is present in the **TP** salt after 6 months of storage.

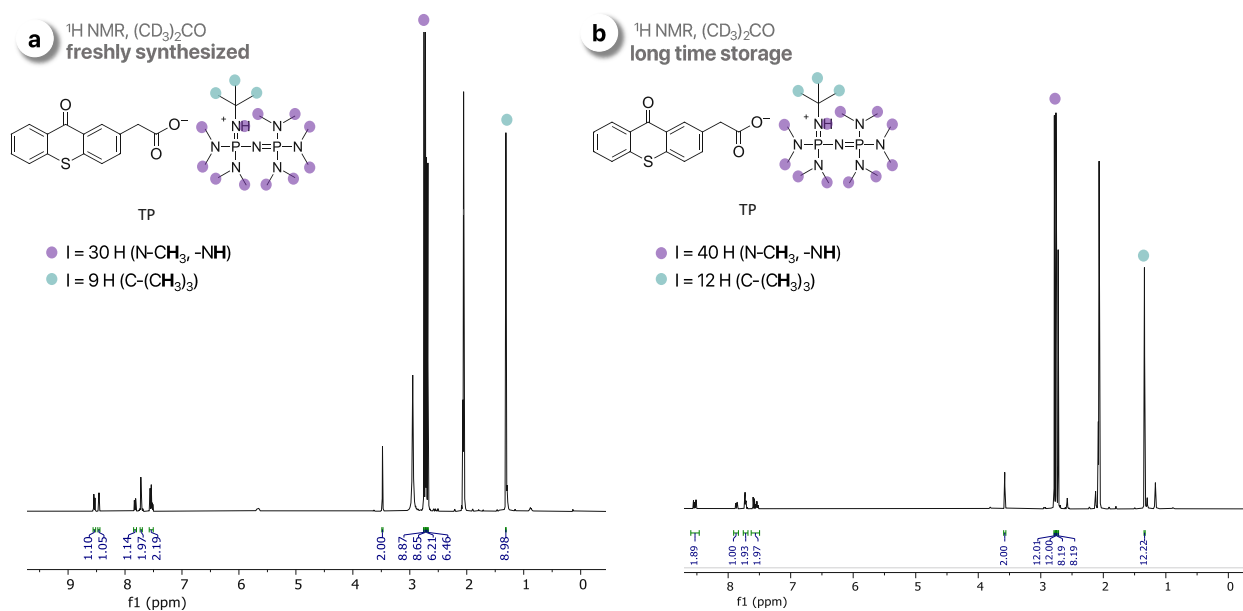


Figure 29: Comparison of proton signals of  $^1\text{H NMR}$  spectra for **TP** a) freshly synthesized and upon b) long term storage (6 months)

Once the stability question was raised, subsequent TLC analysis of **TP** and its chromophoric part (thioxanthone acetic acid) was performed. Surprisingly, each of both compounds exhibited two spots of very different polarities ( $R_{f1} = 0$ ,  $R_{f2} = 0.9$  in 100 % DCM), suggesting that some sort of impurity had been formed along storage of thioxanthone acetic acid and consequently of **TP**.

To identify the impurity, a LC-MS measurement of the thioxanthone acetic acid was conducted. The acquired spectrum confirmed the presence of the pure product ( $m/z$  found: 271) as well as of a by-product, the mass of which corresponds to the decarboxylated form ( $m/z$  found: 227), as summarized in Figure 30. This photocleaved product amounts to 12 % based on the UV detection, given that the absorption intensities of the carboxylated and decarboxylated form are alike.

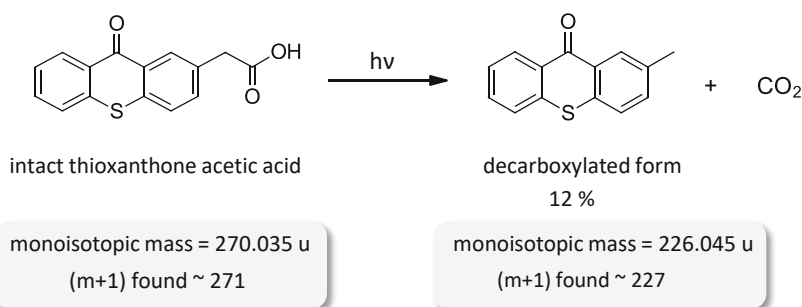
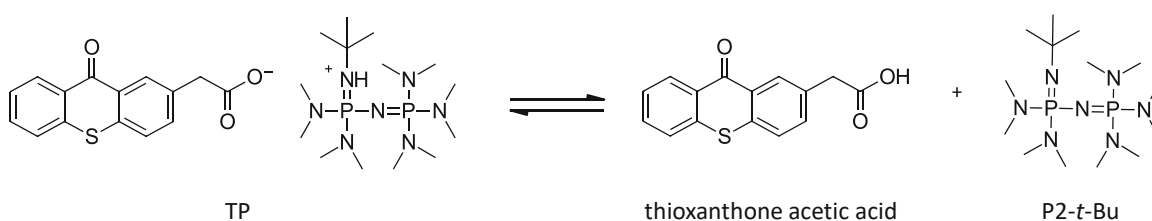


Figure 30: Partial photocleavage of thioxanthone acetic acid in its decarboxylated form and  $\text{CO}_2$  confirmed by LC-MS analysis

Long-term storage had potentially led to partial photodecarboxylation of the thioxanthone acetic acid. When referring to the **TP** salt, this implies that the photodecomposed residues cannot engage in a proton transfer with the free P2-*t*-Bu base in order to “photocage” it, thus shifting the equilibrium to the free base, which is consequently detected in excess (Scheme 15).



Scheme 15: PBG salt equilibrium in the example of **TP**

Afterwards, efforts to separate the intact thioxanthone acetic acid from the photodecomposed by-product were undertaken. To the dark orange powder was added DCM, wherein incomplete solubility was observed. This behavior is expected, as particularly low solubilities are common for thioxanthone derivatives, e.g. ITX, which resembles the structure of the decarboxylated species in this case. Thioxanthone acetic acid, on the other hand, displays a better solubility in DCM due to the polarity of its acidic group.

The mixture in DCM was filtered and the filtrate was flashed through a silica gel column chromatography using DCM with 5-15 % MeOH, affording 146 mg (73 %) of the pure thioxanthone acetic acid.



The storage stability of the isoxepac-based **IP** was investigated analogously after a 9 months storage period. Notably, no change in proton signals was observed, suggesting that the salt composition had remained unimpaired (Figure 31). In this case, storage at a low temperature in the dark seems to successfully prevent any sort of premature chromophore cleavage.

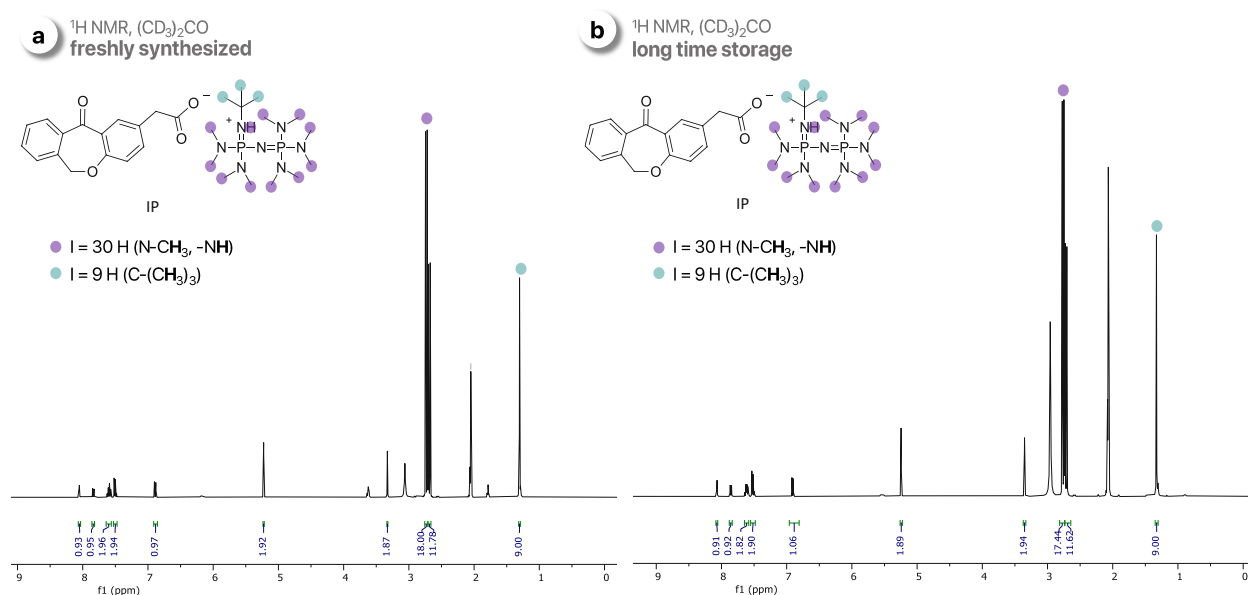


Figure 31: Comparison of proton signals of  $^1\text{H}$  NMR spectra for **IP** a) freshly synthesized and upon b) long term storage (9 months)

The same holds true for the reference ketoprofen-based **KP**, where the  $^1\text{H}$  NMR spectrum retrieved from previously done measurements in our laboratory directly after synthesis<sup>61</sup> was analogously compared to a spectrum recorded after approximately 2 years upon storage under Ar at 4 °C in the dark (Figure 32). The unaffected ratio of the corresponding proton signals indicates no shift in the KP salt equilibrium.

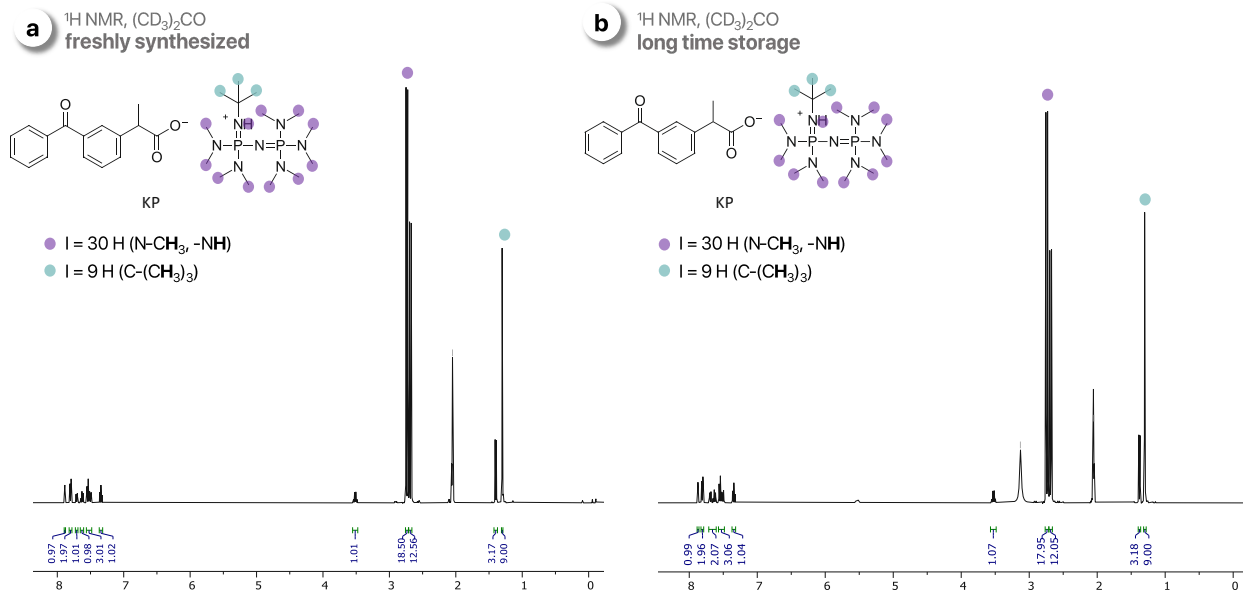


Figure 32: Comparison of proton signals of  $^1\text{H NMR}$  spectra for **KP** a) freshly synthesized, retrieved from previous measurements in our laboratory <sup>61</sup> and upon b) long term storage (2 years)

### 2.3 UV/Vis spectroscopy

The two synthesized PBGs and the reference initiator were further subjected to photochemical analysis via UV/Vis measurements. In a wavelength window ranging from 280 nm to 600 nm, their respective absorption behavior as well as the position of their absorption maxima of the  $\pi\pi^*$  transition band could be observed. The experiments were performed in anhydrous THF solutions at different concentrations and the resulting UV/Vis spectra are presented below.

The absorption profiles of the acquired UV/Vis spectra for the thioxanthone-based **TP** are depicted in Figure 33 and deliver very interesting results. For the two lowest concentrations measured, namely  $0.95 \cdot 10^{-5}$  mol/L and  $4.76 \cdot 10^{-5}$  mol/L, the absorption maxima are located at around 386 nm and their absorption tails extend up to 410 nm, hence falling within the visible light range. Notably, the more concentrated **TP** solution extends the absorption pattern even further to almost 450 nm.

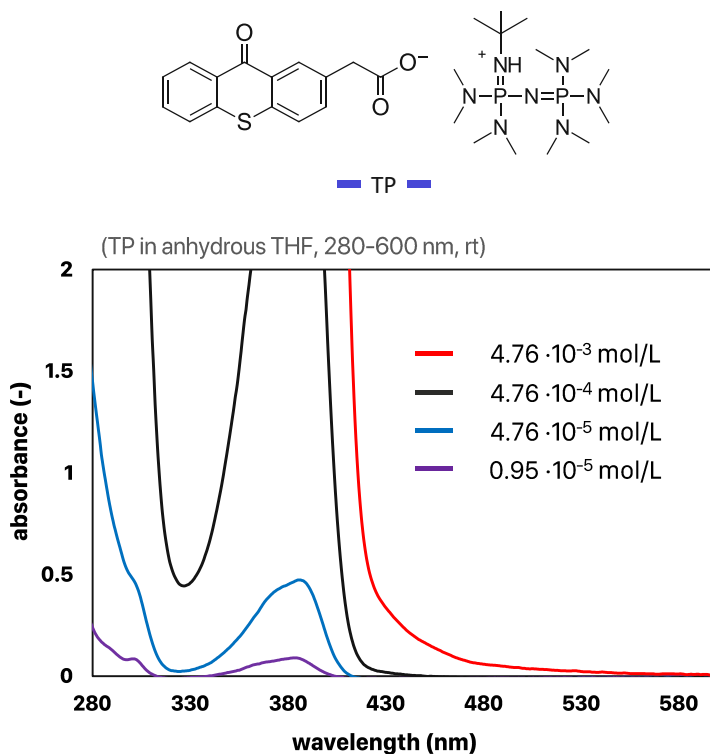


Figure 33: UV/Vis spectra of TP

Similarly, the absorption patterns for the isoxepac-based **IP** at four concentrations are presented in Figure 34. Because of the generally low absorbance of the lowest concentration  $1.17 \cdot 10^{-5}$  mol/L and the rather flat curve, its absorption maximum could not be identified. The maxima of the higher concentrated solutions, namely  $1.17 \cdot 10^{-4}$  mol/L and  $5.85 \cdot 10^{-4}$  mol/L, appear at around 348 nm with tails extending up to about 410 nm.

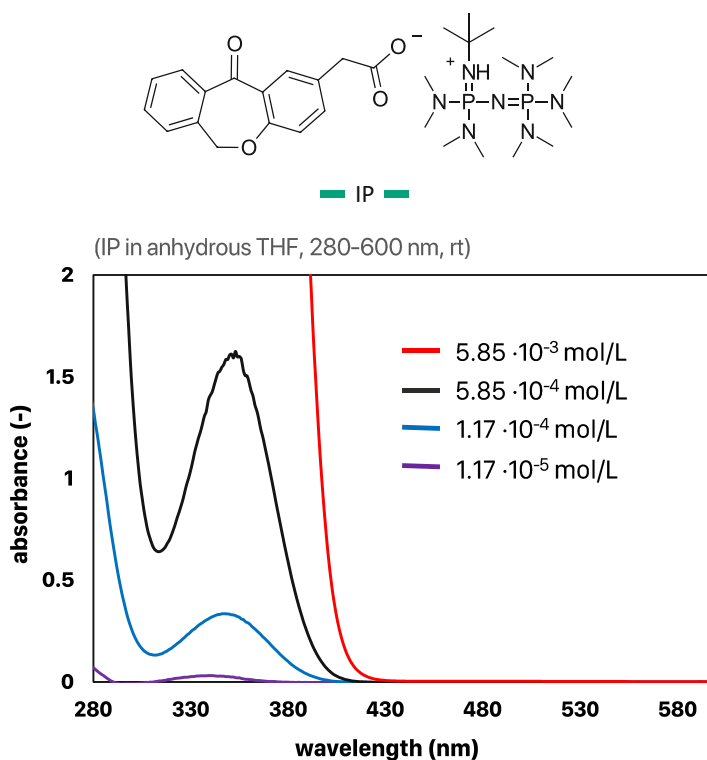


Figure 34: UV/Vis spectra of **IP**

Additionally, the absorption behavior of the reference photocaged ketoprofen chromophore, namely the **KP** PBG is depicted in Figure 35. Its absorption maximum is in good compliance with literature<sup>18</sup> and is located at 248 nm, which is considerably lower than the presented absorption maxima of **TP** and **IP**.

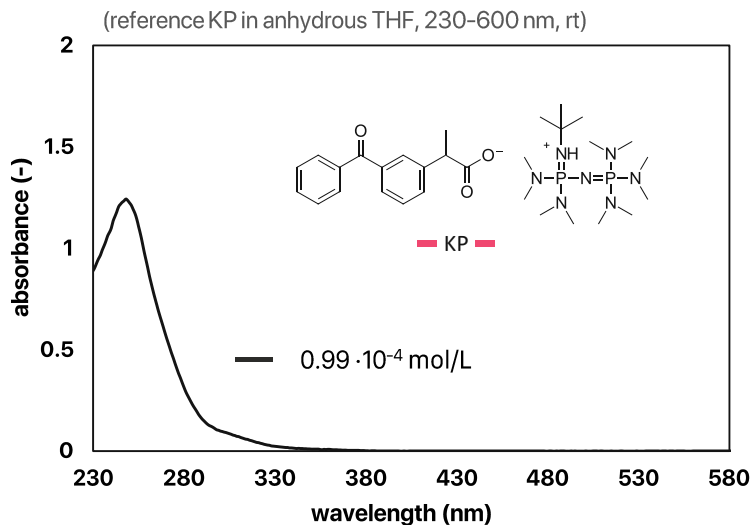


Figure 35: UV/Vis spectrum of reference KP

Further, Lambert-Beer law was applied for the determination of the molar extinction coefficients at the absorption maxima of the most suitable curves for both TP, IP, and KP and the results are displayed in Table 2.

$$A_{max} = \varepsilon_{max} \cdot c \cdot d$$

$A_{max}$  absorbance maximum

$\varepsilon_{max}$  molar extinction coefficient

c concentration (mol/L)

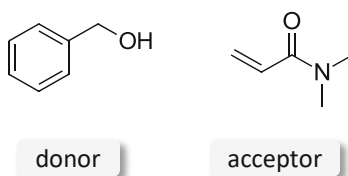
d optical pathlength

Table 2: Molar extinction coefficients of TP, IP, and KP calculated from their absorption maximum

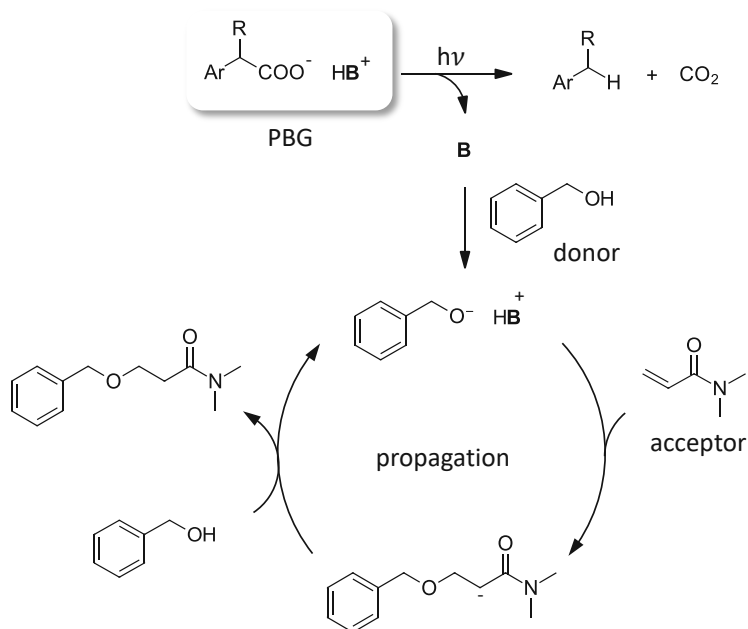
PBG	$\lambda_{max}$ (nm)	$\varepsilon_{max}$ (L mol <sup>-1</sup> cm <sup>-1</sup> )
TP	386	9937
IP	348	2863
reference KP	248	1010

### 3. Monofunctional system

To investigate the applicability of the synthesized PBG salts, a study based on a monofunctional oxa-Michael addition was carried out. The system is composed of a benzyl alcohol substrate emerging as the Michael donor upon deprotonation and an acrylamide Michael acceptor. The selected acrylamide comprises a dimethyl-substituted nitrogen, so that the potential issue of acidic protons competing with the alcohol in the deprotonation step is circumvented.



As outlined in the Introduction, the presence of a base is crucial for the oxa-Michael addition. This is where the photoinduced liberation of the Brønsted P2-*t*-Bu base from the respective PBG comes to play. Details on the mechanistic pathway preceding the addition reaction are presented in Scheme 16.



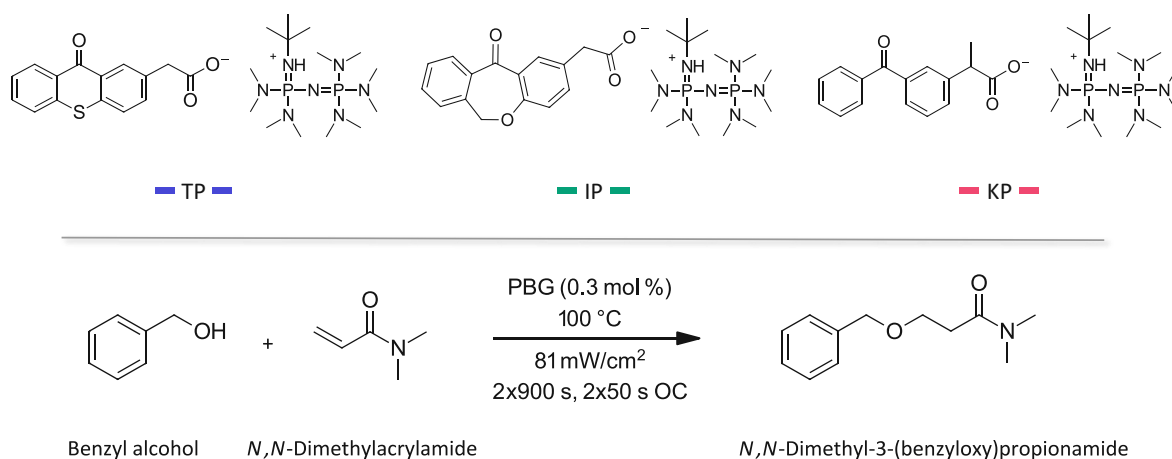
Scheme 16: Mechanistic considerations of the Brønsted base (P2-*t*-Bu) mediated oxa-Michael addition reaction employing a benzyl alcohol and an acrylamide

Direct deprotonation of benzyl alcohol via P2-*t*-Bu affords a benzyloxyde, which will preferably attack the acrylamide double bond in  $\beta$ -position. The resulting  $\alpha$ -positioned carbanion then closes the cycle via H-abstraction from another benzyl alcohol, yielding the ether product.

### 3.1 Preliminary studies

In preliminary experiments, the oxa-Michael addition was performed in a model reaction using an equimolar mixture of benzyl alcohol and *N,N*-dimethylacrylamide with a 0.3 mol % PBG salt loading. Together with the prepared thioxanthone-based **TP** and isoxepac-based **IP** salt, the homologue ketoprofen-based **KP**,<sup>61</sup> was used as a reference (Scheme 17). The three reactions were carried out via a photo-DSC setup, as this allows reproducible and careful monitoring of the reaction parameters, e.g. temperature, irradiation, and reaction time under inert conditions.

In the initially selected set of conditions, a temperature of 100 °C was applied over two cycles of 900 s each, paired with two light exposure cycles of 50 s at a 81 mW cm<sup>-2</sup> intensity of the irradiation source with an emission spectrum of 320-500 nm.



Scheme 17: Oxa-Michael addition reaction utilizing **TP**, **IP**, and **KP** as a PBG

Conversion to the desired oxa-Michael product *N,N*-dimethyl-3-(benzyloxy)propionamide was evaluated via <sup>1</sup>H NMR measurements, which were performed before and after the reaction. The formation of a new singlet, which is shifted upfield relative to the methylene peaks of the benzyl alcohol, is indicative of the desired ether product. Conversion can be determined by comparing

the integral values of the emerging ether signal to the unreacted benzyl alcohol and is therefore calculated as follows (Figure 36).

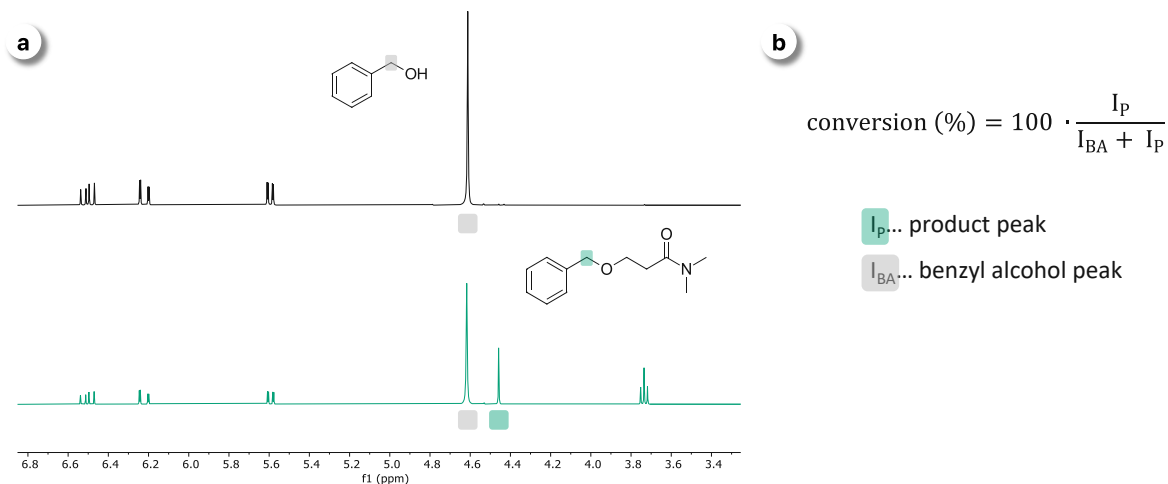


Figure 36: a)  $^1\text{H}$  NMR spectra of the oxa-Michael addition (e.g. using the IP photobase); above: before reaction, below: after reaction, b) conversion calculation

With all three investigated PBGs, the occurrence of an oxa-Michael addition could indeed be confirmed and the resulting conversions are depicted in Figure 37.

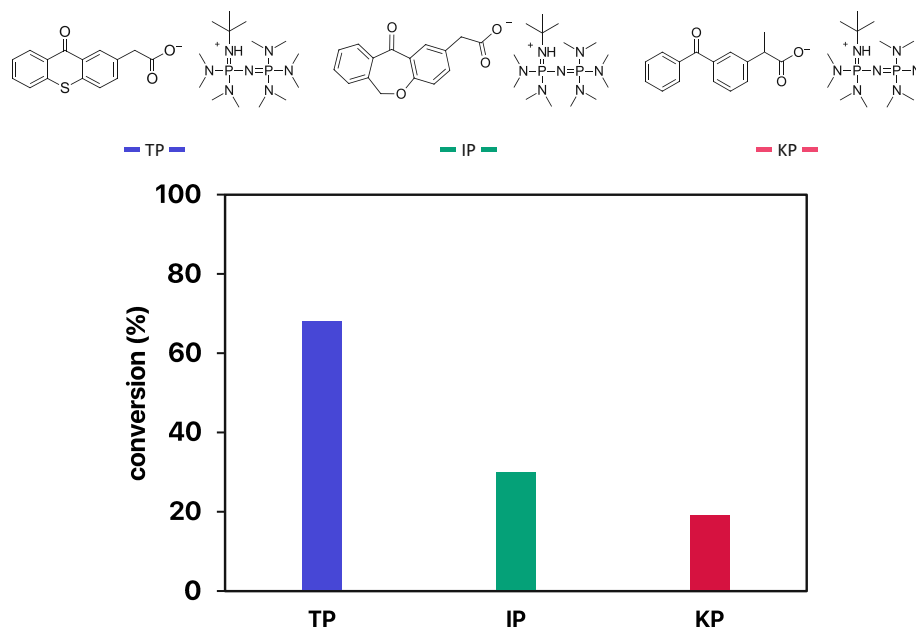


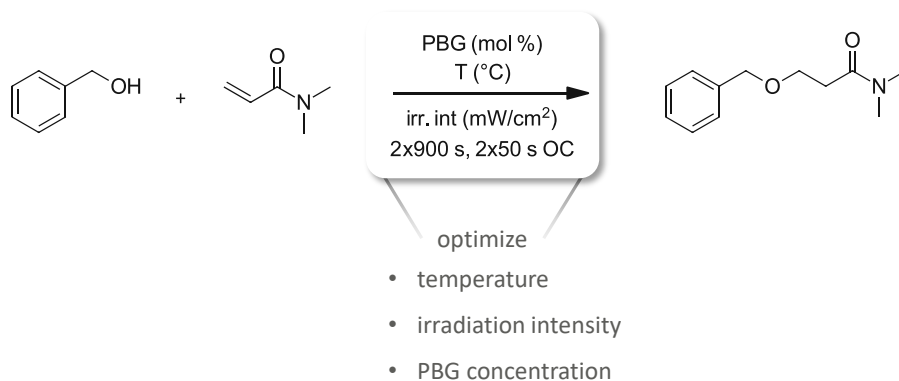
Figure 37: Conversion of the oxa-Michael addition reaction whilst using TP, IP, or KP as a PBG in a preliminary round



Predictably, the highest conversion was reached when **TP** was employed as the PBG of choice owing to its enhanced light absorbing ability expressed through the high molar extinction coefficient. In this case, a remarkable conversion of 68 % could be determined. Then, a notable drop in conversion was detected whilst performing the reaction with **IP**, which afforded the oxa-Michael product in 30 % yield. Lastly, the reference **KP** led to a poor conversion of only 19 %, most probably attributed to its significantly lower photoactivity.

### 3.2 Optimization

We were encouraged by these preliminary results and aimed at finding the optimal reaction conditions for the PBG-mediated oxa-Michael addition whilst comparing the work carried out with this thesis with the thioxanthone-based **TP** and isoxepac-based **IP** to the available reference system ketoprofen-based **KP**. Several parameters were altered in a controlled manner, including temperature, intensity of the incident light, and PBG concentration.



To collect reliable data, all reactions were performed in triplets on a photo-DSC device coupled with a light source emitting in the range 320-500 nm. The conversions presented herein are expressed as arithmetic averages of the values obtained from the recorded  $^1\text{H}$  NMR spectra.

#### 3.2.1 Temperature screening

The oxa-Michael addition reaction was performed with an equimolar mixture of benzyl alcohol and *N,N*-dimethylacrylamide in the presence of the PBG of choice (**TP**, **IP**, and **KP**, 0.3 mol %) at 25, 60, 80, and 100 °C. The irradiation intensity of the light source was set at 81 mW/cm<sup>2</sup>.

Expectedly, temperature has a significant impact on the conversion of the benzyl alcohol to the corresponding ether product. The presented results in Figure 38 clearly indicate and confirm a trend for all three employed PBGs, showing an increase in yield with increasing temperature.

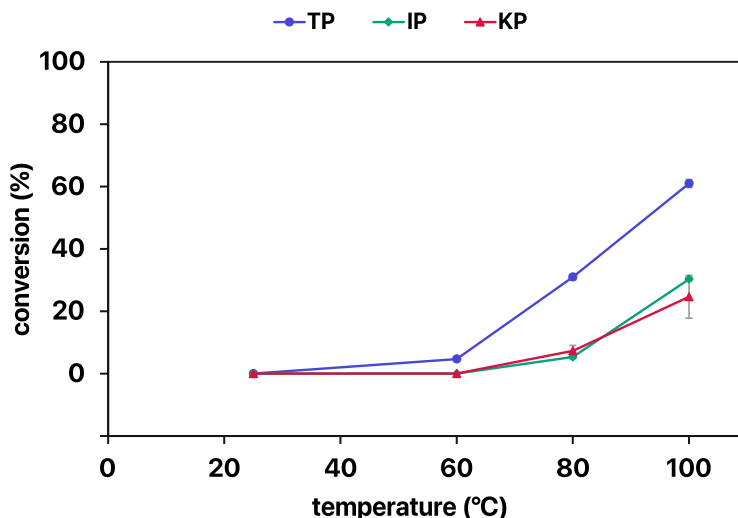


Figure 38: Temperature screening results for the oxa-Michael addition with **TP**, **IP**, and **KP** as initiators

Unfortunately, a mild temperature (25 °C) is insufficient in setting the reaction in motion, as no product could be formed regardless of the used PBG. As far as the thioxanthone-based **TP** is concerned, setting the temperature to 60 °C and further to 80 °C led to improved, yet rather poor conversions (5 and 31 %, respectively). The same does not hold true for the isoxepac-based **IP** and ketoprofen-based **KP**, since the benzyl alcohol remains completely unreacted (60 °C) or is converted to a very limited extend as to form only traces of the oxa-Michael product (80 °C).

Increasing the temperature to 100 °C allows the detection of significantly higher yields when using all three PBGs. Predictably, the best results are obtained via **TP**, which yields the ether at 61 %, thus aligning with precedent findings. Reactions performed with **IP** and **KP** at the same temperature, on the other hand, are not as successful. Poor conversions not surpassing 30 % are observed for both, confirming they are not as effective **TP** in liberating the P2-*t*-Bu base under the given reaction conditions.

Due to the volatility of the Michael acceptor *N,N*-dimethylacrylamide, elevating the temperature above 100 °C for potential yield improvements is not possible.

### 3.2.2 Irradiation intensity screening

The following screening experiments demonstrate the impact of the irradiation intensity on the base-mediated monofunctional oxa-Michael reaction. For this, the reagents benzyl alcohol and *N,N*-dimethylacrylamide were employed in an equimolar ratio together with 0.3 mol % of the investigated PBG (**TP**, **IP**, and **KP**). The reaction was performed at 100 °C and the applied light intensity was altered between 26 to 108 mW cm<sup>-2</sup> (for **TP**) or to 140 mW cm<sup>-2</sup> (for **IP** and **KP**) prior to each triplet measurement.

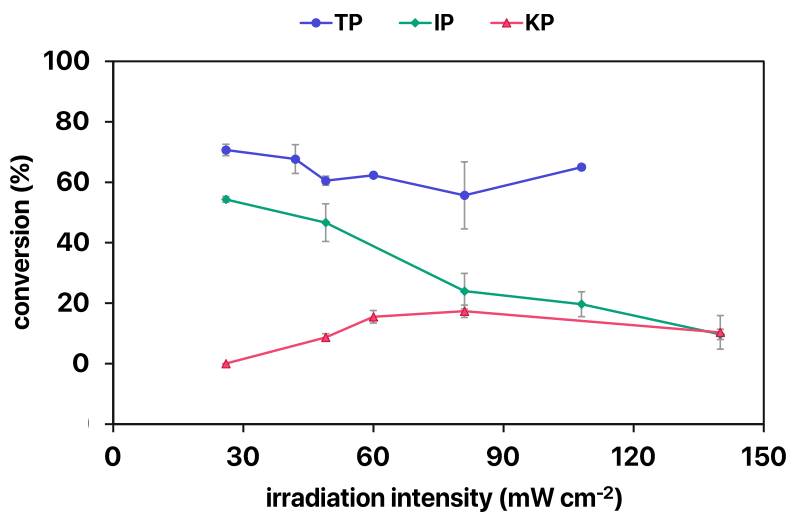


Figure 39: Light source irradiation intensity screening results for the oxa-Michael addition with **TP**, **IP**, and **KP** as initiators

With the thioxanthone-based **TP** as the initiator of choice, no direct correlation between conversion and irradiation intensity was observed (Figure 39). Comparably good results were obtained whilst employing a range of intensities, leading to conversions between 56 and 71 %. Interestingly, the highest conversion was achieved while irradiating with a 26 mW cm<sup>-2</sup> lamp intensity, implying that the corresponding energy of the photons per area is sufficient for successful photocleavage of the PBG. This makes **TP** attractive for potential future applications in 3D printing at mild intensities.

Similarly, for screenings performed with the isoxepac-based **IP**, the mildest applied intensity, i.e. 26 mW cm<sup>-2</sup> affords the best conversion, which amounts to 54 %. However, with higher intensities, a remarkable trend is revealed. Adjusting the intensity level of the light output to e.g. 49, 81, 108 or even 140 mW cm<sup>-2</sup> leads to a significant drop in yields (46, 24, 20, and 10 %, respectively). Considering the slight yellow appearance of the samples after measurement, this behavior might be linked to the potential formation of photolysis products.

Furthermore, very low yields of under 20 % were detected with the ketoprofen-based reference **KP**. Compared to **TP** and **IP**, no oxa-Michael ether is observed at 26 mW cm<sup>-2</sup>. In contrast, at least 49 mW cm<sup>-2</sup> are necessitated for modest product formation (9 %) and the best result among the measured intensities is obtained at 81 mW cm<sup>-2</sup> (17 %).

### 3.2.3 PBG concentration screening

In an attempt to further optimize the reaction conditions for the monofunctional oxa-Michael addition, various initiator concentrations (**TP**, **IP**, and **KP**) ranging between 0.1 and 1.2 mol % were examined. All reactions were performed with an equimolar mixture of benzyl alcohol and *N,N*-dimethylacrylamide at 100 °C. The intensity of the incident light was set at 26 mW cm<sup>-2</sup> in order to ensure comparability between the three PBGs.

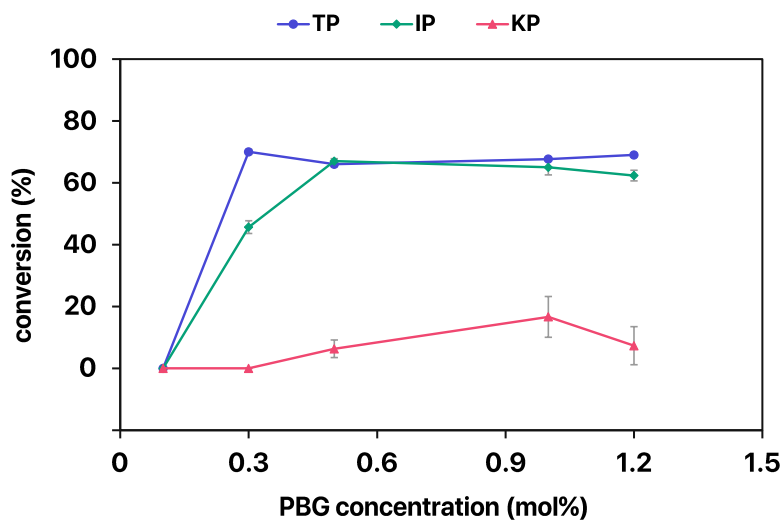


Figure 40: Initiator concentration screening results for the oxa-Michael addition with **TP**, **IP**, and **KP** as initiators

The lowest tested concentration, namely 0.1 mol % **TP**, **IP**, and **KP** proved to be insufficient at initiating the reaction (Figure 40). Regarding the thioxanthone-based **TP**, the best conversion was achieved when using a 0.3 mol % loading thereof, yielding 70 % oxa-Michael ether. Further increasing its concentration (0.5, 1.0, and 1.2 mol %) does not contribute to any detectable extent, implying the maximum capacity of the reaction is already reached with 0.3 mol % **TP**.

As anticipated, when the isoxepac-based **IP** is employed, 0.3 mol % are less effective in enabling oxa-Michael product formation, accounting for 46 % conversion. This is in compliance with the result obtained when altering irradiation intensity, which proves reproducibility and reliability of the screening series. Upon using 0.5 mol % **IP**, a notable increase in yield is detected which extends to 67 %. After reaching this mark, similarly to **TP**, higher concentrations (1 and 1.2 mol %) did not further improve conversion.

For the ketoprofen-based reference system **KP**, rather poor yields are achieved for all concentrations taken into consideration. Traces of the oxa-Michael ether were found when using 0.5 mol % initiator (6 % yield), whereas doubling the concentration led to an improved conversion of 17 %.

### 3.3 Formulation storage stability

The purpose of this storage stability study is to assess how the composition of the formulation for the oxa-Michael addition varies within a defined period of time when stored at 100 °C under exclusion of light. This environment should mimic conditions in possible future applications, e.g. 3D printing.

Therefore, three formulations were prepared using an equimolar mixture of benzyl and *N,N*-dimethylacrylamide, as well as 0.3 mol % of the investigated PBG, i.e. the thioxanthone-based **TP**, isoxepac-based **IP** and ketoprofen-based **KP**. They were subjected to <sup>1</sup>H NMR analysis before and after storage for a two-week period.

As shown in Figure 41, no oxa-Michael product is formed, confirming that without light exposure no premature base release, which would otherwise initiate the addition reaction, is formed. This holds true for all three investigated PBGs.

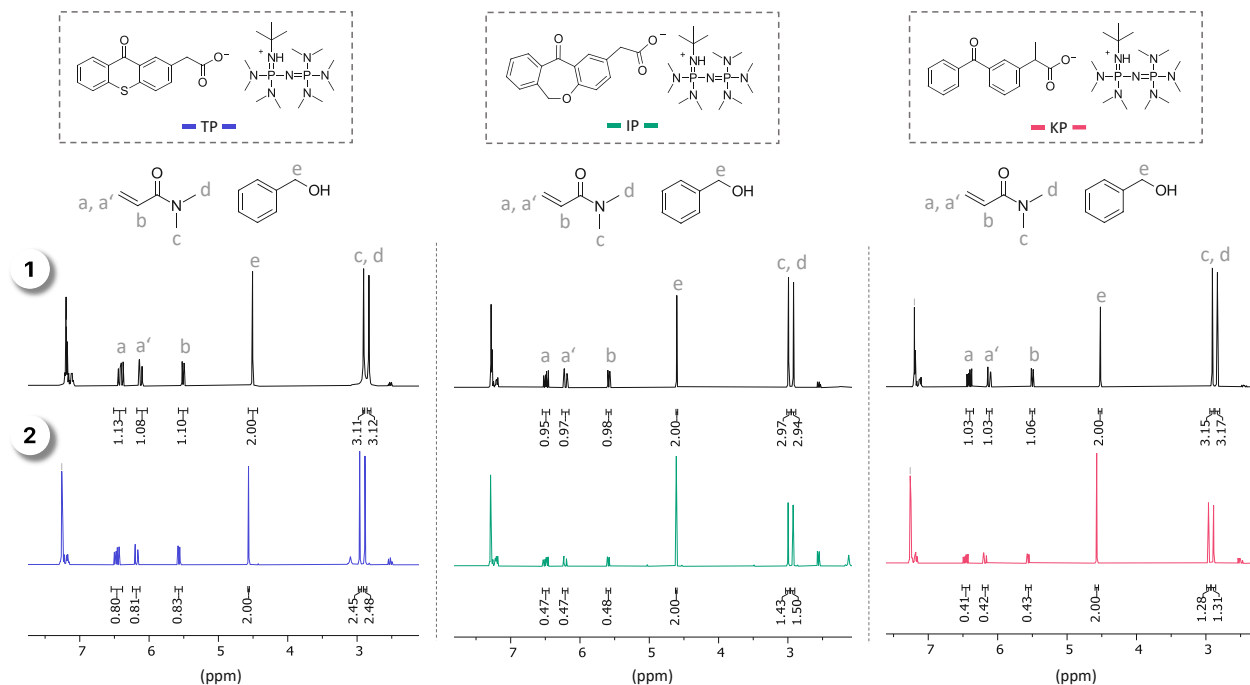
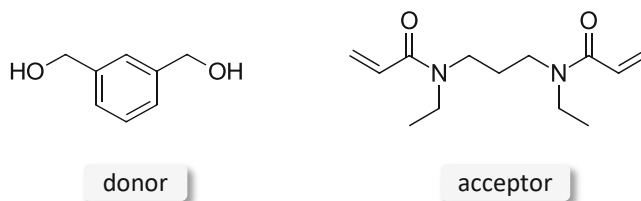


Figure 41:  $^1\text{H}$  NMR spectra of formulations prepared with TP (left), IP (middle), KP (right); 1) pre storage, 2) post storage for 2 weeks at 100 °C

Upon evaluation of their proton signal intensities, however, it becomes evident that the peaks allocated to *N,N*-dimethylacrylamide do not stay intact. In case of TP, a 20 % drop in their intensity is observed. For IP and KP, only half of is detected after storage. This may be linked to potential evaporation of the compound because of its high vapor pressure and subsequent condensation in the screw cap used to seal the employed vial. A further possible explanation for this behavior lies in the susceptibility of *N,N*-dimethylacrylamide to undergo radical homopolymerization, which is favored at elevated temperatures.

## 4. Difunctional system

Building on the successful and optimized monofunctional study for the light sensitive PBG-mediated oxa-Michael reaction, steps towards an extended protocol for the preparation of polymers involving an oxa-Michael addition mechanism were undertaken. This approach comprises the difunctional alcohol (1,3-benzenedimethanol) as the Michael donor and the difunctional acrylamide (*N,N'*-diethyl-1,3-propenebisacrylamide) behaving as the Michael acceptor.



The ability of the three previously introduced PBGs (thioxanthone-based **TP**, isoxepac-based **IP**, and ketoprofen-based reference **KP**) to release the strong P2-*t*-Bu base in a controlled manner upon illumination, therefore initiating the oxa-Michael addition between the diol and bisacrylamide to form poly(ether-amide)s was investigated.

The motivation behind this stems from the broad availability of alcohols as monomers paired with remarkable features such as low toxicity and low odor, thus rendering a broader applicability of the oxa-Michael addition polymerization in a short and straightforward manner possible.

### 4.1 Towards oxa-Michael addition polymerization

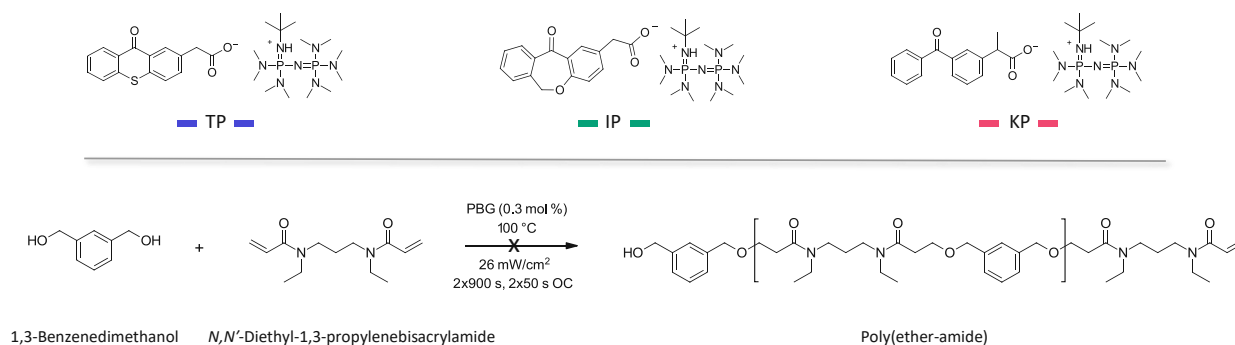
Similar to the monofunctional study, a preliminary round of PBG-mediated oxa-Michael additions was carried out utilizing **TP**, **IP**, and **KP** as initiators. Analogously, a photo-DSC setup with an irradiation source emitting in the range 320-500 nm was employed.

Firstly, 0.3 mol % of the respective PBG was used in an equimolar mixture of 1,3-benzenedimethanol and *N,N'*-diethyl-1,3-propenebisacrylamide and the reactions were carried out at 100 °C for two cycles of 90 s each, combined with two illumination cycles of 50 s at

26 mW cm<sup>-2</sup>. This set of conditions was kept constant for **TP**, **IP**, and **KP**, regardless of the previously determined optimal conditions in order to ensure comparability.

Surprisingly, the initially transparent formulations turned opaque after the measurement. <sup>1</sup>H NMR spectra were measured subsequently after dissolving sample pan contents in CDCl<sub>3</sub>, whereupon incomplete solubility of the reaction performed with the thioxanthone-based **TP** as a PBG was observed, even after ultrasonic bath exposure. Samples of the reactions carried out with the isoxepac-based **IP** and ketoprofen-based **KP**, on the other hand, displayed complete solubility.

Unfortunately, for all three investigated PBGs, no conversion to the targeted oxa-Michael product as a linear polymer was observed upon evaluation of the recorded <sup>1</sup>H NMR spectra (Scheme 18). Following the insolubility hint, as observed in the example of **TP**, it is possible to attribute the unsuccessful oxa-Michael addition to the competing homopolymerization of the bisacrylamide. The light induced PBG cleavage via decarboxylation comprises the intermediate formation of a radical species, which could potentially favor the radical homopolymerization of the double bond containing bisacrylamide. Notably, this behavior was not observed in the monofunctional study, where oxa-Michael product yields extending to 70 % were achieved.

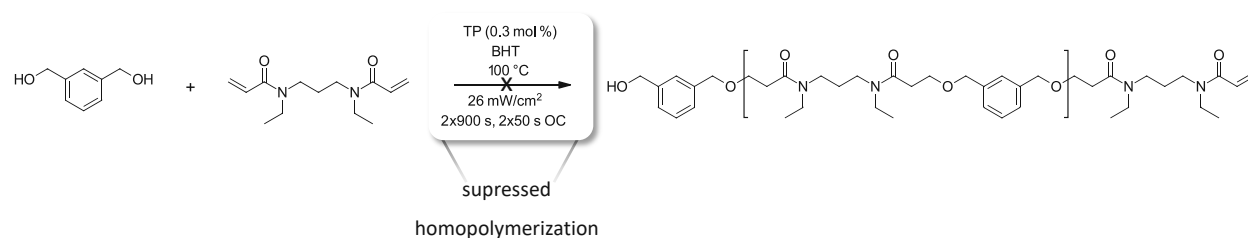


Scheme 18: Oxa-Michael addition polymerization performed with 0.3 mol % PBG (**TP**, **IP**, and **KP**)

To confirm the occurrence of homopolymerization, a formulation composed of only *N,N'*-diethyl-1,3-propylenebisacrylamide and 0.3 mol % **TP** were subjected to the same set of conditions. This afforded a yellow specimen in the shape of the used sample pan, which was insoluble in neither CDCl<sub>3</sub> nor DMSO, which could consequently be assigned to a homopolymer network.



To mitigate the challenge of homopolymerization, a penultimate test experiment employing an equimolar ratio of the diol and bisacrylamide, as well as 0.3 mol % **TP** and butylhydroxytoluol (BHT) as a radical inhibitor (30 mol % of **TP**) (Scheme 19). Although  $^1\text{H}$  NMR spectra indicated yet no oxa-Michael product formation, a complete solubility of the sample pan content in  $\text{CDCl}_3$  was achieved, proving successful suppression of radical species.



Scheme 19: Oxa-Michael addition polymerization performed with 0.3 mol % **TP** and BHT

With the final goal to enhance the reactivity of the system so that an oxa-Michael addition polymerization takes place, a higher PBG loading of 3 mol % (**TP**, **IP**, and **KP**) per formulation was used in combination with BHT as a radical suppresser (30 mol % of the PBG). The ratio of diol and bisacrylamide donor-acceptor pair and the applied reaction conditions were not altered.

Upon evaluation of  $^1\text{H}$  NMR spectra before and after the oxa-Michael addition in  $\text{CDCl}_3$ , which are presented in Figure 42, it was found that utilization of the thioxanthone-based **TP** as a PBG led to successful, although modest conversion to the oxa-Michael product.

The conversion was estimated via comparison of NMR proton signals following a similar approach to the monofunctional study. There are three hints pointing to the same results. Firstly, attention was focused on the double bond conversion of the bisacrylamide. The respective double bond signals between 5 ppm and 7 ppm drop by 15 %. This should correspond to the yield in oxa-Michael polymer, provided that homopolymerization does not occur because of successful radical suppression via BHT.

Further, the second monomer 1,3-benzenedimethanol was taken into consideration. The signal of the two meta-arranged chemically equivalent benzylic  $-\text{CH}_2-$  residues decreases by 12 %, thus suggesting a 12 % conversion to the oxa-Michael product. The newly formed ether bonds between

the diol and bisacrylamide double bonds are shifted upfield, with two broad peaks of nearly same intensities, namely 0.57 ppm. This value can additionally be set in relation to the four protons of the two ether bonds formed per molecule diol, resulting in 14 % oxa-Michael yield.

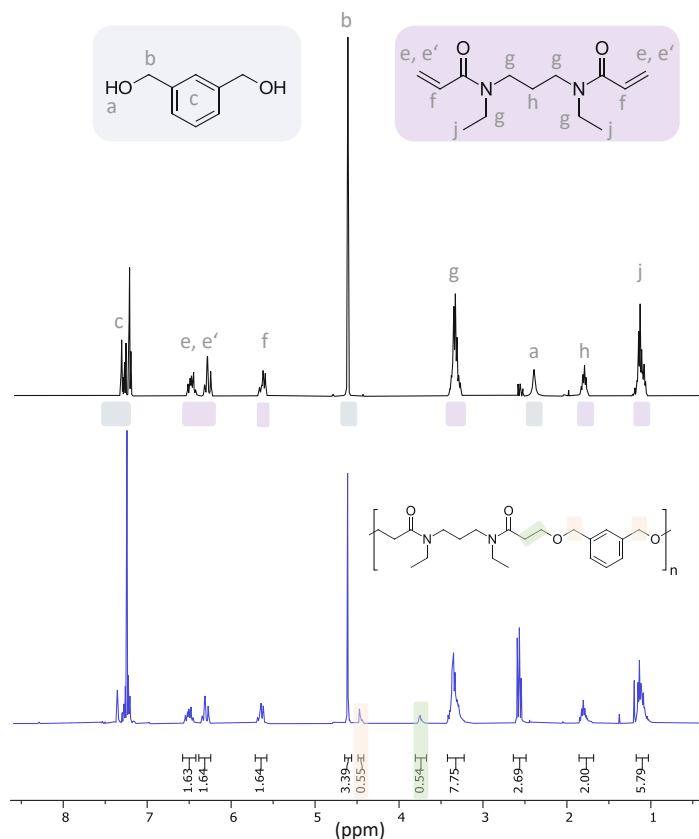
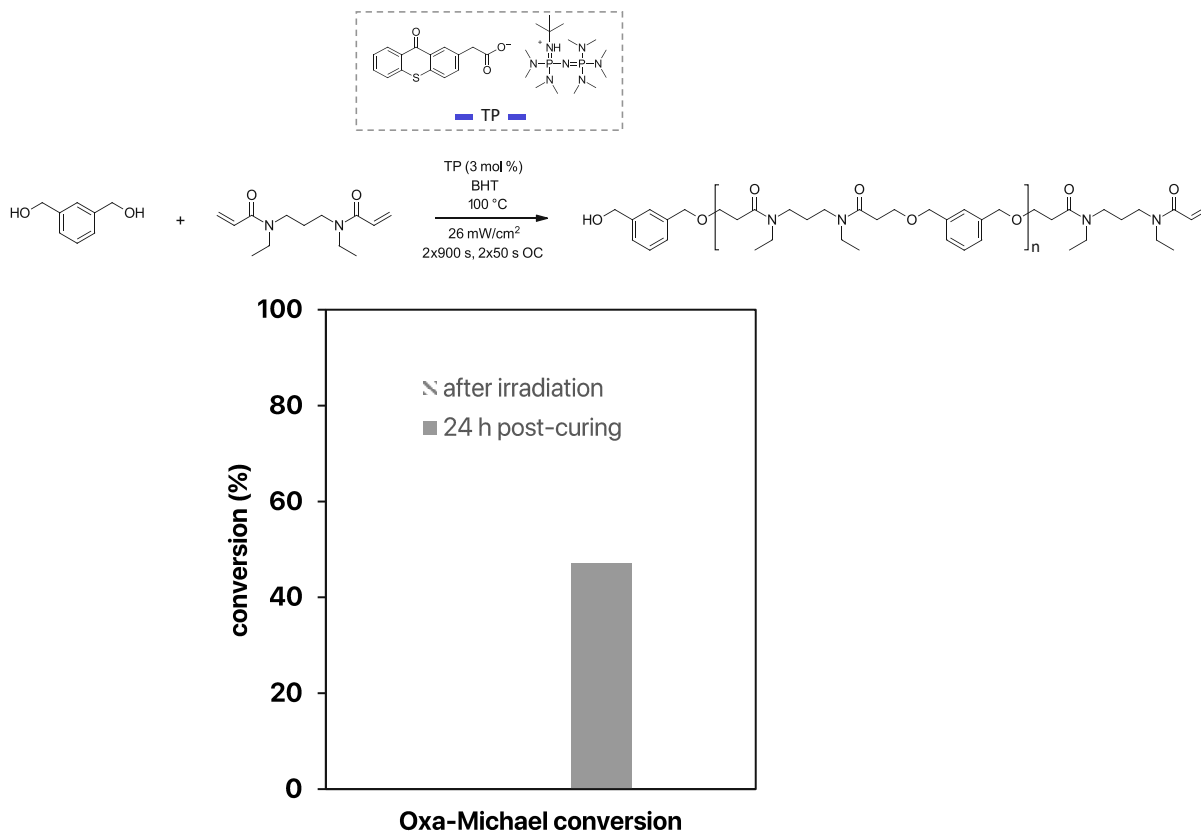


Figure 42: <sup>1</sup>H NMR spectra of the oxa-Michael addition polymerization with **TP**, top: before reaction, bottom: after reaction.

Unfortunately, for the isoxepac-based **IP** and ketoprofen-based **KP**, no conversion was observed, underlining the overall lower performance of these PBG salts compared to the thioxanthone-based **TP** at the given set of reaction conditions.

To explore the possibility of increasing the conversion via post-curing, irradiated photo-DSC oxa-Michael formulations with **TP**, **IP**, and **KP**, were placed in an oven at 100 °C overnight.

Notably, evaluation of the resulting <sup>1</sup>H NMR spectrum for the **TP**-mediated addition revealed quite interesting results. A remarkable increase in oxa-Michael polymer yield amounting to almost 50 % was calculated, displaying the positive effect of post-curing (Scheme 20).



Scheme 20: Post-curing effect on the conversion to the oxa-Michael linear polymer conversion using **TP** as a PBG

Polymerizations performed with **IP** and **KP**, however, do not profit from this, as they still remained unreacted and did not hit the mark as envisioned. However, reporting these preliminary results may be seen as a step forward to unfold new areas where further investigations should be focused.

## Experimental part

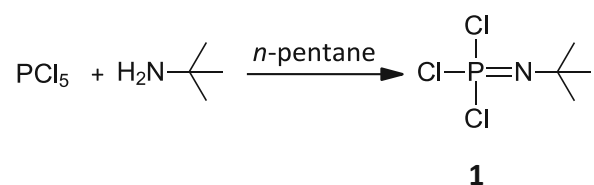
### 1. Synthesis

#### 1.1 Phosphazene superbase

##### 1.1.1 First P-fragment

##### 1.1.1.1 The *n*-pentane route

The synthesis was performed in accordance with literature.<sup>63</sup> Dry *n*-pentane was stored over molecular sieves prior to use. Water content determination via Karl Fischer titration resulted in 21.27 ppm.



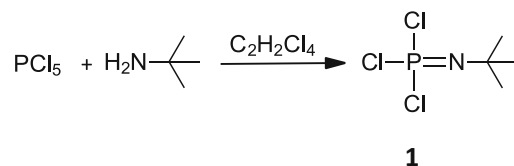
In a three-necked flask, equipped with an Ar-inlet and dropping funnel, PCl<sub>5</sub> (3.15 g, 15.2 mmol, 1 equiv.) was suspended in 75 mL of *n*-pentane. Then, a solution of *t*-butylamine (5.2 mL, 49 mmol, 3 equiv.) in 15 mL of *n*-pentane was added dropwise over a period of 30 min while the mixture was cooled with an ice bath, whereupon gas formation was observed. The cloud-white suspension was refluxed under Ar-atmosphere for 1.5 h and stirred overnight at rt. The mixture was then filtered over a Schlenk frit and washed with *n*-pentane, leading to a clear liquid. An NMR sample of the crude material was measured in CDCl<sub>3</sub>.

The crude product was then purified by fractioned distillation in vacuo under inert conditions. At around 700 mbar and 30 °C (oil bath temperature), pentane was distilled off of the mixture. However, at 400 mbar and 40 °C the pentane fraction as well as the liquid sump residue disappeared completely, suggesting that *n*-pentane, as well as other species with high vapor pressures had been already collected into the pump without prior condensation in the distillation apparatus. The experiment was repeated again following the same procedure with no major changes in parameters. The filtrate was obtained as a clear liquid, similar to the previous

experiment. Distillation led to no product isolation. An NMR analysis of the significantly reduced amount of the liquid residue in the sump flask was performed in  $\text{CDCl}_3$ .

#### 1.1.1.2 The tetrachloroethane route

The synthesis was adapted from literature.<sup>64</sup>



In a three-necked flask equipped with an Ar-inlet and condenser, *t*-butylamine (3.58 equiv., 49 mmol, 5.11 mL) was dissolved in 40 mL 1,1,2,2-tetrachloroethane. Subsequently,  $\text{PCl}_5$  (1 equiv., 19 mmol, 4 g) was added via a solid addition tube over a 15 min timeframe. The mixture was then allowed to stir for 1 h at rt and then warmed to 80-100 °C for further 6 h. This afforded a clear solution with a suspended turbid upper layer, which was insoluble in neither  $\text{CDCl}_3$  nor  $(\text{CD}_3)_2\text{CO}$ . An NMR sample of the soluble crude was measured in  $\text{CDCl}_3$ , confirming the presence of the desired product, along with two other unidentifiable phosphorous species.

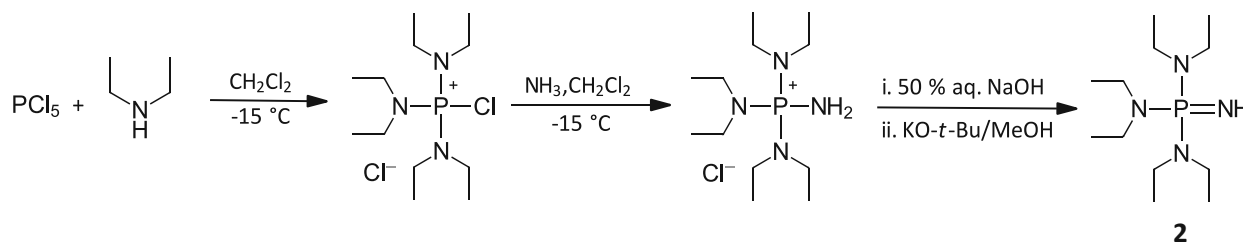
The crude mixture was distilled in vacuo under Ar atmosphere. Thereupon, three fractions were collected between 60 and 80 °C at 100 mbar, 70 mbar, and minimum pressure, i.e., 30 mbar, respectively. In all three fractions, the presence of the solvent and product could be detected in the recorded  $^1\text{H}$  NMR spectrum.

$^1\text{H}$  NMR  $\delta$  (ppm, 400 MHz,  $\text{CDCl}_3$ ): 1.34 (d,  $J = 2.5$  Hz, C-( $\text{CH}_3$ )<sub>3</sub>).

$^{31}\text{P}$  NMR  $\delta$  (ppm, 162 MHz,  $\text{CDCl}_3$ ): 8.94 (s), 4.69 (s), -74.61 (s,  $\text{P}=\text{N}$ ).

### 1.1.2 Second P-fragment

The synthesis was adapted from two reported procedures.<sup>34, 65</sup>



Phosphorous pentachloride (1 equiv., 15 mmol, 3.124 g) was added into a 100 mL three-necked flask equipped with a gas inlet for  $\text{N}_2$  and ammonia and a dropping funnel. Then, 30 mL anhydr. DCM were added in a low temperature methanol bath ( $-15\text{ }^\circ\text{C}$ ). Diethylamine (6.60 equiv, 99 mmol, 10 mL) was added dropwise under careful stirring, whereupon gas formation in the reaction apparatus could be observed. Small portions of liquid  $\text{N}_2$  were added into a cooling bath to avoid temperature elevation. After complete addition of the amine, an orange mixture was obtained. The reaction was allowed to stir at rt for 1h.

The temperature was lowered again at  $-13\text{ }^\circ\text{C}$  and gaseous ammonia was introduced through the gas inlet slightly above the surface of the reaction mixture for 30 min until a white turbidity could be observed, indicating saturation. Afterwards, a faint stream of ammonia was passed through the solution for further 2h at rt. Conversion was confirmed via  $^1\text{H}$  and  $^{31}\text{P}$  NMR analysis in  $\text{CDCl}_3$ , for a sample taken under  $\text{N}_2$  flow, which was filtered through a syringe filter, resulting in a yellow solution.

To examine the stability of the product, an additional NMR tube was charged with 0.1 mL of the crude mixture and allowed to be in contact with atmospheric air for 2h. Then, a drop of distilled water was added, and the thoroughly mixed solution was transferred to an empty NMR tube through a syringe filter and diluted in  $\text{CDCl}_3$ .  $^1\text{H}$  and  $^{31}\text{P}$  NMR spectra were recorded.

Since formation of possible hydrolysis by-products was not observed, two protocols were performed on a 0.25 mL for product isolation and purification (see 1.1.2.1 the NaOH approach and 1.1.2.2 the KO-*t*-Bu/MeOH approach).

Finally, the NaOH route was followed. Insoluble materials were filtered off from the crude mixture and washed with DCM (3 x 5 mL). The resulting orange filtrate was freed from the solvent under reduced pressure, affording a highly viscous orange oil. Subsequently, 30 mL of a 50 % aq. NaOH solution were added, and the mixture was allowed to stir for 1h at rt under ambient conditions. The precipitate was filtered off and the turbid aqueous solution was transferred to a separation funnel and extracted with DCM (3 x 30 mL). The combined organic layers were dried over anhydr. Na<sub>2</sub>SO<sub>4</sub> and concentrated under reduced pressure, yielding 1.706 g (43 %, based on PCl<sub>5</sub>) of the target P1 base as an orange oil.

<sup>1</sup>H NMR δ (ppm, 400 MHz, CDCl<sub>3</sub>): 3.07 (dq, J = 10.2, 7.1 Hz, 12H, -(N-CH<sub>2</sub>)<sub>6</sub>), 1.10 (t, J = 7.1 Hz, 18H, (-CH<sub>2</sub>-CH<sub>3</sub>)<sub>6</sub>).

<sup>31</sup>P NMR δ (ppm, 162 MHz, CDCl<sub>3</sub>): 42.31.

#### 1.1.2.1 The NaOH approach

0.25 mL of the crude mixture (containing 22 mg product, based on theory, 100 % yield) were transferred to an 8 mL vial equipped with a septum screw cap and a magnetic stirring bar. The solvent was removed in vacuo, affording a yellow solid. Upon addition of a 50 % aq. NaOH solution (20 mL) and stirring at rt for 1h, the yellow turbid solution was extracted with DCM. After concentration under reduced pressure of the organic layer, the product was dissolved in CDCl<sub>3</sub>, filtered through a syringe filter into an NMR tube, and <sup>1</sup>H and <sup>31</sup>P NMR spectra were recorded.

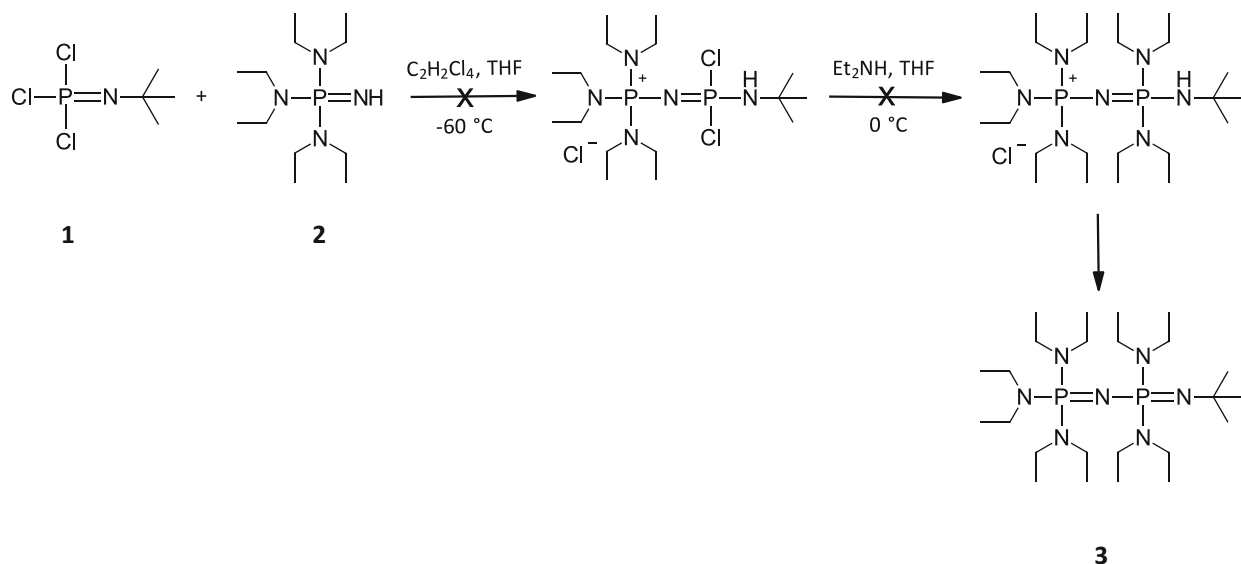
#### 1.1.2.2 The KO-*t*-Bu/MeOH

0.25 mL of the crude mixture (containing 22 mg product, based on theory, 100 % yield) were transferred to an 8 mL vial equipped with a septum screw cap and a magnetic stirring bar. The solvent was removed in vacuo, affording a yellow solid, which was dissolved in 0.5 mL methanol. The solution was stirred over an ice bath, whereupon a solution of 54 mg KO-*t*-Bu in 1 mL of methanol was added dropwise over 10 min. The yellow solution was then allowed to stir overnight at rt under inert atmosphere (Ar balloon).

The mixture was filtered through a syringe filter and transferred to a 10 mL flask with methanol. After evaporation of the solvent under reduced pressure, the obtained orange oil was analyzed via  $^1\text{H}$  and  $^{31}\text{P}$  NMR in  $\text{CDCl}_3$ .

### 1.1.3 Coupling of the two P-fragments

This synthesis was adapted from the reported procedure for the P2-*t*-Bu methylated base according to Schwesinger et al.<sup>34</sup> It was performed in a dry Ar atmosphere using Schlenk techniques.



A three-necked round bottom flask equipped with a septum was charged with the precursor **1** ( $\text{Cl}_3\text{PN-}t\text{-Bu}$ ) in 1,1,2,2-tetrachloroethane under Ar counter flow. A solution of the synthesized P-fragment **2** ( $(\text{Et}_2\text{N})_3\text{PNH}$ ) (9 mmol, 1.612 g) in 5 mL anhydrous THF was added dropwise via a syringe at  $-80\text{ }^\circ\text{C}$  (cooling with liquid  $\text{N}_2$ ). After stirring overnight at  $0\text{ }^\circ\text{C}$ , diethylamine (30 mmol, 2.50 mL) was added dropwise, and the mixture was allowed to stir at  $0\text{ }^\circ\text{C}$  for 2h.

After  $^1\text{H}$  and  $^{31}\text{P}$  NMR measurements, the crude mixture was freed from the solvent in vacuo, affording 7.884 g of a highly viscous orange oil. Further, a LC-MS sample was prepared in a  $\text{H}_2\text{O}$ /acetonitrile solution and measured in a basic C18 column.



### 1.1.3.1 Reaction in THF at 30 °C

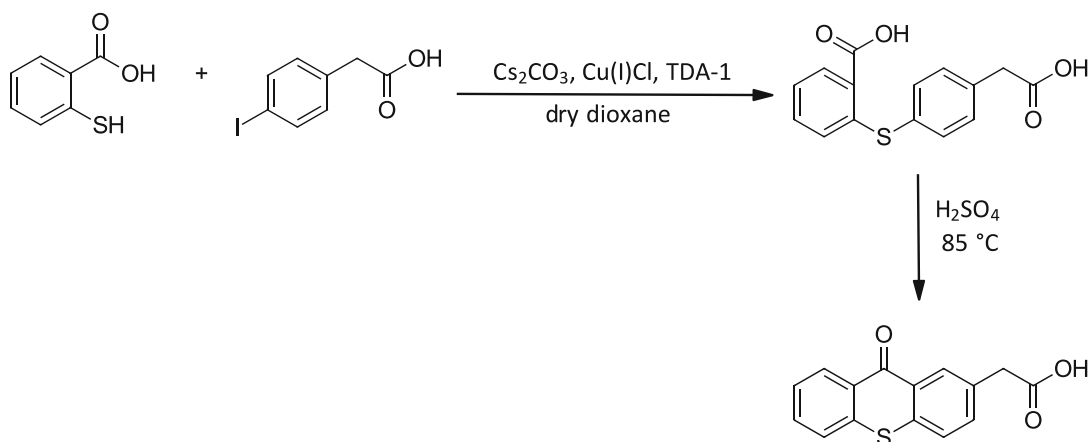
In a screw cap vial equipped with a septum and a magnetic stirring bar, 26.7 mg of the crude mixture were dissolved in 4 mL THF and stirred at 30 °C for 2.5 h under Ar atmosphere. After evaporation of the solvent under reduced pressure, <sup>1</sup>H and <sup>31</sup>P NMR analysis of the resulting orange solid was performed in CDCl<sub>3</sub>.

### 1.1.3.2 Reaction in toluene at 120 °C

50.5 mg of the crude mixture were dissolved in toluene and the solution was allowed to stir overnight at 120 °C. The solvent was removed in vacuo and the obtained orange solid was taken up in CDCl<sub>3</sub> for <sup>1</sup>H and <sup>31</sup>P NMR measurements.

## 1.2 Chromophore

The procedure was adapted from a literature known synthesis of the analog xanthone acetic acid.<sup>62</sup> For the reaction standard Schlenk techniques were applied. The catalyst Cu(I)Cl was manipulated in the glove box.



To a dried Schlenk flask were added thiosalicylic acid (1 equiv., 3 mmol, 0.786 g), 2-(4-iodophenyl)acetic acid (1.5 equiv., 4.5 mmol, 0.694 g), the base Cs<sub>2</sub>CO<sub>3</sub> (3.33 equiv., 10 mmol, 3.258 g) and 30 mL anhydrous dioxane. The slightly yellow solution was allowed to stir at rt for 15 min. Then, TDA-1 (0.13 equiv., 0.4 mmol, 1 mL) was added using a cannula, followed by the addition of Cu(I)Cl (0.26 equiv., 0.8 mmol, 80 mg). The solution was refluxed for 24 h at 130 °C, turning from yellow to green.

The reaction mixture was then transferred to a round bottom flask with dioxane. All volatiles were removed in vacuo, resulting in a light green solid, which was dissolved in 50 mL 0.1 M NaOH. Due to a light turbidity, the mixture was filtered and washed with further 20 mL 0.1 M NaOH. Subsequently, 100 mL of a 1 M HCl solution were added slowly, whereupon the formation of a white turbidity, turning into a forest green color, was observed. The aqueous mixture was then transferred to a separatory funnel and extracted with ethyl acetate (3 x 60 mL). The organic layers were washed with brine, dried over anhydrous Na<sub>2</sub>SO<sub>4</sub>, and concentrated under reduced pressure, affording 0.79 g of the crude intermediate product as a dark orange powder, which was used in the next step without further purification.

<sup>1</sup>H NMR (ppm, 400 MHz, DMSO-d<sub>6</sub>): 7.90 (dd, *J* = 7.8, 1.6 Hz, 1H, H<sub>arom</sub>), 7.63 – 7.52 (m, 1H, H<sub>arom</sub>), 7.50 – 7.44 (m, 2H, H<sub>arom</sub>), 7.40 – 7.36 (m, 2H, H<sub>arom</sub>), 7.19 (td, *J* = 7.5, 1.2 Hz, 1H, H<sub>arom</sub>), 6.72 (dd, *J* = 8.2, 1.1 Hz, 1H, H<sub>arom</sub>), 3.65 (s, 2H, -CH<sub>2</sub>-).

To the intermediate were added 20 mL concentrated H<sub>2</sub>SO<sub>4</sub>, forming a dark brown solution. After heating for 2 h at 100 °C, the mixture was poured over 500 mL distilled water at 0 °C. The turbid green aqueous solution was subsequently extracted with ethyl acetate (4x80 mL) and dried over Na<sub>2</sub>SO<sub>4</sub>. Filtration and concentration under reduced pressure afforded the target compound as an orange solid (0.59 g, 73 %). The product was stored under argon and light exclusion at 4 °C.

TLC analysis: R<sub>f</sub> = 0.2 (LP:EtOAc = 1/4)

m.p. = 198.1-201.3 °C

<sup>1</sup>H NMR δ (ppm, 400 MHz, DMSO-d<sub>6</sub>): 12.49 (s, 1H, -COOH), 8.48 (dd, *J* = 8.2, 1.5 Hz, 1H, H<sub>arom</sub>), 8.38 (d, *J* = 2.0 Hz, 1H, H<sub>arom</sub>), 7.89 – 7.74 (m, 2H, H<sub>arom</sub>), 7.69 (dd, *J* = 8.3, 2.0 Hz, 1H, H<sub>arom</sub>), 7.64 – 7.56 (m, 1H, H<sub>arom</sub>), 3.80 (s, 2H, -CH<sub>2</sub>-).

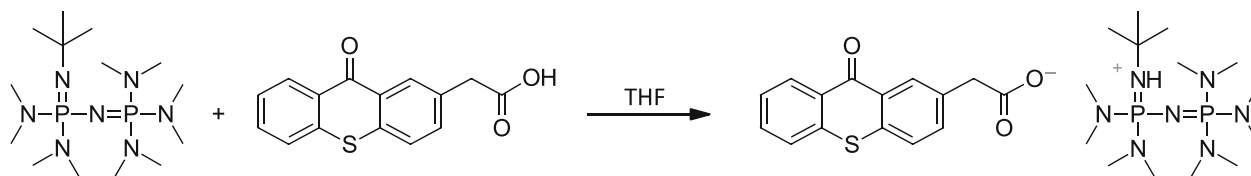
<sup>13</sup>C NMR δ (ppm, 101 MHz, DMSO-d<sub>6</sub>): 178.74 (C=O, chromophore), 172.40 (C=O, carboxylic), 136.56 (C-S, C<sub>arom</sub>), 134.82 (C-S, C<sub>arom</sub>), 134.51; 134.03; 132.97; 129.64; 129.11; 128.34; 128.17; 126.77; 126.60; 126.50 (C<sub>arom</sub>), 40.20 (-CH<sub>2</sub>-).

## 1.3 PBGs

### 1.3.1 Thioxanthone-based TP

The thioxanthone-based **TP** salt was prepared in alignment with a literature known procedure.<sup>29</sup>

In a dried 25 mL round-bottom flask, (10-oxa-9-thia-3-anthryl)acetic acid (1 equiv., 0.5 mmol, 0.135 g) was dissolved in 2.5 mL anhydrous THF, resulting in an orange solution. Then, P2-*t*-Bu (1 equiv., 0.5 mmol, 0.25 mL, 2 M in THF) was added via a cannula and the solution was allowed to stir for 1 h at rt. The solvent was removed using the high vacuum pump. The resulting product was characterized via <sup>1</sup>H and <sup>31</sup>P NMR in acetone-d<sub>6</sub>.



The dark orange photobase was stored under Ar in the dark at 4 °C and used without further purification.

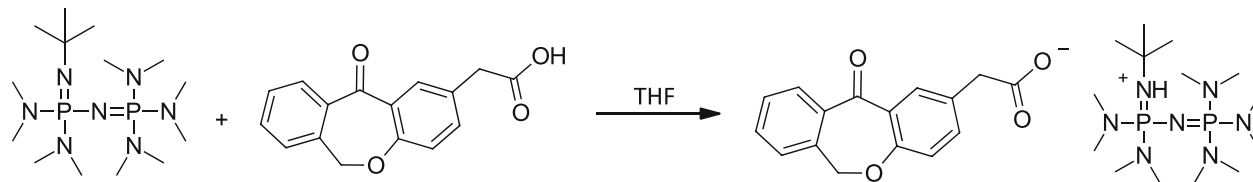
<sup>1</sup>H NMR δ (ppm, 400 MHz, acetone-d<sub>6</sub>): 8.56 – 8.52 (m, 1H, H<sub>arom</sub>), 8.46 (dt, *J* = 2.1, 0.7 Hz, 1H, H<sub>arom</sub>), 7.82 (dd, *J* = 8.3, 2.0 Hz, 1H, H<sub>arom</sub>), 7.73 – 7.70 (m, 2H, H<sub>arom</sub>), 7.58 – 7.50 (m, 2H, H<sub>arom</sub>), 3.48 (s, 2H, -CH<sub>2</sub>-), 2.75 (s, 10H, N-CH<sub>3</sub>, -NH), 2.73 (s, 9H, N-CH<sub>3</sub>), 2.71 (s, 6H, N-CH<sub>3</sub>), 2.68 (s, 6H, N-CH<sub>3</sub>), 1.31 (d, *J* = 0.8 Hz, 9H, C-(CH<sub>3</sub>)<sub>3</sub>).

<sup>31</sup>P NMR δ (ppm, 162 MHz, acetone-d<sub>6</sub>): 17.86, 17.43, 11.73, 11.31.

### 1.3.2 Isoxepac-based IP

The isoxepac-based **IP** salt was prepared according to a reported procedure.<sup>29</sup>

To a 10 mL dried flask, 2-(11-oxo-6,11-dihydrodibenzo[*b,e*]oxepin-2-yl)acetic acid (isoxepac) (1 equiv., 0.5 mmol, 0.135 g) was added and dissolved in 1.5 mL anhydrous THF. Then, P2-*t*-Bu (1 equiv., 0.5 mmol, 0.25 mL, 2M in THF) was added via a syringe. The mixture was stirred for 1 h at rt. Evaporation of the solvent using high vacuum afforded the target compound as a milky white viscous liquid, which was analyzed via <sup>1</sup>H and <sup>31</sup>P NMR in acetone-d<sub>6</sub>.



The photobase was stored at 4 °C under Ar and light exclusion and used without further purification.

$^1\text{H}$  NMR  $\delta$  (ppm, 400 MHz, acetone- $d_6$ ): 8.07 – 8.03 (m, 1H,  $\text{H}_{\text{arom}}$ ), 7.84 (dt,  $J = 7.5, 0.9$  Hz, 1H,  $\text{H}_{\text{arom}}$ ), 7.64 – 7.56 (m, 2H,  $\text{H}_{\text{arom}}$ ), 7.53 – 7.47 (m, 2H,  $\text{H}_{\text{arom}}$ ), 6.89 (d,  $J = 8.4$  Hz, 1H,  $\text{H}_{\text{arom}}$ ), 5.23 (s, 2H,  $-\text{CH}_2-$ ), 2.71 (dd,  $J = 18.7, 10.2$  Hz, 3H,  $\text{N}-\text{CH}_3, -\text{NH}-$ ), 1.30 (d,  $J = 0.8$  Hz, 9H,  $\text{C}-(\text{CH}_3)_3$ ).

$^{31}\text{P}$  NMR  $\delta$  (ppm, 162 MHz, acetone- $d_6$ ): 17.67, 17.26, 12.04, 11.62.

## 2. Characterization

### 2.1 Thermogravimetric analysis (TGA)

The thioxanthone-based **TP** and isoxepac-based **IP** were subjected to TGA measurements. The samples were weighted into aluminum DSC pans and covered with a lid. A temperature ramp from 25 °C to 400 °C for **TP** and to 300 °C for **IP** was performed with a heating rate of 10 K  $\text{min}^{-1}$  and  $\text{N}_2$  (constant flow rate, 40 mL  $\text{min}^{-1}$ ) was used as a measurement atmosphere. The mass loss signal was recorded over time.

The TGA measurement of the reference ketoprofen-based **KP** was retrieved from previous work performed in our laboratory.<sup>61</sup> A temperature ramp program from 25 °C to 300 °C with a heating rate of 5 K  $\text{min}^{-1}$  was performed under a  $\text{N}_2$  measuring atmosphere (constant flow rate, 40 mL  $\text{min}^{-1}$ ).

### 2.2 Storage stability

The prepared PBG salts, namely the thioxanthone-based **TP** and isoxepac-based **IP**, which were stored under light exclusion and Ar atmosphere at 4 °C, were tested regarding their stability via NMR measurements in acetone- $d_6$ . NMR signals of spectra recorded after 6 months (**TP**) or even

9 months (**IP**) were compared to the measurements performed directly after synthesis to detect possible PBG equilibrium shift.

For the reference ketoprofen-based **KP**,  $^1\text{H}$  NMR spectral data were retrieved from already performed measurements in our laboratory directly after synthesis.<sup>61</sup> Proton signals were compared to an  $^1\text{H}$  NMR spectrum acquired approximately after 2 years of storage within the context of this work.

### 2.3 UV/Vis spectroscopy

The two synthesized PBGs, thioxanthone-based **TP** and isoxepac-based **IP** were dissolved in anhydrous THF and diluted to form four solutions at different concentrations, as presented in Table 3 and Table 4. Subsequently, the solutions were placed into quartz cuvettes of 10 mm optical path length to record their absorption spectra. Dry THF was applied as a background measurement. The molar extinction coefficients were calculated from the maximum absorbance at a given wavelength using the Lambert-Beer law.

Table 3: Concentrations of **TP** solutions in THF for UV/Vis measurements

TP solution	1	2	3	4
c (mol/L)	$4.76 \cdot 10^{-3}$	$4.76 \cdot 10^{-4}$	$4.76 \cdot 10^{-5}$	$0.95 \cdot 10^{-5}$

Table 4: Concentrations of **IP** solutions in THF for UV/Vis measurements

IP solution	1	2	3	4
c (mol/L)	$5.85 \cdot 10^{-3}$	$5.85 \cdot 10^{-4}$	$1.17 \cdot 10^{-5}$	$1.17 \cdot 10^{-5}$

For the reference ketoprofen-based **KP**, a  $0.99 \cdot 10^{-4}$  mol/L solution in anhydrous THF was prepared and measured analogously to **TP** and **IP**.

### 3. Monofunctional system

#### General procedure

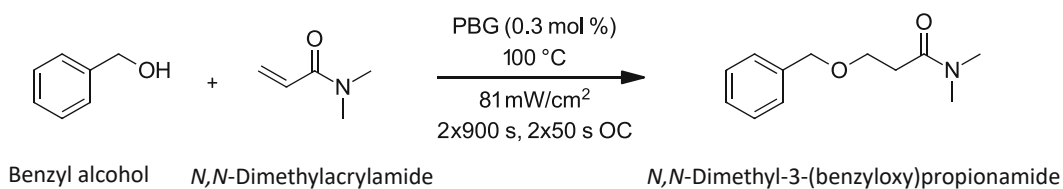
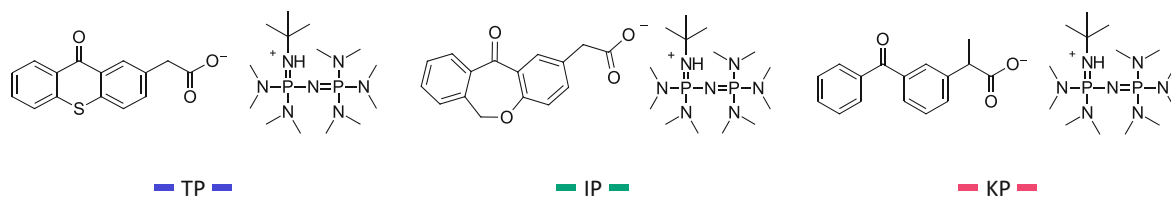
All oxa-Michael addition reactions were carried out in a photo-DSC setup coupled with an Omnicure light source equipped with a 200 W Hg and glass fiber light wave guides. Calibration via an Omnicure R2000 radiometer was executed prior to each measurement, whereupon the intensity light source (320 to 500 nm) was set to the desired luminous energy per second and surface unit (expressed in  $\text{mW cm}^{-2}$ ). Approximately 20 mg of each formulation was weighed into a 25  $\mu\text{L}$  aluminum crucible and sealed with a glass lid.

Except for the preliminary studies, every experiment was performed in triplets for ensuring reproducibility. All reactions were carried out under  $\text{N}_2$ -atmosphere at a 20  $\text{mL min}^{-1}$  flow rate at a constant given temperature with 2x50 s light exposure and an overall reaction time of 2x900 s. Light with wavelengths below 520 nm was excluded during preparation and measurement of all formulations.

For the conversion evaluation, the content of each sample pan after reaction was dissolved in  $\text{CDCl}_3$  and  $^1\text{H}$  NMR spectra were recorded. For all conversions calculated for the screening series according to  $^1\text{H}$  NMR, Tables S1-S9 in the appendix are to be consulted.

#### 3.1 Preliminary studies

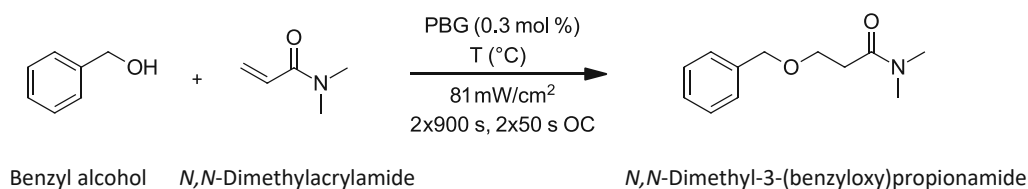
Three formulations, each composed of benzyl alcohol and *N,N*-dimethylacrylamide in an equimolar ratio as well as 0.3 mol % of either the thioxanthone-based **TP**, isoxepac-based **IP** or ketoprofen-based **KP** as an initiator were irradiated with an intensity of  $81 \text{ mW cm}^{-2}$  at a constant temperature of 100 °C following the general procedure (Chapter 3). Evaluation of  $^1\text{H}$  NMR spectra gave a 68 %, 30 %, and 19 % conversion for **TP**, **IP**, and **KP**, respectively.



## 3.2 Optimization

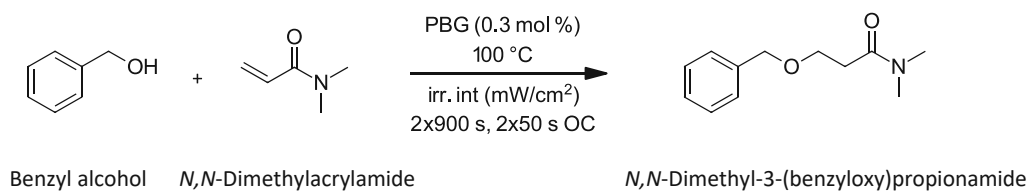
### 3.2.1 Temperature screening

Oxa-Michael additions were performed in agreement with the general procedure employing an equimolar mixture of benzyl alcohol and *N,N*-dimethylacrylamide and 0.3 mol % of the respective PBG (**TP**, **IP**, and **KP**). For each system, the temperature was varied between 25, 60, 80, and 100 °C. The samples were illuminated with an intensity of 81 mW cm<sup>-2</sup>.



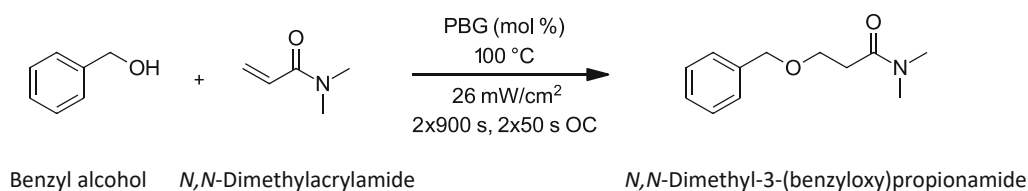
### 3.2.2 Irradiation intensity screening

Oxa-Michael additions were investigated in agreement with the general procedure with equimolar concentrations of benzyl alcohol and *N,N*-dimethylacrylamide and for each investigated series, 0.3 mol % loadings of **TP**, **IP**, and **KP**. Experiments were conducted at 100 °C and the intensity of the light source was altered between 26 to 108 mW cm<sup>-2</sup> for **TP**, or further extended to 140 mW cm<sup>-2</sup> for **IP** and **KP**.



### 3.2.3 PBG concentration screening

Oxa-Michael additions were carried out in accordance with the general procedure using benzyl alcohol and *N,N*-dimethylacrylamide in an equimolar ratio whilst testing different **TP**, **IP**, and **KP** concentrations, i.e. 0.1, 0.3, 0.5, 1.0, and 1.2 mol %. The reaction temperature was kept constant at 100 °C and the irradiation intensity was set at 26 mW cm<sup>-2</sup>.



### 3.3 Formulation storage stability

Similar to the procedure for the oxa-Michael addition reaction, three formulations were prepared with an equimolar ratio of benzyl alcohol and *N,N*-dimethylacrylamide as well as 0.3 mol % of each investigated PBG, namely the thioxanthone-based **TP**, isoxepac-based **IP**, and reference ketoprofen-based **KP** under exclusion of light (orange-light lab) in brown glass vials equipped with closed-top screw caps.

They were subsequently placed in an oven at constant 100 °C and stored for a 2 weeks period. Thereafter, they were dissolved in CDCl<sub>3</sub> and again subjected to <sup>1</sup>H NMR analysis. The thus obtained data was compared to the spectra of each formulation prior to storage. Loss of the reagent *N,N*-dimethylacrylamide upon storage was evaluated via integral decrease of double bond proton signals after storage.



## 4. Difunctional system

### General procedure

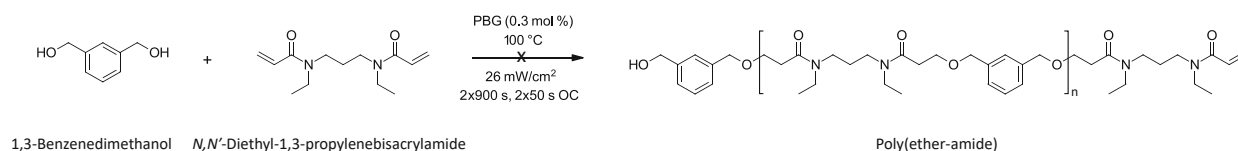
The oxa-Michael addition polymerizations were carried out in compliance with the monofunctional system in a photo-DSC set up utilizing an Omnicure light source with a 200 W Hg broadband lamp. Similarly, the irradiation source was calibrated prior to each measurement sequence via an Omnicure R2000 radiometer. Approximately 20 mg of each prepared formulation was weighed into a 25  $\mu$ L aluminum crucible, which was then sealed with a glass lid. Light with wavelengths below 520 nm was excluded during preparation and measurement of all formulations (orange light lab).

All reactions were carried out under  $N_2$ -atmosphere at a 20 mL  $min^{-1}$  flow rate at a constant given temperature with 2x50 s light exposure at an intensity of 26 mW  $cm^{-2}$  and an overall reaction time of 2x900 s at 100  $^{\circ}C$ .

### 4.1 Towards oxa-Michael addition polymerization

#### 1<sup>st</sup> preliminary round

The first round of photopolymerizations was carried out using all three PBGs (thioxanthone-based **TP**, isoxepac-based **IP**, and ketoprofen-based **KP**) at a 0.3 mol % loading together with an equimolar ratio of 1,3-benzenedimethanol and *N,N'*-diethyl-1,3-propylenebisacrylamide. Heating via a heat-gun and ultrasonic bath cycles of 5 min each were applied to ensure homogeneously mixed formulations. The clear formulations were then subjected to photo-DSC measurements.



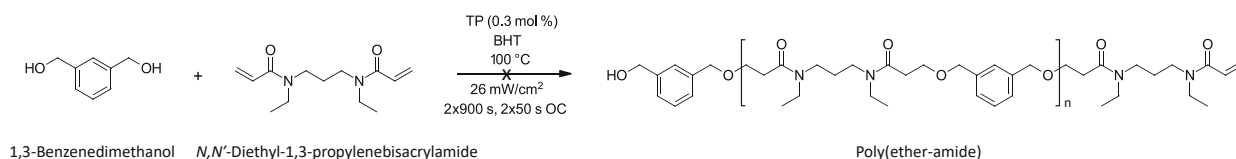
Sample pan contents were dissolved in  $CDCl_3$  for  $^1H$  NMR analysis. In case of the **TP**-mediated addition, incomplete solubility was observed.  $^1H$  NMR spectra showed no conversion for all three PBGs.

## Homopolymerization of bisacrylamide

The homopolymerization of *N,N'*-diethyl-1,3-propenebisacrylamide in presence of the **TP** PBG was tested out in an experiment employing the bisacrylamide and 0.3 mol % TP. The photo-DSC measurement afforded a yellow polymer which displayed no solubility in CDCl<sub>3</sub> and DMSO.

## Radical suppression with BHT

A further formulation for an oxa-Michael addition polymerization was prepared with **TP** PBG (0.3 mol %), followed by addition of BHT as a radical suppressor (30 mol % of **TP**), and an equimolar mixture of 1,3-benzenedimethanol and *N,N'*-diethyl-1,3-propenebisacrylamide. Heating via a heat-gun and ultrasonic bath cycles of 5 min each were applied to ensure homogeneously mixed formulations.

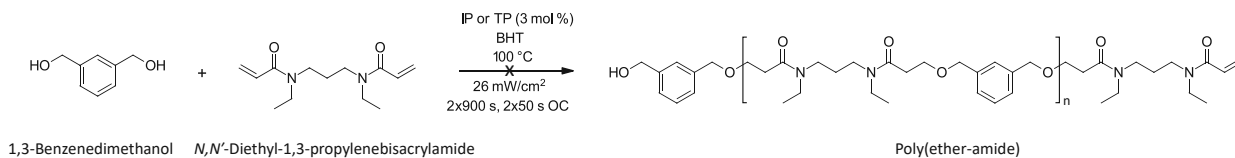
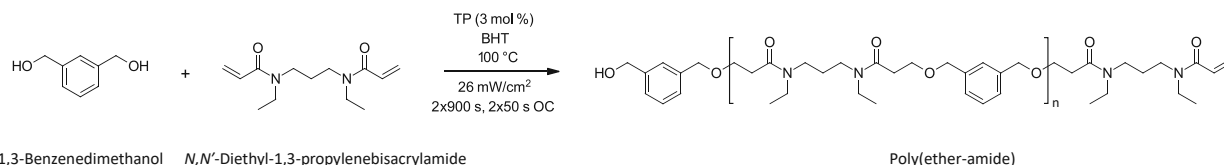


The transparent sample obtained after photo-DSC measurement was fully dissolved in CDCl<sub>3</sub> for <sup>1</sup>H NMR analysis. No conversion was observed in the respective <sup>1</sup>H NMR spectra.

## Final attempt

Three formulations were prepared in duplicates with 3 mol % of the initiators (**TP**, **IP**, and reference **KP**), BHT (30 mol % of the respective PBG), and an equimolar ratio of the Michael donor-acceptor pair 1,3-benzenedimethanol and *N,N'*-diethyl-1,3-propenebisacrylamide.

After complete photo-DSC measurements, the first half of the samples was subjected to <sup>1</sup>H NMR analysis in CDCl<sub>3</sub>. The **TP**-mediated addition polymerization yielded 14 % oxa-Michael product, calculated via NMR proton signals. No conversion was obtained for **IP** and **KP**.



The second half of the sample pans was stored in brown glass vials sealed with screw caps in an oven at 100 °C overnight for post-curing. Then,  $^1\text{H}$  NMR spectra were recorded after dissolving the contents in  $\text{CDCl}_3$ . For the **TP**-mediated addition polymerization, 50 % conversion to the oxamichael product was calculated. Samples comprising **IP** and **KP** displayed no conversion according to their  $^1\text{H}$  NMR spectra.

## Conclusions

The aim of this thesis is developing new photo base generators (PBGs) based on the generation of a basic active species upon light-triggered photodecarboxylation. PBGs represent an intriguing alternative to conventional radical or even acid counterparts, due to the long list of advantages that comes with their use, e.g. insensitivity towards oxygen, a potentially broad scope of compatible monomers, generally lower susceptibility of the final material to experience volume shrinkage after irradiation, as well as no corrosion of metallic substrates. Following up on recent reports demonstrating their feasibility when employing strong bases, e.g. amidines and guanidines, it is a logical step to design new PBGs with a wider variety of both bases and chromophores.

Firstly, attempts towards the synthesis of a modified phosphazene P2-*t*-Bu superbase were made. The designed structure replaces methyl residues of the commercially available Schwesinger base with ethyl branches (Figure 43), hence substituting gaseous dimethylamide with liquid diethylamine as a reagent, aiming for a safer synthesis in a lab-scale. Despite completing the synthesis of the first two phosphorous-based building blocks, the final coupling reaction to give the desired ethylated P2-*t*-Bu proved to be unsuccessful.

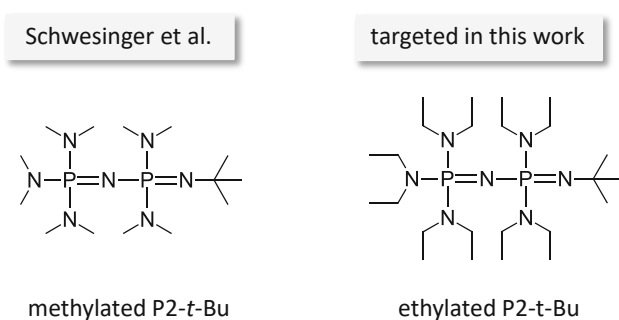


Figure 43: Schwesinger phosphazene P2-*t*-Bu and its ethylated homologue

As far as the chromophoric structures were concerned, thioxanthone acetic acid was targeted because of its ability to absorb high wavelengths, hence avoiding harmful UV light. Previous work in our laboratory had disclosed that its literature-known synthesis delivered a mixture of two possible isomers, with the acetic acid group positioned in a meta- or para-arrangement to the

chromophoric ketone, whereas the latter is photoinactive. This gap was successfully bridged in this thesis via demonstration of a new route based on a copper-catalyzed Ullmann coupling reaction, affording the isomeric-pure thioxanthone acetic acid at a high yield (Figure 44).

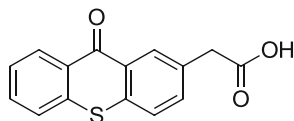


Figure 44: Structure of the thioxanthone acetic acid

Two new PBGs corresponding to the commercially obtained P2-*t*-Bu superbase were prepared as salts. The first one, **TP**, employed the synthesized thioxanthone acetic acid, whereas for the second PBG, namely **IP**, a structurally similar chromophore known as isoxepac was used. A ketoprofen-based analogous PBG (**KP**) was used as a reference for comparison (Figure 45).

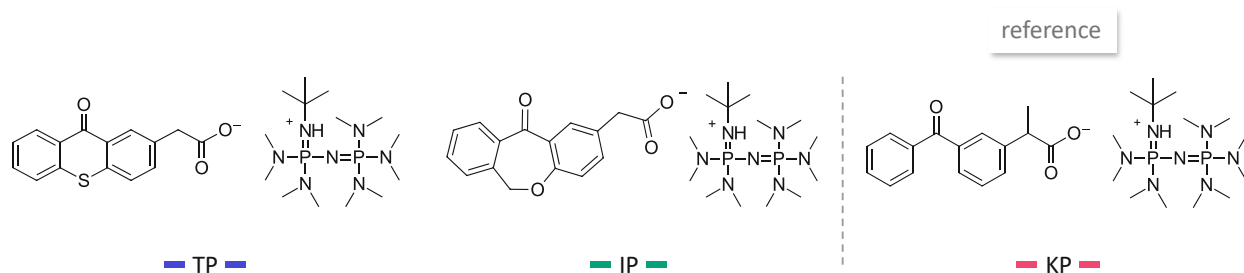


Figure 45: The two synthesized PBGs (**TP**, **IP**) and the reference **KP**

Thermogravimetric analysis (TGA) of both thioxanthone-based **TP** and isoxepac-based **IP** showed a thermal decomposition starting from temperatures as high as 170 °C or 200 °C, respectively. Further, their absorption patterns were studied via UV/Vis spectroscopy, revealing quite remarkable results. Notably, **TP** absorbs at a maximum of 386 nm, which corresponds to blue light with an excellent molar extinction coefficient of 9937 L mol<sup>-1</sup> cm<sup>-1</sup> at the same wavelength. The absorbance of **IP**, on the other hand, reaches its maximum at 348 nm, where the extinction coefficient amounts to 2863 L mol<sup>-1</sup> cm<sup>-1</sup>.

The long-time storage stability of **TP** and **IP** was additionally investigated via <sup>1</sup>H NMR analysis. In case of the **TP** salt, an equilibrium shift to the free base resulting from partial photocleavage of

the thioxanthone acetic acid of up to 12 % could be determined. For **IP**, no equilibrium shift was observed.

The applicability of **TP**, **IP**, and reference **KP** was demonstrated via an oxa-ene Michael addition model system in a photo-DSC setup, comprising a benzyl alcohol as the Michael donor and an electron-deficient  $\alpha,\beta$ -unsaturated acrylamide (Figure 46).

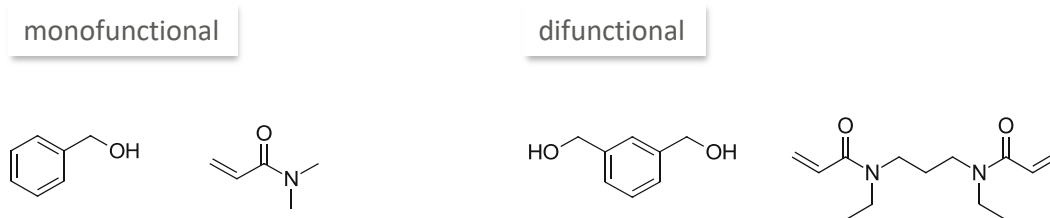


Figure 46: Monofunctional and difunctional donor-acceptor pairs for the Oxa-Michael addition

First, a monofunctional study was conducted, where **TP** outperformed the other two PBGs in terms of conversion to the oxa-Michael ether product with yields extending to 70 %. The impact of temperature, irradiation screening, and PBG concentration was then assessed. In line with our observations in Chapter 3, performing the addition reaction at 100 °C was necessary for satisfactory product formation. Remarkably, a mild irradiation intensity of only 26 mW cm<sup>-2</sup> proved to be enough to set the photocleavage in motion in case of **TP** and **IP**, however insufficient for **KP**. Altering of PBG concentration revealed that a comparably low loading of only 0.3 mol % **TP** amounts to the best oxa-Michael conversion. For **IP**, at least 0.5 mol % were required to achieve comparable results, whereas even 1.0 mol % of **KP** could only afford less than one third of the yield obtained with **TP**.

Finally, attempts towards extending this methodology to a difunctional system were undertaken with the prospect of introducing the light-induced PBG-mediated synthesis linear poly(ether-amide)s. In a preliminary round, the utility of **TP** could be demonstrated, while also showing post-curing behavior when stored at 100 °C overnight. **IP** and the reference **KP**, on the other hand, deem further extensive investigations necessary. This work carried out with this thesis, however, adds a fundamental contribution in the relatively uncharted field of PBGs and lays the groundwork for further research effort.

## Materials and methods

All chemicals were purchased from commercial suppliers and, unless otherwise noted, used without further purification.

Thin layer chromatography (TLC) analysis was performed on aluminum-backed unmodified Merck silica gel 60 F<sub>245</sub> plates and visualization was realized under UV irradiation.

Flash column chromatography was performed on silica gel 60 (40-63  $\mu\text{m}$ ) by hand.

NMR spectroscopy was used to record  $^1\text{H}$ ,  $^{13}\text{C}$  and  $^{31}\text{P}$  NMR spectra on a Bruker Avance UltraShield 400 MHz spectrometer. Chemical shifts ( $\delta$ ) are reported in ppm, using  $\text{Me}_4\text{Si}$  as internal standard. Coupling constants (J) are given in Hertz (Hz) and multiplicities are assigned as s = singlet, d = doublet, t = triplet, q = quartet, and m = multiplet.

Liquid chromatography mass spectroscopy (LC-MS) was carried out on a Nexera X2<sup>®</sup> UHPLC system by Shimadzu. Detection was performed via an SPD-M20A photo diode array, a RF-20Axs fluorescence detector, and ELS-2041 light scattering detector, as well as an LC-MS-2020 mass spectrometer (ESI/APCI). Water/acetonitrile was used as a solvent.

UV/Vis spectroscopy was used for photochemical characterization of the synthesized photoinitiators employing a Lambda 950 device from Perkin Elmer with a PMT detector, using PeakFit v4.12 by SigmaPlot for spectral evaluation. The spectra were recorded using standard 10 mm pathlength quartz cuvettes.

Thermal gravimetric analysis (TGA) was performed on a Netzsch Jupiter STA 449 F1 thermal analysis instrument with an autosampler, which combines differential scanning calorimetry (DSC) with TGA in one measurement. Samples were weighed into DSC aluminum pans and subjected to a temperature ramp measurement (25 °C-300 or 400 °C, at a  $\text{K min}^{-1}$  rate) in a constant  $\text{N}_2$  gas flow (40  $\text{mL min}^{-1}$ ). The obtained data, i.e. the mass loss expressed in weight %, was analyzed with the software Netzsch-Proteus.

Photo-DSC measurements were conducted on a Photo-DSC 204 F1 with autosampler from Netzsch, using 25  $\mu\text{L}$  aluminum crucibles and glass lids. A  $\text{N}_2$  atmosphere at 20  $\text{mL min}^{-1}$  flow rate

was used for all measurements. Light with wavelengths below 520 nm was excluded (orange light lab) during preparation of all formulations. Triplets were measured for each experiment.

An Omnicure 2000 from Lumen Dynamics with a 200 W broadband Hg lamp and glass fiber light waveguides was used as the light source with an emission spectrum spanning a 320-500 nm wavelength range. The calibration of the light intensity was performed prior to each measurement series via Omnicure R2000 radiometer, which provides a calibrated flat output response in a given wavelength range in terms of the luminous energy per second and surface unit.



## Bibliography

- (1) *The History of Protective Coatings*. D&D Coatings, <https://www.ddcoatings.co.uk/3852/history-protective-coatings> (accessed 2024 26 Mar).
- (2) *75 Years in Coating: A Historic Look at the Coatings Industry's Evolution*. Paint & Coatings Industry, <https://www.pcimag.com/articles/110313-75-years-in-coatings-a-historic-look-at-the-coatings-industrys-evolution> (accessed 2024 26 Mar).
- (3) Cavallaro, G.; Milioto, S.; Konnova, S.; Fakhrullina, G. I.; Akhatova, F.; Lazzara, G.; Fakhrullin, R.; Lvov, Y. Halloysite/keratin nanocomposite for human hair photoprotection coating. *ACS applied materials & interfaces* **2020**, *12* (21), 24348-24362.
- (4) Schwalm, R. UV coatings: basics, recent developments and new applications. **2006**.
- (5) Pélissier, K.; Thierry, D. Powder and high-solid coatings as anticorrosive solutions for marine and offshore applications? A review. *Coatings* **2020**, *10* (10), 916.
- (6) Hill, L. W.; Wicks Jr, Z. W. Design considerations for high solids coatings. *Progress in Organic Coatings* **1982**, *10* (1), 55-89.
- (7) Javadi, A.; Cobaj, A.; Soucek, M. D. Commercial waterborne coatings. In *Handbook of waterborne coatings*, Elsevier, 2020; pp 303-344.
- (8) Waterborne Coatings. In *Organic Coatings*, 2017; pp 366-373.
- (9) Kumar, V.; Bhardwaj, Y.; Goel, N.; Francis, S.; Dubey, K.; Chaudhari, C.; Sarma, K.; Sabharwal, S. Coating characteristics of electron beam cured Bisphenol A diglycidyl ether diacrylate-co-aliphatic urethane diacrylate resins. *Surface and coatings technology* **2008**, *202* (21), 5202-5209.
- (10) Khudyakov, I. V. Fast photopolymerization of acrylate coatings: Achievements and problems. *Progress in Organic Coatings* **2018**, *121*, 151-159.
- (11) Dworak, C. Novel concepts for photoinitiating moieties. PhD Thesis, TU Wien, 2009.
- (12) Patil, R. S.; Thomas, J.; Patil, M.; John, J. To Shed Light on the UV Curable Coating Technology: Current State of the Art and Perspectives. *Journal of Composites Science* **2023**, *7* (12), 513.
- (13) Corrigan, N.; Yeow, J.; Judzewitsch, P.; Xu, J.; Boyer, C. Seeing the light: advancing materials chemistry through photopolymerization. *Angewandte Chemie International Edition* **2019**, *58* (16), 5170-5189.
- (14) Yagci, Y.; Jockusch, S.; Turro, N. J. Photoinitiated polymerization: advances, challenges, and opportunities. *Macromolecules* **2010**, *43* (15), 6245-6260.
- (15) Lang, M.; Hirner, S.; Wiesbrock, F.; Fuchs, P. A review on modeling cure kinetics and mechanisms of photopolymerization. *Polymers* **2022**, *14* (10), 2074.
- (16) Gruber, H. F. Photoinitiators for free radical polymerization. *Progress in polymer Science* **1992**, *17* (6), 953-1044.
- (17) Fouassier, J.-P.; Lalevée, J. *Photoinitiators: Structures, Reactivity and Applications in Polymerization*; John Wiley & Sons, 2021.
- (18) Zivic, N.; Kuroishi, P. K.; Dumur, F.; Gignes, D.; Dove, A. P.; Sardon, H. Recent advances and challenges in the design of organic photoacid and photobase generators for polymerizations. *Angewandte Chemie International Edition* **2019**, *58* (31), 10410-10422.
- (19) Kiker, M. T.; Uddin, A.; Stevens, L. M.; Chung, K.-Y.; Lu, P.; Page, Z. A. Visible light activated coumarin photocages: an interplay between radical and organobase generation to govern thiol-ene polymerizations. *Polymer Chemistry* **2023**, *14* (33), 3843-3850.

- (20) Fréchet, J.; Cameron, J.; Chung, C.; Haque, S.; Willson, C. Photogenerated base as catalyst for imidization reactions: a new design of photosensitive polymers. *Polymer Bulletin* **1993**, *30*, 369-375.
- (21) Chemtob, A.; De Paz-Simon, H.; Dietlin, C.; Croutxé-Barghorn, C.; Salmi, H.; Allonas, X.; Chany, A.-C.; Vidal, L.; Rigolet, S. A highly reactive photobase catalytic system for sol-gel polymerization. *Thin solid films* **2014**, *550*, 177-183.
- (22) Zheng, Y.; Yang, Y.; Yang, H.; Han, F.; Li, Z. Thioxanthone-based amidine: An efficient nonionic photobase generator for thiol-based click polymerization under visible LED light. *Progress in Organic Coatings* **2020**, *148*, 105842.
- (23) Noon, A.; Hamieh, T.; Toufaily, J.; Morlet-Savary, F.; Schmitt, M.; Dumur, F.; Lalevée, J. Phenothiazine-based oxime ester as a photobase generator for thiol-acrylate reactions. *European Polymer Journal* **2024**, *204*, 112679.
- (24) Kutal, C.; Willson, C. G. Photoinitiated cross-linking and image formation in thin polymer films containing a transition metal compound. *Journal of the Electrochemical Society* **1987**, *134* (9), 2280.
- (25) Cameron, J. F.; Frechet, J. M. Base catalysis in Imaging Materials. 1. Design and synthesis of novel light-sensitive urethanes as photoprecursors of amines. *The Journal of Organic Chemistry* **1990**, *55* (23), 5919-5922.
- (26) Beecher, J. E.; Cameron, J. F.; Fréchet, J. M. Photogeneration of polymeric amines: synthesis, photocrosslinking and photoimaging of copolymers containing photoactive carbamate pendant groups. *Journal of Materials Chemistry* **1992**, *2* (8), 811-816.
- (27) Chae, K. H. Thermal curing reaction of poly (glycidyl methacrylate) using photogenerated amines from oxime-urethane derivatives. *Macromolecular rapid communications* **1998**, *19* (1), 1-4.
- (28) Salmi, H.; Allonas, X.; Ley, C.; Defoin, A.; Ak, A. Quaternary ammonium salts of phenylglyoxylic acid as photobase generators for thiol-promoted epoxide photopolymerization. *Polymer Chemistry* **2014**, *5* (22), 6577-6583.
- (29) Arimitsu, K.; Endo, R. Application to photoreactive materials of photochemical generation of superbases with high efficiency based on photodecarboxylation reactions. *Chemistry of Materials* **2013**, *25* (22), 4461-4463.
- (30) Yilmaz, G.; Guler, E.; Barlas, F. B.; Timur, S.; Yagci, Y. Polymeric thioxanthenes as potential anticancer and radiotherapy agents. *Macromolecular Rapid Communications* **2016**, *37* (13), 1046-1051.
- (31) Suyama, K.; Shirai, M. Photobase generators: Recent progress and application trend in polymer systems. *Progress in Polymer Science* **2009**, *34* (2), 194-209. DOI: <https://doi.org/10.1016/j.progpolymsci.2008.08.005>.
- (32) Leito, I.; Koppel, I. A.; Koppel, I.; Kaupmees, K.; Tshepelevitsh, S.; Saame, J. Basicity limits of neutral organic superbases. *Angewandte Chemie International Edition* **2015**, *54* (32), 9262-9265.
- (33) Weitkamp, R. F.; Neumann, B.; Stammer, H. G.; Hoge, B. Phosphorus-Containing Superbases: Recent Progress in the Chemistry of Electron-Abundant Phosphines and Phosphazenes. *Chemistry—A European Journal* **2021**, *27* (42), 10807-10825.
- (34) Schwesinger, R.; Schlemper, H.; Hasenfratz, C.; Willaredt, J.; Dambacher, T.; Breuer, T.; Ottaway, C.; Fletschinger, M.; Boele, J.; Fritz, H. Extremely strong, uncharged auxiliary bases;

monomeric and polymer-supported polyaminophosphazenes (P2–P5). *Liebigs Annalen* **1996**, *1996* (7), 1055-1081.

(35) Kárpáti, T.; Veszprémi, T.; Thirupathi, N.; Liu, X.; Wang, Z.; Ellern, A.; Nyulászi, L.; Verkade, J. G. Synthesis and Photoelectron Spectroscopic Studies of N (CH<sub>2</sub>CH<sub>2</sub>NMe) <sub>3</sub> P E (E= O, S, NH, CH<sub>2</sub>). *Journal of the American Chemical Society* **2006**, *128* (5), 1500-1512.

(36) Kolomeitsev, A. A.; Koppel, I. A.; Rodima, T.; Barten, J.; Lork, E.; Röschenthaler, G.-V.; Kaljurand, I.; Kütt, A.; Koppel, I.; Mäemets, V. Guanidinophosphazenes: design, synthesis, and basicity in THF and in the gas phase. *Journal of the American Chemical Society* **2005**, *127* (50), 17656-17666.

(37) Coles, M. P.; Aragón-Sáez, P. J.; Oakley, S. H.; Hitchcock, P. B.; Davidson, M. G.; Maksic, Z. B.; Vianello, R.; Leito, I.; Kaljurand, I.; Apperley, D. C. Superbasicity of a bis-guanidino compound with a flexible linker: a theoretical and experimental study. *Journal of the American Chemical Society* **2009**, *131* (46), 16858-16868.

(38) Vazdar, K.; Margetic, D.; Kovacevic, B.; Sundermeyer, J. r.; Leito, I.; Jahn, U. Design of novel uncharged organic superbases: Merging basicity and functionality. *Accounts of chemical research* **2021**, *54* (15), 3108-3123.

(39) Tokoroyama, T. Discovery of the Michael reaction. Wiley Online Library: 2010.

(40) Loydl, F. Ueber die künstliche Aepfelsäure aus Fumarsäure. *Justus Liebigs Annalen der Chemie* **1878**, *192* (1-2), 80-89.

(41) Ratzenböck, K.; Fischer, S. M.; Slugovc, C. Poly (ether) s derived from oxa-Michael polymerization: a comprehensive review. *Monatshefte für Chemie-Chemical Monthly* **2023**, *154* (5), 443-458.

(42) Hu, J.; Bian, M.; Ding, H. Recent application of oxa-Michael reaction in complex natural product synthesis. *Tetrahedron Letters* **2016**, *57* (50), 5519-5539.

(43) Mather, B. D.; Viswanathan, K.; Miller, K. M.; Long, T. E. Michael addition reactions in macromolecular design for emerging technologies. *Progress in Polymer Science* **2006**, *31* (5), 487-531.

(44) Love, D.; Kim, K.; Domaille, D. W.; Williams, O.; Stansbury, J.; Musgrave, C.; Bowman, C. Catalyst-free, aza-Michael polymerization of hydrazides: polymerizability, kinetics, and mechanistic origin of an  $\alpha$ -effect. *Polymer chemistry* **2019**, *10* (42), 5790-5804.

(45) Podgórski, M.; Chatani, S.; Bowman, C. N. Development of Glassy Step-Growth Thiol-Vinyl Sulfone Polymer Networks. *Macromolecular rapid communications* **2014**, *35* (17), 1497-1502.

(46) Matsuoka, S.-i.; Hoshiyama, Y.; Tsuchimoto, K.; Suzuki, M. Oxa-Michael addition reaction and polymerization of Morita–Baylis–Hillman adducts and derivatives. *Chemistry Letters* **2017**, *46* (12), 1718-1720.

(47) Yu, Y.; Chau, Y. One-step “click” method for generating vinyl sulfone groups on hydroxyl-containing water-soluble polymers. *Biomacromolecules* **2012**, *13* (3), 937-942.

(48) Yang, H.; Zuo, Y.; Zhang, J.; Song, Y.; Huang, W.; Xue, X.; Jiang, Q.; Sun, A.; Jiang, B. Phosphazene-catalyzed oxa-Michael addition click polymerization. *Polymer Chemistry* **2018**, *9* (38), 4716-4723.

(49) Nising, C. F.; Bräse, S. The oxa-Michael reaction: from recent developments to applications in natural product synthesis. *Chemical Society Reviews* **2008**, *37* (6), 1218-1228.

- (50) Thiyagarajan, S.; Krishnakumar, V.; Gunanathan, C. KOtBu-catalyzed Michael addition reactions under mild and solvent-free conditions. *Chemistry—An Asian Journal* **2020**, *15* (4), 518-523.
- (51) Stewart, I. C.; Bergman, R. G.; Toste, F. D. Phosphine-catalyzed hydration and hydroalkoxylation of activated olefins: use of a strong nucleophile to generate a strong base. *Journal of the American Chemical Society* **2003**, *125* (29), 8696-8697.
- (52) Fischer, S. M.; Kaschnitz, P.; Slugovc, C. Tris (2, 4, 6-trimethoxyphenyl) phosphine—a Lewis base able to compete with phosphazene bases in catalysing oxa-Michael reactions. *Catalysis Science & Technology* **2022**, *12* (20), 6204-6212.
- (53) Sarker, A. M.; Kaneko, Y.; Neckers, D. Synthesis of tetraorganylborate salts: photogeneration of tertiary amines. *Chemistry of materials* **2001**, *13* (11), 3949-3953.
- (54) Sarker, A.; Neckers, D. Tetraorganylborate salts as convenient precursors for photogeneration of tertiary amines. *Journal of the Chemical Society, Perkin Transactions 2* **1998**, (10), 2315-2322.
- (55) Jensen, K. H.; Hanson, J. E. Synthesis and photochemistry of tertiary amine photobase generators. *Chemistry of materials* **2002**, *14* (2), 918-923.
- (56) Sun, X.; Gao, J. P.; Wang, Z. Y. Bicyclic guanidinium tetraphenylborate: a photobase generator and a photocatalyst for living anionic ring-opening polymerization and cross-linking of polymeric materials containing ester and hydroxy groups. *Journal of the American Chemical Society* **2008**, *130* (26), 8130-8131.
- (57) Li, Z.; Shen, W.; Liu, X.; Liu, R. Efficient unimolecular photoinitiators for simultaneous hybrid thiol–yne–epoxy photopolymerization under visible LED light irradiation. *Polymer Chemistry* **2017**, *8* (9), 1579-1588.
- (58) Feillé, N.; De Fina, M.; Ponche, A.; Vaulot, C.; Rigolet, S.; Jacomine, L.; Majjad, H.; Ley, C.; Chemtob, A. Step-growth thiol–thiol photopolymerization as radiation curing technology. *Journal of Polymer Science Part A: Polymer Chemistry* **2017**, *55* (1), 117-128.
- (59) Zivic, N.; Sadaba, N.; Almandoz, N.; Ruiperez, F.; Mecerreyes, D.; Sardon, H. Thioxanthone-Based photobase generators for the synthesis of polyurethanes via the photopolymerization of polyols and polyisocyanates. *Macromolecules* **2020**, *53* (6), 2069-2076.
- (60) Esen, D. S.; Temel, G.; Balta, D. K.; Allonas, X.; Arsu, N. One-component thioxanthone acetic acid derivative photoinitiator for free radical polymerization. *Photochemistry and Photobiology* **2014**, *90* (2), 463-469.
- (61) Ableidinger, K. Novel Photo Base Generators for Step Growth Polymerization. Progress Report, PhD, TU Wien, 2022.
- (62) Blake, J. A.; Gagnon, E.; Lukeman, M.; Scaiano, J. Photodecarboxylation of xanthone acetic acids: C–C bond heterolysis from the singlet excited state. *Organic letters* **2006**, *8* (6), 1057-1060.
- (63) Weitkamp, R. F.; Neumann, B.; Stammner, H. G.; Hoge, B. Generation and Applications of the Hydroxide Trihydrate Anion, [OH (OH)<sub>2</sub>]<sup>3-</sup>, Stabilized by a Weakly Coordinating Cation. *Angewandte Chemie International Edition* **2019**, *58* (41), 14633-14638.
- (64) Bell, S. A.; Meyer, T. Y.; Geib, S. J. Catalytic double-bond metathesis without the transition metal. *Journal of the American Chemical Society* **2002**, *124* (36), 10698-10705.
- (65) Zhibo, L.; Zhao, N.; Chuanli, R.; Xiaohui, F.; Liu, S. Phosphazene compound, preparation method and use thereof. Google Patents: 2022.
- (66) Giri, R.; Brusoe, A.; Troshin, K.; Wang, J. Y.; Font, M.; Hartwig, J. F. Mechanism of the Ullmann biaryl ether synthesis catalyzed by complexes of anionic ligands: Evidence for the reaction of

iodoarenes with ligated anionic CuI intermediates. *Journal of the American Chemical Society* **2018**, *140* (2), 793-806.

(67) SCOTT, J.; Huskisson, E. Analgesic action of isoxepac. *Rheumatology* **1982**, *21* (1), 48-50.

(68) Bissett, D. L.; Bush, R. D.; Chatterjee, R. Photoprotection compositions comprising chelating agents. Google Patents: 1996.

## Appendix

Table S1: Monofunctional oxa-Michael temperature screening with TP

temperature screening TP				
annotation	T (°C)	conversion (%)	average (%)	st. dev. (%)
A1		0		
A2	25	0	0	0
A3		0		
B1		4		
B2	60	5	4.7	0.62
B3		5		
E1		31		
E2	80	32	31	0.82
E3		30		
C1		62		
C2	100	59	61	1.29
C3		62		
D1		0		
D2	120	0	0	0
D3		0		

Table S1: Monofunctional oxa-Michael temperature screening with IP

temperature screening IP				
annotation	T (°C)	conversion (%)	average (%)	st. dev. (%)
A1		0		
A2	25	0	0	0
A3		0		
B1		0		
B2	60	0	0	0
B3		0		
E1		5		
E2	80	6	5	0.47
E3		5		
C1		30		
C2	100	31	30	0.47
C3		30		

Table S3: Monofunctional oxa-Michael temperature screening with **KP**

temperature screening <b>KP</b>				
annotation	T (°C)	conversion (%)	average (%)	st. dev. (%)
A1		0		
A2	25	0	0	0
A3		0		
B1		0		
B2	60	0	0	0
B3		0		
E1		8		
E2	80	9	7	1.70
E3		5		
C1		29		
C2	100	30	25	6.85
C3		15		

Table S4: Monofunctional oxa-Michael irradiation intensity screening with **TP**

irr. intensity screening <b>TP</b>				
annotation	intensity (mW/cm <sup>2</sup> )	conversion (%)	average (%)	st. dev. (%)
A1		72		
A2	26	68	71	1.89
A3		72		
B1		72		
B2	42	61	68	4.78
B3		70		
C1		59		
C2	49	62	61	1.5
C3		58		
D1		62		
D2	60	63	62	0
D3		62		
E1		40		
E2	81	63	56	11.09
E3		64		
F1		66		
F2	108	64	65	0.82
F3		65		

Table S5: Monofunctional oxa-Michael irradiation intensity screening with **IP**

irr. intensity screening <b>IP</b>				
annotation	intensity (mW/cm <sup>2</sup> )	conversion (%)	average (%)	st. dev. (%)
A1		53		
A2	26	55	54	0.94
A3		55		
B1		40		
B4	49	45	47	6.24
B3		55		
C1		31		
C2	81	17	24	5.89
C3		21		
D1		25		
D2	108	19	20	4.11
D3		15		
E1		12		
E2	140	8	10	1.7
E3		9		

Table S6: Monofunctional oxa-Michael irradiation intensity screening with **KP**

irr. intensity screening <b>KP</b>				
annotation	intensity (mW/cm <sup>2</sup> )	conversion (%)	average (%)	st. dev. (%)
A1		0		
A2	26	0	0	0
A3		0		
B1		7		
B4	49	9	8.7	1.25
B3		10		
C2		14		
C3	60	17	16	2.05
C4		19		
D1		15		
D2	81	17	17	2.05
D3		20		
E1		8		
E2	140	5	10	5.56
E3		18		



Table S7: Monofunctional oxa-Michael screening of **TP** concentration

TP concentration screening				
annotation	TP (mol%)	conversion (%)	average (%)	st. dev. (%)
A1		0		
A2	0.1	0	0	0
A3		0		
B1		71		
B2	0.3	69	70	0.82
B3		70		
C1		67		
C2	0.5	65	66	0.82
C3		66		
D1		67		
D2	1.0	68	68	0.47
D3		68		
E1		69		
E2	1.2	69	69	0
E3		69		

Table S8: Monofunctional oxa-Michael screening of **IP** concentration

IP concentration screening				
annotation	IP (mol%)	conversion (%)	average (%)	st. dev. (%)
A1		0		
A2	0.1	0	0	0
A3		0		
B1		43		
B2	0.3	48	46	2.05
B3		46		
C1		68		
C2	0.5	66	67	0.82
C3		67		
D1		68		
D2	1.0	65	65	2.45
D3		62		
E1		64		
E2	1.2	60	62	1.7
E3		63		

Table S9: Monofunctional oxa-Michael screening of **KP** concentration

KP concentration screening				
annotation	KP (mol%)	conversion (%)	average (%)	st. dev. (%)
A1		0		
A2	0.1	0	0	0
A3		0		
B1		0		
B2	0.3	0	0	0
B3		0		
C1		3		
C2	0.5	10	6	2.87
C3		6		
D1		8		
D2	1.0	18	17	6.6
D3		24		
E1		7		
E2	1.2	0	7	6.13
E3		15		